Scale-up of an advanced oxidation process for the degradation of citric acid

Chee, Gan Poh

Award date:
1996

Awarding institution:
University of Bath

SCALE-UP OF AN ADVANCED OXIDATION PROCESS FOR THE DEGRADATION OF CITRIC ACID

submitted by Gan Poh Chee
for the degree of PhD
of the University of Bath
1996

Gan Poh Chee

ProQuest LLC
789 East Eisenhower Parkway
P.O. Box 1346
Ann Arbor, MI 48106-1346

CONTENTS:

Acknowledgements

First and foremost, I would like to thank Prof. P. L. Yue for his support and supervision in my first two years of my research. I am also grateful and indebted to Dr. M. R. Bird who read and commented on the thesis. I would also like to acknowledge Dr. U. Ullah for his continuous advice on modelling and for his valuable suggestions. The co-operation of the technical staff of the university is much appreciated. Special thanks are due to my best friend Anne Chen for her encouragement and help in my experiments. Further, I want to express my gratitude to the Science Research Council and the university for financial support.

List of Figures

List of Tables

ABSTRACT

This research has determined the most efficient Advanced Oxidation Process (AOP) in the degradation and mineralization of citric acid. A mineralization rate model has also been formulated for the purpose of scaling-up the process. The UV/H_2O_2/Ferric sulphate pentahydrate process has proved to be the most efficient in the mineralization of citric acid. Results have shown that the process efficiency increases with increasing reactant concentration. However, for the process to be efficient and economical, the right balance is needed in the usage of the reactants. The mineralization rate was determined to be $r = -1.0094\text{x}10^{-4}[TOC]_o^{0.74}[H_2O_2]_o^{0.39}[I_{abs}]_o^{-0.11}$. When this rate equation is incorporated with the relevant mass balances, a good prediction of the mineralization profile in the batch and pilot plant is achieved.

CHAPTER 1
INTRODUCTION

Our society is becoming increasingly concerned over the state of our environment and quality of life, and the "purity" of water discharged by industry. In addition, drinking water quality is becoming a major issue. Even minute quantities of organic compounds in water may pose a threat to the public health. It is thus desirable to completely oxidise (or mineralise) organic contaminants in water to relatively harmless substances such as carbon dioxide and water.

Removal of low levels of hazardous organic compounds from water can be a difficult and expensive task. Conventional treatment methods such as packed bed aeration and granular activated carbon absorption can effectively remove some compounds but not others. Aeration is only useful for highly volatile pollutants. Carbon adsorption has the disadvantage that the carbon must be replaced or regenerated when its adsorptive capacity is reached. And chlorination in conventional water treatment has been shown to enhance the production of toxic haloforms and other halogenated compounds. Also, ozonation doses typically used in drinking water treatment are not sufficient to mineralise most micropollutants. Ozone is a powerful oxidant and a disinfectant aid, and in principle should be able to oxidise inorganic substances to their highest stable oxidation states and organic compounds to carbon dioxide and water. However in practice ozone is quite selective in its oxidation reactions.

The destruction of refractory compounds upon ozonation of water is actually due to the production of hydroxyl radicals from ozone decomposition. The development of advanced oxidation processes (AOPs) is an attempt to take advantage of the rapid, non-selective nature of the hydroxyl radical. Examples of AOPs are ozone/UV, ozone/hydrogen peroxide and hydrogen peroxide/UV

processes. Some processes have ferrous or ferric ions added to catalyze the photo-oxidation reaction. In this research, AOPs are used to degrade citric acid, one of the most widely used chemical in the food and pharmaceutical industries, finding application from nuclear power to cosmetic plants. Another reason for its choice is because of its simple chemical structure which in theory can be easily photodegraded into smaller molecules and eventually only carbon dioxide and water is left. At the present moment no limit is set by the law the maximum concentration of citric acid that could be discharged to drain by industry. Citric acid is non-toxic and fairly soluble in water.

The objective of this research is to scale-up a batch reactor for the photo-degradation of citric acid, i.e. to produce a kinetic rate model which is capable of predicting the performance of the pilot plant. Since mineralization profile shows the sum of the total organic compounds present at any time, this is the best method to determine the efficiency of any AOPs and is used as a basis for modelling the rate model. Experimental data from batch experiments are collected for modelling purposes. If the model obtained is proved to be successful when applied to the pilot plant, it means we are one step closer to the use of the process in large industrial applications. Research in this area involves determination of the most efficient AOP to degrade and mineralise citric acid and its optimum reaction conditions, identification of the intermediate compounds so as to understand the reaction paths, and isolation of any toxic compounds formed. The following chapters will systematically present the results of work done to achieve these aims.

The next chapter will present a literature review on work done by researchers in this and related fields. This is followed by a detailed description of the apparatus, equipment and chemicals used, and the procedures involved in experiments and analysis. The results obtained in this research are presented in Chapter 5 onwards. Firstly, the most efficient AOP is determined and the experimental conditions to be used for modelling purpose are discussed in Chapter 5. Factors which might influence the process and which need to be taken into

account in the modelling are also determined and discussed in the followed chapter. In addition efforts are made to determine if any toxic by products are formed in using the process by identifying the intermediate compounds (Chapter 7). In Chapter 8 radiation field models are used to evaluate the photon flux emitted by the ultra-violet lamp. Everything is set then to carry out the modelling of the mineralization rate which is presented in Chapter 9. The model obtained is tested on batch reactor before being apply to the pilot plant in Chapter 10 which showed mineralization profile of model and experiment results. Finally the last two chapters will conclude this thesis with critical appraisal and recommendations followed by conclusions and future work.

CHAPTER 2
LITERATURE SURVEY

Many researchers have contributed to the field of photochemical engineering and advanced oxidation processes (AOPs). These two fields of research have been studied almost independently of each other when in fact they are closely inter-related since in AOPs one of the major contributing factors is the UV light. This chapter will attempt to present a comprehensive review on the work (related to this research) that has been done to date by these researchers. This chapter consists of two main parts : a review on AOPs (Sec.2.1) and radiation field models (Sec. 2.2).

2.1 AOPs

Advanced oxidation processes (AOPs) rely on the generation of very reactive free radicals, such as hydroxyl radicals, to be considered as initiators of oxidative degradation. They have been defined as ambient temperature processes that involve the generation of highly reactive radical intermediates, particularly the hydroxyl radical (·OH). These processes show promise for the destruction of hazardous organic substances in municipal and industrial wastes, and in drinking water. The appeal of AOPs is the prospect of complete oxidation of organic contaminants through a "combustion" process that operates at or near ambient temperature and pressure.

Oxidation of organic pollutants by the combination of ultraviolet light and oxidants (H_2O_2,O_3 etc.) implies in most cases generation and subsequent reaction of hydroxyl radicals. The oxidation potentials for common oxidants are listed in Table 2.1 and show that the most powerful oxidising species after fluorine is in fact the hydroxyl radical.

TABLE 2.1 Oxidation Potentials of Some Common Oxidants (Hager et al, 1990)

Species	Oxidation Potential (V)
fluorine	3.03
hydroxyl radical	2.80
atomic oxygen	2.42
ozone	2.07
hydrogen peroxide	1.78
perhydroxyl radical	1.70
permanganate	1.68
hypobromous acid	1.59
chlorine dioxide	1.57
hypochlorous acid	1.49
hypoiodous acid	1.45
chlorine	1.36
bromine	1.09
iodine	0.54

The hydroxyl radical is a short lived, extremely potent oxidising agent, capable of oxidising organic compounds mostly by hydrogen abstraction (Eqn.2.1). This reaction generates organic radicals which by addition of molecular oxygen yield peroxyl radicals (Eqn.2.2). These intermediates initiate thermal (chain) reactions of oxidative degradation, leading finally to carbon dioxide, water and inorganic salts (Legrini et al, 1993).

$$HO\cdot + RH \rightarrow R\cdot + H_2O \quad \cdots(2.1)$$

$$R\cdot + O_2 \rightarrow RO_2\cdot \rightarrow\rightarrow \quad \cdots(2.2)$$

$$HO\cdot + RX \rightarrow RX\cdot^{+} + HO^{-} \quad \cdots(2.3)$$

Besides hydrogen abstraction, electron transfer to hydroxyl radicals (Eqn.2.3) constitutes another mechanism of oxidative degradation. The reaction scheme demonstrates clearly that rate and efficiency of oxidative degradation processes, which are primarily based on the production and the reactivity of radical intermediates, depend (i) on the energy needed in order to homolyze a given chemical

bond, and (ii) to a large extent on the concentration of dissolved molecular oxygen (Legrini et al, 1993).

Four types of AOPs are considered in this section : photolysis of hydrogen peroxide with ultraviolet radiation (UV/H_2O_2), photolysis of ozone with ultraviolet radiation (UV/O_3), ozone with hydrogen peroxide (O_3/H_2O_2) and hydrogen peroxide with ultraviolet radiation in the presence of ferric salt ($UV/H_2O_2/Fe^{3+}$).

2.1.1 UV/H_2O_2 Process

In principle this is the most direct method for the generation of hydroxyl radicals. Baxendale and Wilson (1957) demonstrated that photolysis of hydrogen peroxide produces hydroxyl radicals directly, i.e. absorption of a UV photon by a hydrogen peroxide molecule causes it to dissociate into two hydroxyl radicals (Table 2.2). This was further confirmed by Guittinneau et al (1987), who had examined this process in detail, and later by Glaze et al (1989).

The principal reactions in this process are (Glaze et al, 1989) :

Initiation $H_2O_2 + h\upsilon \rightarrow 2HO\cdot$

Propagation $HO\cdot + H_2O_2 \rightarrow \cdot HO_2 + H_2O$

$\cdot HO_2 + H_2O_2 \rightarrow HO\cdot + H_2O + O_2$

Termination $2HO_2\cdot \rightarrow H_2O_2 + O_2$

$HO\cdot + \cdot HO_2 \rightarrow H_2O + O_2$

As mentioned earlier the hydroxyl radical ·OH has an oxidation potential of 2.87 volts relative to hydrogen, which makes it a stronger oxidising agent then either ozone or hydrogen peroxide (Weir et al, 1987). And it is known to be extremely reactive with most organic molecules with H-atom donor properties, and promptly attacks such species to produce new types of radicals which may subsequently initiate

several radical chain reactions (Anbar et al, 1967). Also, OH radicals are more effective than ·OR and ·OOR (R = alkyl or aryl group) in producing carbon radicals from organics and hence the use of H_2O_2 as the source of free radicals is very attractive (Anbar et al, 1967). The reaction scheme above also shows that portion of the peroxide which is used for creating hydroxyl radicals in the first place is regenerated.

However, Glaze et al (1987) stated that the molar extinction coefficient ($\in$) of hydrogen peroxide at 254 nm is only 19.6 $M^{-1}s^{-1}$, compare to ozone which has a value of 3300 $M^{-1}s^{-1}$ (Table 2.3), which is exceptionally low for a primary absorber in a photochemical process. So in order to generate a sufficient level of OH radicals, high concentration of hydrogen peroxide is required.

A simplified reaction scheme for UV/H_2O_2 treatment is shown in Fig.2.1 (Peyton, 1990) :

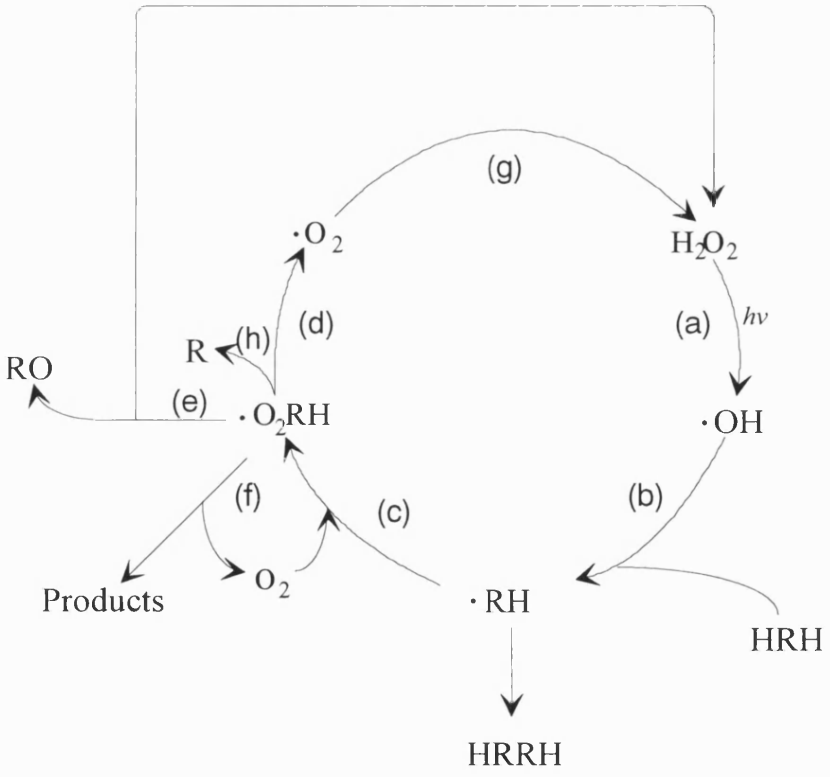

Fig. 2.1 Reaction System for the Peroxide / UV System

Peroxide photolysis a yields hydroxyl radical (path a), which reacts with organic compound (HRH in Fig.2.1) either by addition to a double bond or by hydrogen abstraction, to create (b) and organic radical (·RH). This radical reacts quickly with oxygen (if present) to give (c) an organic peroxyl radical ($\cdot O_2RH$), which decays either directly or via a short-lived tetroxide. Decay of peroxyl radicals, either directly or through the tetroxide, appears to follow one or more of three distinct pathways : (d) creation of superoxide, (e) generation of hydrogen peroxide and (f) oxygen liberation. Superoxide produced is disproportionate to hydrogen peroxide (path g). If oxygen is not present, the organic radicals can combine with themselves (path h) or attack hydrogen peroxide.

Generated at high (local) concentration, hydroxyl radicals will readily dimerize to H_2O_2 (Eqn.2.4). If an excess of H_2O_2 is use, HO· radicals will produce hydroperoxyl radicals (Eqn.2.5) which are much less reactive and do not appear to contribute to the oxidative degradation of organic substrates (Legrini et al, 1993). The concentration of HO_2^- is controlled by the pH of the reaction system, the latter controlling, therefore, the efficiency of superoxide dismutation (Legrini et al, 1993).

$$HO\cdot + HO\cdot \rightarrow H_2O_2 \qquad \cdots(2.4)$$

$$H_2O_2 + HO\cdot \rightarrow H_2O + HO_2\cdot \qquad \cdots(2.5)$$

Also, electrophilic addition of HO· radicals to organic π systems will lead to organic radicals the subsequent reactions of which are quite similar to those mentioned in Fig.2.1.

For substrate M which is both a radical scavenger and UV absorber, the steady state concentration of OH radicals is given by (Glaze and Lay, 1989) :

$$[OH]_{ss} = \frac{2\phi I_o\left(1-\exp\left(-a_{H_2O_2}b[H_2O_2]\right)\right)}{k_2[H_2O_2]+k_3[HO]^- +\left(k_{HCO_3,OH}+k_{CO_3,OH}\,10^{pH-pK'}\right)\left[HCO_3^-\right]} \qquad \ldots(2.6)$$

and the rate equation is given as:

$$-\frac{dM}{dt} = k_p + k_{ps}[PS] + k_{m,OH}[OH]_{SS}[M] \qquad ...(2.7)$$

where I_o is the effective incident radiation power.

$k_{HCO_3,OH}$ and $k_{CO_3,OH}$ are rates of scavenging of OH by bicarbonate and carbonate respectively.

pK' is the carbonate-bicarbonate equilibrium constant.

k_p is the rate constant of direct photolysis of M

k_{ps} is the rate constant for induced decomposition by the photosentizer (PS).

Yue et al (1989, 1992) studied the degradation rate for the oxidative removal of several organic compounds. Results show that conversion (diminution of TOC) of trichloroethylene, phenol, 4-chlorophenol and catechol (Peyton et al, 1986) is higher if the initial H_2O_2 concentration is increased. For all organics studied, TOC removal rate follows first order kinetics. After numerous studies on the photo-oxidation of organics in water in an annular batch reactor, Yue and Legrini (1989) proposed a model for the rate of TOC reduction :

$$r = k_1[H_2O_2]^a[TOC]^b \qquad ...(2.8)$$

$$r = k_2[TOC]^c \qquad ...(2.9)$$

where k_1 and k_2 = rate constants

a, b and c = exponential constants

Eqn.2.9 is only applicable when excess hydrogen peroxide is used. The exponents of the power law were found to vary with the initial TOC concentration. Their results showed that TOC can be effectively reduced to very low levels, provided the concentration of hydrogen peroxide used exceeds 0.05% v/v.

The UV/H_2O_2 process has a number of advantages in comparison with other methods of chemical or photochemical water treatment (Legrini et al, 1993): commercial availability of the oxidant, thermal stability and storage on-site, infinite solubility in water, and no mass-transfer problems associated with gases. In addition, two hydroxyl radicals are formed for each molecule of H_2O_2 photolyzed, peroxyl radicals are generated after HO· attack on most organic substrates, leading to subsequent thermal oxidation reactions. Minimal capital investment is required, very cost-effective source of hydroxyl radicals exists and simple operation procedure results.

There are, however, obstacles encountered with the UV/H_2O_2 process. The rate of chemical oxidation of the contaminant is limited by the rate of formation of hydroxyl radicals, and there is a rather small absorption cross-section of H_2O_2 at 254 nm particularly in cases where organic substrates will act as inner filters (Legrini et al, 1993).

2.1.2 UV/O_3 Process

This process has been studied by more workers and in greater detail than other AOPs. It is the most frequently applied AOP for a wide range of compounds. This is mainly due to the fact that ozonation is a well-known procedure in water technology and that ozonizers are therefore in most cases readily available in drinking water treatment stations. Studies have shown that UV lamps emitting primary 254 nm radiation are the most efficient for ozone photolysis because of their coincidence with the centre of ozone absorption band. Also, UV photons at 180 - 400 nm provide 72 - 155 Kcal/mol energy which is able to produce more and other oxidising free radicals from O_3 (Prengle, 1983). However, there are many questions related to mechanisms of free radicals production and subsequent oxidation of organic substrates. In fact, the literature contains many conflicting reports on the efficiency of this oxidation method

which may be linked to the difficult tasks of dissolving and photolyzing ozone with high efficiency.

Glaze et al (1984) and Peyton et al (1988, 1987), in agreement with the findings of Taube (1956), have provided additional confirmation that ozone photolysis in aqueous solution leads directly to the formation of hydrogen peroxide which then produces hydroxyl radical by secondary reaction of the anion (HO_2^-) and subsequent species with ozone.

$$O_3 + H_2O \xrightarrow{h\upsilon} H_2O_2 + O_2 \quad \cdots(2.10)$$

$$E_{254} = 3185\ M^{-1}cm^{-1}$$

$$H_2O_2 \xrightarrow{h\upsilon} 2 \cdot OH \quad \cdots(2.11)$$

$$E_{254} = 17.2\ M^{-1}cm^{-1}$$

Further studies by Peyton et al (1985) provide kinetic evidence that ozone at 2537 Å in aqueous solution yields peroxide followed by reaction of the conjugate base hydroperoxyl anion (HO_2^-) with ozone to yield superoxide ($\cdot O_2^-$) and hydroxyl radical (Eqn.2.13).

$$H_2O_2 + H_2O \Leftrightarrow H_3O^+ + HO_2^- \quad \cdots(2.12)$$

$$O_3 + HO_2^- \rightarrow O_2 + \cdot O_2^- + OH \quad \cdots(2.13)$$

Based largely on the work of Staehelin and Hoigne (1982, 1983), Peyton et al (1987) developed a mass balance model for the photolytic ozonation (ozone/UV) treatment of organic compounds in water. The scheme used is shown in Fig.2.2.

In the presence of excess ($\geq 10^{-4}$ M) organic compounds, containing an abstractable hydrogen atom, ·OH reacts with organic substrate to produce an organic radical :

$$\cdot OH + RH \rightarrow H_2O + R\cdot \quad \cdots(2.14)$$

followed by a quick reaction between R· and dioxygen to give organic peroxyl radicals :

$$R\cdot \quad + \quad O_2 \quad \rightarrow \quad RO_2^- \qquad \cdots(2.15)$$

which can photolyze, disproportionate to more stable molecules, or regenerate further superoxide.

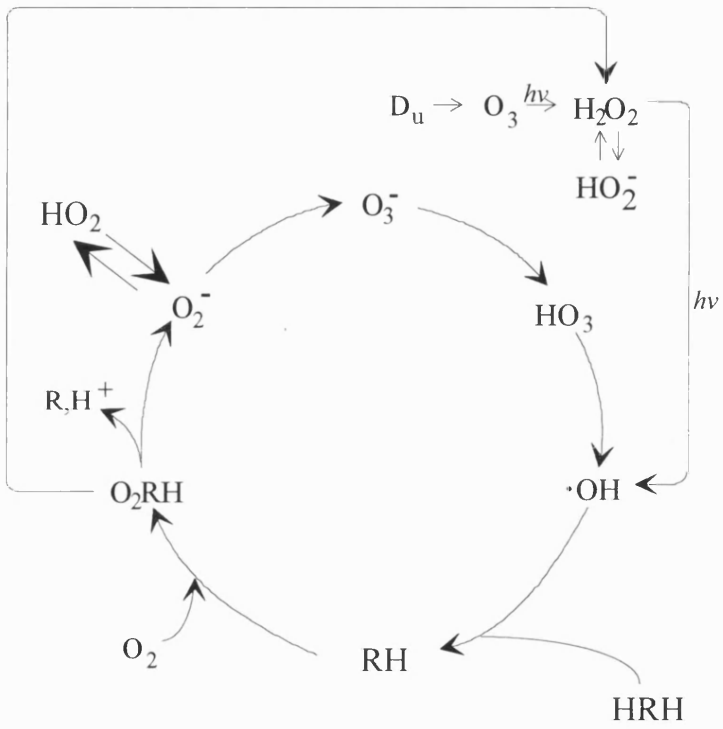

Fig.2.2 Reaction Pathway in the Ozone/UV and Ozone/Peroxide System.

Some peroxyl radicals formed can rapidly eliminate superoxide (Staehelin et al, 1983, 1985), which quickly reacts with ozone to yield hydroxyl radical (Staehelin et al, 1983). Because this reaction is so fast, the disproportion of superoxide to hydrogen peroxide is not important in ozonation systems and is therefore not included in Fig.2.2. The attack of ozone and peroxide by the hydroxyl radical is also not shown. At low organic and high oxidant concentrations, these reactions have a direct effect in process efficiency and must be considered.

Glaze et al (1984) observed that the efficiency of the hydroxyl radical product would be lowered if more than one third of the transferred ozone was photolyzed. This depended on the rate of the secondary ozone reactions relative to the rate of photon absorption by ozone.

In acidic media where chain reaction of ozone with H_2O_2/HO_2^- are inhibited Eqn.2.10 takes place with almost exact stoichiometry (>0.9 mole of H_2O_2 formed per mole of O_3 decomposed) (Verhaeghe et al, 1988). H_2O_2 formed in this reaction accumulates in solution because of the slow photolysis rate of H_2O_2 (Eqn.2.11). The quantum yields for ozone decomposition at 253.7 nm and 313.5 nm are, respectively, 0.62 and 0.23.

At high pH values (pH > 7) hydrogen peroxide in its ionised form (HO_2^-) reacts with residual ozone quite rapidly and initiates a complex chain reaction mechanism ozone decomposition (Guittonneau et al, 1990). Therefore, the photo-decomposition pathway of ozone by UV light at neutral pH produces less H_2O_2 and more ·OH radicals (Hoigne et al, 1987).

The reactions present in this process are complex, and the oxidation process is likely to be a mixture of photo-oxidation, ozonation and reactions with the free radicals produced from the photolysis of ozone (Francis, 1987). Several parameters can influence the degree of efficiency of the O_3/UV system, especially the pH, the alkalinity, rate of ozonation, radiation power and reactor characteristics (Paillard et al, 1987).

Francis (1987) proposed that the UV-ozone reaction sequence can be considered as a series of slow and fast reactions shown in Fig.2.3. The overall rate of reduction of TOC concentration expressed in terms of independent variables of the experiment is given by :

$$-\frac{d[TOC]}{dt} = k_{TOC} I^a [O_3]^b [TOC]^d \qquad ...(2.16)$$

where k_{TOC} is a constant,

$[O_3]$ is the concentration of dissolved ozone,

I is the UV radiation intensity.

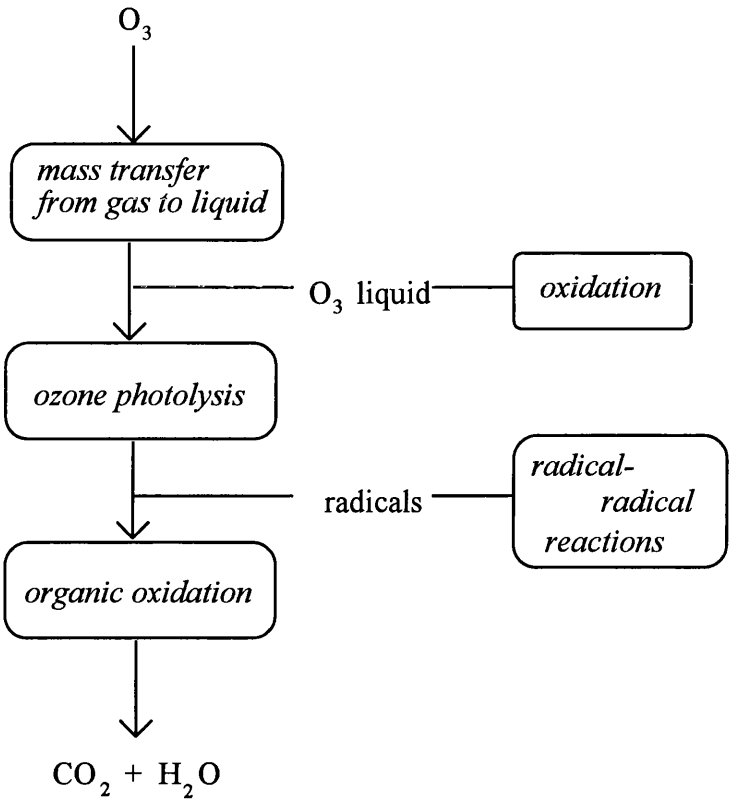

Fig.2.3 Sequence of Reactions in the UV - Ozone Oxidation Process

Francis also suggested an expression for the decomposition rate of dissolved ozone, derived from the product of the light intensity due to radial light rays emitted from the lamp and the ozone optical absorption coefficient. Thus the decomposition of ozone due to photolysis by UV radiation in a plug flow reactor is given as (Francis, 1987) :

$$C_o - C = C_o\left[1 - \exp\left(-\frac{2K}{\psi(\lambda+1)(1-e^{-\psi})}\right)\right] \qquad \cdots(2.17)$$

where C_o is the initial concentration of dissolved ozone in the reactor and K, ψ and λ are expressed in terms of the UV radiation intensity, the residence time in the reactor and the ratio of the radii of the UV lamp and the reactor.

2.1.3 O_3/H_2O_2 Process

It can be seen from Fig.2.2 that the same mechanistic model used for the ozone/UV process can be applied simply by settling the photolysis rates to zero.

Hart et al (1982) and Staehelin and Hoigne (1982) showed that the conjugate base of H_2O_2 can inhibited the ozone decomposition cycle by a single electron transfer process involving the conjugate base of hydrogen peroxide (HO_2^-) :

$$H_2O_2 + H_2O \Leftrightarrow HO_2^- + H_3O^+ \qquad k_a = 10^{-11} \qquad \cdots(2.18)$$

$$HO_2^- + O_3 \xrightarrow{k_1} HO_2 + O_3^- \qquad \cdots(2.19)$$

This initiates the decomposition of ozone resulting in the formation of hydroxyl radicals. The above reactions can be represented by the following scheme (Brunet et al, 1984):

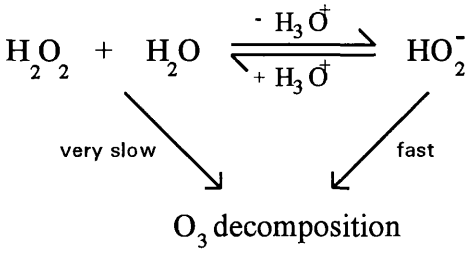

Brunet et al (1984) observed that with the acidity constant of hydrogen peroxide, $k_a = 10^{-11}$, the quantity of HO_2^- ions will decrease as the pH drops. This was confirmed by Staehelin and Hoigne (1982) who observed that at pH = 2, H_2O_2 reacts only very slowly with O_3. However at pH values above 5, a strong acceleration of the decomposition of O_3 by H_2O_2 is observed. For pH values well below pK_a, the degree of dissociation will have the following form :

$$\log \alpha = pH - pk_a$$

However at high pH values, when the ratio between the ozone consumed and the hydrogen peroxide destroyed is of the order of one, hydroxyl radicals react with hydrogen peroxide as follows :

$$\cdot OH + H_2O_2 \rightarrow H_2O + HO_2\cdot$$
$$\cdot OH + HO_2\cdot \rightarrow O_2 + H_2O$$

with overall reaction of :

$$O_3 + H_2O_2 \rightarrow 2O_2 + H_2O \qquad \cdots(2.20)$$

The rate increases by one order of magnitude per pH unit. This observation suggests that H_2O_2 also reacts with O_3 only when present in its ionised form :

$$O_3 + H_2O_2 \xrightarrow{\text{very slow}}$$
$$-H^+ \Updownarrow +H^-$$
$$O_3 + HO_2^- \xrightarrow{\text{fast}} \text{decomposition } O_3$$

When no promoters (i.e. OH_2) are formed and inorganic carbon species are the principal ·OH scavengers, the pseudo-first order rate constant $k_{o,m}$ for a micropollutant M is given by

$$k_{o,m} = \frac{k_{m,OH}\, k_L\, a\, P / H}{k_{m,OH}[M] + \left(k_7 10^{pH-pK} + k_8\right)[H_2O_2] + \left(k_{10} + k_{11}10^{pH-pK'}\right)[HCO_3^-]} \qquad \cdots(2.21)$$

where $\left(k_7 10^{pH-pK} + k_8\right)[H_2O_2]$ represents reaction of OH with hydrogen peroxide and its conjugate base.

$\left(k_{10} + k_{11}10^{pH-pK'}\right)[HCO_3^-]$ is for reaction of ·OH with bicarbonate and carbonate respectively.

P is the partial pressure of ozone in the gas phase entering the reactor.

H is the Henry's Law constant for ozone-water.

The ozone/peroxide process has the obvious advantages over ozone/UV process in that (i) it is simpler and (ii) the maintenance associated with cleaning of the lamp wells and the expense of electrical power and lamp replacement are eliminated. There are, however, also disadvantages to the ozone/peroxide system :

(i).any effect due to direct photolysis of the substrate is lost,

(ii).no peroxide photolysis can occur and this disadvantages can be significant if promoters are absent,

(iii).there is no "self-regulation" when promoters are absent. The ozone reaction with superoxide is rapid and the ozone concentration is maintained at a low level, with the result that very little ozone photolysis occurs. However, when superoxide production (and thus chain production of hydroxyl) decreases, the ozone concentration in solution increases and more photolysis to peroxide occurs, providing an automatically regulated dose of initiator.

Summary for UV/H_2O_2, UV/O_3, and O_3/H_2O_2 Processes

Summary of the chemistry involved in the generation of hydroxyl radical from the four processes is given by Brunet et al, 1984 :

TABLE 2.2 Theoretical Amounts of Oxidants and UV Required For Formation of Hydroxyl Radical In Ozone-Peroxide-UV System.

	Moles of Oxidant Consumed		
System	O_3	UV[b]	H_2O_2
O_3 -- Hydroxide Ion[c]	1.5	-----	-----
O_3 -- UV	1.5	0.5	0.5[d]
O_3 -- H_2O_2	1.0	-----	0.5
H_2O_2 -- UV	-----	0.5	0.5

TABLE 2.3 Theoretical Formation of Hydroxyl Radicals From Photolysis of Ozone and Hydrogen Peroxide.

	Molar Absorptivity 254 nm ($M^{-1}cm^{-1}$)	Stoichiometry	OH Radical Formed per Incident Photon
H_2O_2	20	H_2O_2 ---> 2(·OH)	0.09
O_3	3300	$3(O_3)$ ---> 2(·OH)	2.00

2.1.4 $UV/H_2O_2/Fe^{3+}$ Process

This process is relatively new in comparison with other AOPs. However it has evolved as a result of years of work on closely related process : Fenton's reagent (Fe^{2+}/H_2O_2 process) and Fe^{3+}/H_2O_2 process. This section will start by briefly describing these two processes as they help one to understand more about the $UV//H_2O_2/Fe^{3+}$ process, how it came about and the reactions involved.

---

b moles of photons (Einsteins) required for each mole of OH radical formed.

c assumed that superoxide formed in the primary step yields one OH radical per O_2^- which may not be the case in certain water.

d H_2O_2 formed in situ.

2.1.4.1 Fe^{2+}/H_2O_2 Process

Direct photolysis of H_2O_2 produces OH radicals, but, because H_2O_2 weakly absorbs ultra-violet radiation, OH radical formation by this process is comparatively slow (Zepp et al, 1992). Hydrogen peroxide, however, can serve as an ·OH source via other pathways involving iron. Past studies have shown that Fe(II) (Fe^{2+} and complexes thereof) and H_2O_2 can oxidise a wide variety of organic substances (Fenton, 1894). Since then the combination of a ferrous salt and hydrogen peroxide, known as the Fenton's reagent has been used as one of the most effective oxidants substances (Walling, 1975). Fenton's reactions have been shown to involve hydroxyl radicals as the actual oxidants. This was been proved by many techniques, including ESR spectroscopy (Dixon and Norman, 1964).

The classic procedure for oxidation by Fenton's reagent consists of the addition of hydrogen peroxide to a solution or a suspension of the organic compound in the presence of iron (II) ions. The following mechanism has been demonstrated (Walling and Weil, 1974):

$$Fe^{2+} + H_2O_2 \xrightarrow{k_1} Fe^{3+} + HO^- + HO\cdot \quad \cdots(2.22)$$

$$Fe^{2+} + HO\cdot \rightarrow Fe^{3+} + HO^- \quad \cdots(2.23)$$

$$H_2O_2 + HO\cdot \rightarrow HO_2\cdot + H_2O \quad \cdots(2.24)$$

$$Fe^{2+} + HO_2\cdot \rightarrow Fe^{3+} + HO_2^- \xleftrightarrow{H^+} H_2O_2 \quad \cdots(2.25)$$

$$Fe^{3+} + HO_2\cdot \rightarrow Fe^{2+} + H^+ + O_2 \quad \cdots(2.26)$$

$$Fe^{3+} + H_2O_2 \xrightarrow{k_2} Fe^{2+} + HO_2\cdot + H^+ \quad \cdots(2.27)$$

In the presence of excess of Fe^{2+} ions reactions (2.22) and (2.23) take place, with an excess of hydrogen peroxide in acid solution -- (2.22), (2.24) and (2.25) occur.

2.1.4.2 Fe^{3+}/H_2O_2 Process

Barb et al (1951) showed that hydrogen peroxide and iron salts separately are not effective oxidants of the complex organic materials in municipal waste waters. They found that when ferrous salts are used, the hydroxyl radical is produced immediately by the rapid reaction between ferrous ion and hydrogen peroxide (Eqn.2.22, rate constant $k_1 = 4.45 \times 10^8\ e^{-9400/RT}$ moles litre^{-1} second^{-1}). With ferric salts, however, the hydroxyl radical is produced by a two-stage process with the slow reaction between ferric ion and hydrogen peroxide (Eqn.2.27, $k_2 = 1.1 \times 10^{24}\ e^{28000/RT}$ moles litre^{-1} second^{-1}) followed by the rapid reaction between the produced ferrous ion and additional hydrogen peroxide. According to Barb et al (1951) and later substantiated by Walling and Goosen (1973), Walling and Weil (1974) and Walling and Cleary (1977) the redox sequence is :

$$Fe^{3+} + H_2O_2 \xrightarrow{k_3} Fe^{2+} + HO_2\cdot + H^+ \quad \ldots(2.28)$$

$$Fe^{2+} + H_2O_2 \xrightarrow{k_4} Fe^{3+} + HO\cdot + OH^- \quad \ldots(2.29)$$

$$HO\cdot + H_2O_2 \xrightarrow{k_5} H_2O + HO_2\cdot \quad \ldots(2.30)$$

$$HO_2\cdot + Fe^{3+} \xrightarrow{k_6} Fe^{2+} + H^+ + O_2 \quad \ldots(2.31)$$

$$HO_2\cdot + Fe^{2+} \xrightarrow{k_7} HO_2^- + Fe^{3+} \quad \ldots(2.32)$$

$$HO\cdot + Fe^{2+} \xrightarrow{k_8} Fe^{3+} + OH^- \quad \ldots(2.33)$$

OH radical generated in the rate-limiting step (Eqn.2.29) may be scavenged by reaction with another Fe^{2+} (Eqn.2.33) or react with an organic compound (Walling, 1975). According to Walling and Weil (1974), Eqn.2.28 and Eqn.2.31 also involve equilibria with hydrogen ion prior to going to completion. As such, both Eqn.2.28 and Eqn.2.31 can each be considered as the summation of two reactions. For Eqn.2.28, the first of these two reactions is the equilibria with hydrogen ion which may be written as :

$$Fe^{3+} + H_2O_2 \leftrightarrow H^+ + FeOOH^{2+} \quad \ldots(2.34)$$

This equilibrium reaction is then followed by the completion of the step :

$$FeOOH^{2+} \rightarrow Fe^{2+} + HO_2\cdot \quad ...(2.35)$$

Similarly, Eqn.2.31 can be considered as the sum of two reactions. First, is the equilibrium with hydrogen ion (Walling and Weil, 1974) :

$$HO_2\cdot \rightarrow H^+ + O_2^- \quad ...(2.36)$$

followed by step completion,

$$O_2^- + Fe^{3+} \rightarrow O_2 + Fe^{2+} \quad ...(2.37)$$

More recently Kremer and Stein (1959) and Kremer (1962, 1963, 1985) have proposed an alternative non-chain scheme involving two intermediate complexes :

$$Fe^{3+} + HO_2^- \Leftrightarrow Fe^{3+}HO_2^-$$
$$Fe^{3+}HO_2^- \rightarrow FeO^{3+} + OH^-$$
$$FeO^{3+} + HO_2^- \rightarrow Fe^{3+} + O_2 + OH^-$$

It is now known that the oxidising power of the Fenton type systems can be greatly enhanced by irradiation with UV/visible light (Sedlak et al, 1987; Pignatello, 1992; Haag and Yao, 1992).

2.1.4.3 The UV/H_2O_2/Fe^{3+} Process

Bishop et al (1968) found that both ferrous and ferric salts were efficient catalysts when applied to the oxidation of organic residuals, being effective only between pH 3 and 5. In a closely related ferric system, Fe^{3+} acts as a catalyst for decomposition of peroxide to O_2 and H_2O, during which 'steady state' concentrations of Fe^{2+} (as a source of OH^- via Eqn.2.29) are generated as in Eqn.2.31 and Eqn.2.28 (Sun and Pignatello, 1993).

The generation of ·OH in $Fe^{3+}/H_2O_2/UV$ systems was suggested by kinetic experiments by Haag and Yao (1992). Sun and Pignatello (1993) carried out a detailed investigation of 2,4-D mineralization by $Fe^{2+}/H_2O_2/UV$, focusing on the photochemical reactions that contribute to enhancement. It seemed likely that at least one contributing reaction to photoenhancement is photolysis of aquated ferric ion (only H_2O or OH^- ligands are present) (Sun and Pignatello, 1993) :

$$Fe(III)_{aq} \xrightarrow{h\upsilon} Fe^{2+} + OH\cdot \qquad ...(2.38)$$

The photoreduced iron may be a precursor to a second ·OH when peroxide is present via the Fenton reaction (Eqn.2.29).

The authors have shown that (i) the first stage is dominated by ·OH reactions, and light contributes to production of ·OH, and (ii) the second stage occurs without ·OH and is entirely the result of photochemical reactions. The steps leading to ·OH are as proposed in Scheme I (Sun and Pignatello, 1993).

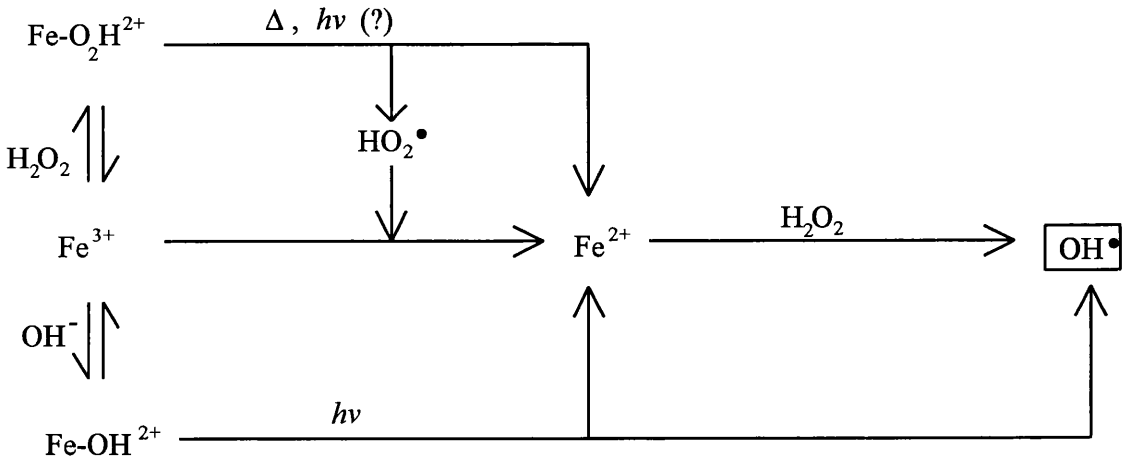

Scheme I. Pathway of OH· Generation

The thermal and photolytic reactions of $FeOH^{2+}$ generate ·OH directly. All photolytic reactions may contribute indirectly to generation of ·OH via production of Fe^{2+} by the Fenton reaction. The importance of individual reactions depends on concentration of hydrogen peroxide and light intensity (Sun and Pignatello, 1993).

Their study also indicated that other reactions besides photolysis of $Fe(III)_{aq}$ are involved in $Fe^{3+}/H_2O_2/UV$ systems. Behar and Stein (1966) studied H_2O_2 photolysis in the presence of ferric ions at various pH. They showed that the photolysis of H_2O_2 in the presence of ferric ions is initiated by 365 nm radiation, i.e. by radiation which at the concentration used ($[H_2O_2]$=0.16 M, $[Fe^{3+}]$=0.005 M) is not absorbed to any important degree by the H_2O_2 alone or by ferric ions alone. This radiation (365 nm) is, however, absorbed by a complex arising from an interaction between H_2O_2 and ferric ions, and is assumed to have a composition $Fe^{3+}HO_2^-$:

$$H_2O_2 + Fe^{3+} \Leftrightarrow [FeHO_2]^{2+} + H^+ \quad ...(2.39)$$

According to the authors, the photocatalytic effects can be attributed to the photochemical generation of Fe^{2+} described by :

$$[FeHO_2]^{2+} \xrightarrow{h\upsilon} Fe^{2+} + HO_2\cdot \quad ...(2.40)$$

The arising Fe^{2+} initiates the decomposition of H_2O_2 via the classical Fenton reaction (Eqn.2.22).

However, Sun and Pignatello (1993) argued that although their results supported Eqn.2.39, this is not sufficient to prove the existence of photoproducts. Thus the identity of the additional contributing reaction(s) remains speculative at this time.

Kozlov et al (1974) used $C(NO_2)_4$, known as an effective inhibitor of the photolysis of H_2O_2, in the measurement of the rate of initiation of photolytic reactions in the presence of Fe^{3+} ions. In addition to the generation of Fe^{3+} suggested by Behar and Stein (1966), the authors (Kozlov et al, 1974) assume that Fe^{3+} is also formed according to :

$$[FeHO_2]^{2+} + [FeOH]^{2+} \rightarrow 2Fe^{2+} + O_2 + H_2O \quad ...(2.41)$$

2.1.4.4 Advantages

Ferric systems are attractive because degradation of organic can be catalytic in iron (Sun and Pignetallo, 1993). This method of generating Fe(II) from Fe(III) in aqueous H_2O_2 solutions was also selected instead of directly mixing solutions of Fe(II) and H_2O_2. This was done in order to avoid artifacts that can results from locally high concentrations of the reagents that are inherent in the initial stages of the mixing process (Zepp et al, 1992). In addition, it has an advantage over the classical method, in that it uses a substantially lower iron concentration (Lunak et al, 1989). In the classical method, only a single ·OH radical is formed for every added Fe^{2+} ion, whereas the photochemical reduction Fe(III) - Fe(II) is coupled to reaction (2.22) to close a cycle, which produces many radicals.

2.1.4.5 Photoactive Fe^{3+} Salts

Several $Fe(III)_{aq}$ species are known to be photoactive, including Fe^{3+}, $FeOH^{2+}$, and $Fe(OH)_2^{4+}$, and their importance depends on pH and wavelength of the emitted light (Sun and Pignatello 1993). Sedlak et al (1987) have studied the effects of 3d transition metal ions (Cr(III), Mn(II), Fe(III), Co(II), Ni(II), Cu(II) and Zn(II) ions) on the quantum yields of hydrogen peroxide photolysis. They found that only Cu(II) and Fe(III) are the only species to exhibit photocatalytic effects under the conditions employed[e]. Cu(II) is efficient in increasing the quantum yields of the photolysis, while Fe(III) dominates in catalysing the hydroxylation.

Cater et al (1991) have found that organics from many different classes of organic contaminants may be efficiently removed from liquid effluents and ground waters using a method employing hydrogen peroxide, transition metal ions and a UV source having a polychromatic output between 200 to 400 nm. The source of transition metal ions is selected for optimal removal efficiency. Particular anions with

---

[e] $I_o = 9.8 \times 10^{14}$ quantum s^{-1}, T = 298 K, $[H_2O_2] = 0.09$ mol dm^{-3}, $[2\text{-hydroxybenzoic acid}]_o = 4 \times 10^{-4}$ mol dm^{-3}.

which the transition metal ions are added (i.e. Cl^-, SO_4^{2-}) may improve the removal efficiency. Copper, zinc and/or iron compounds are preferably used as sources of transition metal ions : iron compounds being most particularly preferred. Iron compounds such as $Fe(OH)_3$, $FeCl_3$, Fe_2O_3, $Fe_2(SO_4)_3$, FeO, $Fe(OH)_2$, $FeCl_2$, $FeCO_3$ or $FeSO_4$ may be used in the process, preferably $FeSO_4.7H_2O$ may be used as a source of iron ions.

2.2 Modelling Of The Radiation Field In Photoreactors

There are many radiation field models which describe the distribution of light intensity or radiation flux in the photoreactor. These models are employed in the determination of the local volumetric rate of energy absorption (LVREA) by the reactant which undergoes photoactivation, which is the most fundamental property for the analysis and design of a reactor. A comprehensive review of radiation field modelling in photoreactors is given in Alfano et al (1986) and Cassano et al (1986). The majority of researchers have carried out model calculations which are often very sophisticated. However, experimental work is rare and in general carried out in the absence of absorbing substances (Cassano et al, 1967; Jacob and Dranoff, 1970; Williams, 1979). This section will review the different models proposed to described the radiant energy field, which will be used in this research.

For homogeneous photoreactors, Alfano et al (1986) divided ten models into two categories : incident and emission models. The incident model is based on incident radiation which comes from outside of the reactor such as the cylindrical and parallel types as shown in Fig.2.4. It assumes a given radiation distribution in the vicinity of the reactor (Hill and Felda, 1965; Matsuura and Smith, 1970). The emission model is based on the annular type as shown in Fig.2.5 and proposes a model for the source emission. The latter can be classified into line source and extense source models and the line source models can further be subdivided into two and three dimensional models (Table 2.4). In line source model, the thickness of the lamp in the reactor is neglected while the dimension of the lamp is considered in the extense source model. Among them the simplest one is the linear source emitting in parallel planes (LSPP model). A better approximation to reality is the line source with spherical emission (LSSE model). The three dimensional emission model proposed by Irazoqui et al (1973) is even closer to the actual performance but it requires a more elaborated and time consuming computational work.

In this research only LSSE and ESVE models will be considered since they had been found to predict reasonably accurately the radiation flux profiles in an

annular reactor when there is no dispersion or absorption effect (Irazoqui et al, 1973; Jacob and Dranoff, 1970). In addition, the ESVE model appears to be the best available representation for a UV arc source.

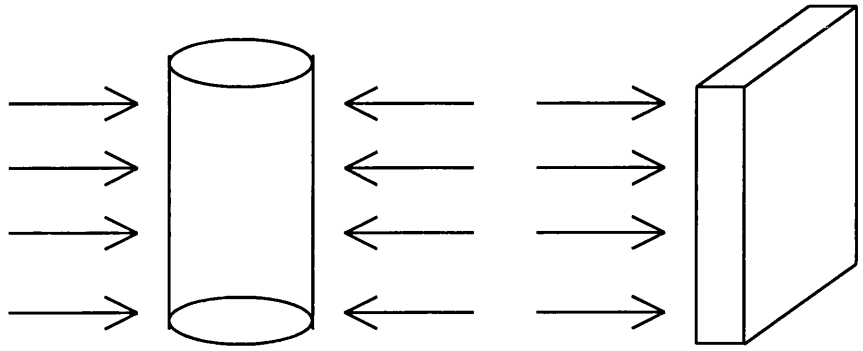

(a) Cylindrical (tubular) (b) Parallel plate

Fig.2.4 Cylindrical and Parallel Plate Photoreactors

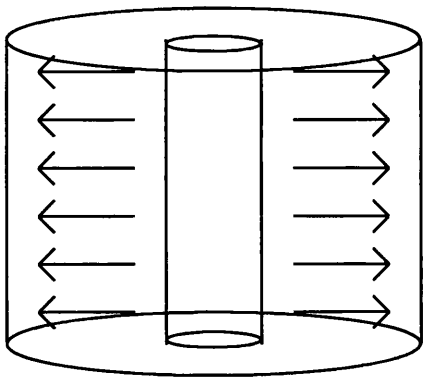

Fig.2.5 Annular Photoreactor

TABLE 2.4 Main Source Emission Models (Alfano et al, 1986)

Source Characteristic	Emission Characteristic		Model Name	Authors
Line source	Parallel planes perpendicular to the lamp axis	2-dimensional propagation of rays	LSSP	Harris and Dranoff (1965)
	Spherical and isotropic	3-dimensional propagation of rays	LSSE	Jacob and Dranoff (1966)
Extense source	Volumetric source	3-dimensional	ESVE	Irazoqui et al (1973)
	Superficial source	3-dimensional	ESSE	Stramigioli et al (1977)

2.2.1 LSSE Model (Cassano et al, 1986)

The Line Source with Spherical Emission (LSSE) Model allows a reasonably good analysis of the radiant energy distribution within the reaction space with the object of predicting with the source placed at its axis. Basically, the model assumes the lamp as a lone source where each one of its points emits radiation in every direction and isotropically, i.e. source is made up of a finite number of segments ("points" source), whose contribution are later added up in order to calculate the radiant energy distribution within the reactor.

The specific intensity can be written as :

$$I_o'' \, d\upsilon = \frac{dE_\upsilon}{dz \, d\Omega} \qquad ...(2.42)$$

and since

$$|dq_\upsilon| = \frac{dE_\upsilon}{dA \cos\theta_n} \qquad ...(2.43)$$

$\therefore$

$$|dq_\upsilon| = \frac{I_\upsilon'' \, d\upsilon \, dz}{\rho^2} \qquad ...(2.44)$$

Rearranging and using Lambert's equation :

$$\frac{1}{\rho^2} \frac{d(|q_\upsilon|\rho^2)}{d\rho} = -\mu |dq_\upsilon| \qquad ...(2.45)$$

Integrating through the optical path and using Eqn.2.42 and Eqn.2.43 gives :

$$|dq_\upsilon| = \frac{dE_{\upsilon,o}}{4\pi L_L} \frac{dz}{\rho^2} \exp\left(-\int_{\rho_o}^{\rho} \mu_\upsilon \, d\rho^*\right) \qquad ...(2.46)$$

Integration along lamp length :

$$|dq_\upsilon| = \frac{dE_{\upsilon,o}}{4\pi L_L} \int_0^{L_L} \frac{1}{\rho^2} \exp\left(-\int_{\rho_o}^{\rho} \mu_\upsilon \, d\rho^*\right) dz \qquad ...(2.47)$$

and since $de_\upsilon^a = \mu_\upsilon |dq_\upsilon|$ ...(2.48)

by substituting Eqn.2.45 and integrating over all wavelengths gives local volumetric rate of energy absorption (LVREA) :

$$e^a = \int_{\upsilon=0}^{\upsilon=\infty} \mu_\upsilon \frac{dE_{\upsilon,o}}{4\pi L_L} \int_0^{L_L} \frac{1}{\rho^2} \exp\left(-\int_{\rho_o}^{\rho} \mu_\upsilon \, d\rho^*\right) dz \qquad ...(2.49)$$

2.2.2 **ESVE Model** (Irazoqui et al, 1973)

Whereas the previous model simplified the geometry of the emission of the light source, this model will take into account this geometry. The Extense Source with Volumetric Emission (ESVE) Model is based on the following assumptions about emission :

(i) The emitters of the radiation source are uniformly distributed inside its volume,

(ii) Each elementary volume inside the source has an isotropic emission. That means the specific intensity associated with each bundle of radiation coming from the same element of volume is independent of direction,

(iii) Any elemental volume inside the source emits, at any frequency, an amount of energy proportional to its extension,

(iv) The energy emitted from any elementary volume of the lamp is due to spontaneous emission, and each of these differential volumes is transparent to the emission of its surroundings.

Assumptions about the source are :

(i) The lamp is a perfect cylinder, bounded by mathematical surfaces with zero thickness. Thus any bundle of radiation coming from inside does not change its intensity or direction when it crosses this boundary,

(ii) The lamp is long enough and is adequately masked to neglect end effects. That means the emission characteristics are constant along the z-direction (see Fig.2.9 and Fig.2.10; this assumption does not say anything about the radiation field along the z-direction).

Assumptions about the reactor :

(i) The reactor is bounded by two concentric cylindrical mathematical surfaces without thickness. That means no refraction or absorption occurs at any of the walls of the reactor,

(ii) The reactor is filled with a transparent fluid. That means no absorption occurs inside the reaction vessel.

(iii) The opaque zones at the top and bottom parts of the reactor do no reflect or emit radiation.

Fig.2.9 and Fig.2.10 shows the geometrical variables of the model.

From the assumptions about the source the rate of energy emission by an elementary volume at frequency υ may be represented by :

$$dE_{\upsilon} = N_e P_{\upsilon} h\upsilon \; dV \, d\upsilon \qquad ...(2.50)$$

where N_e = number of emitters per unit volume of source

P_{υ} = probability of emission at a given frequency

From assumption about the emission, the energy emitted in a solid angle about a given direction is :

$$dE_{\upsilon,W} = \frac{N_e P_{\upsilon} h\upsilon}{4\pi} \, d\upsilon \, dV \, d\Omega \qquad ...(2.51)$$

which can be written, for a θ,ϕ direction as :

$$dE_{\upsilon,\theta,\phi} = \frac{N_e P_\upsilon h\upsilon}{4\pi} \sin\theta \cos\phi_n \, d\theta \, d\phi \, d\rho \, dA \, d\upsilon \qquad ...(2.52)$$

The specific intensity is defined by :

$$dE_{\upsilon,\theta,\phi} = dI_\upsilon \sin\theta \cos\phi_n \, d\theta \, d\phi \, dA \, d\upsilon \qquad ...(2.53)$$

which for the isotropic emission of the differential volume of source at frequency ν gives a specific intensity equal to :

$$dI_\upsilon = \frac{N_e P_\upsilon h\upsilon}{4\pi} \, d\rho \qquad ...(2.54)$$

At any point in space (z, r), the radiation flux density coming from the elementary volume dV with direction θ,ϕ, and for the whole range of frequencies, is given by :

$$dq(\theta,\phi,\rho)\big|_{r,z} = \kappa \sin\theta \cos\theta_n \, d\theta \, d\phi \, d\rho \qquad ...(2.55)$$

where

$$\kappa = \int_{\upsilon=0}^{\upsilon=\infty} \frac{N_e P_\upsilon h\upsilon}{4\pi} \, d\upsilon \qquad ...(2.56)$$

is a property of the radiation source and its operating conditions.

The total energy per unit area and unit time impinging on the differential area at the point (z, r), from all directions in space and from the whole volume of the lamp, can be obtained by proper integration of Eqn.2.55. Substituting $\cos\theta_n = \cos\phi\sin\theta$, and performing the integration :

$$q_\lambda = \kappa \int_\phi \int_\theta \int_\rho \sin^2\theta \cos\phi \, d\rho \, d\theta \, d\phi \qquad ...(2.57)$$

For annular reactor the limits for the variables θ, ϕ and ρ are :

$$\rho_{1,2} = \frac{r\cos\phi \mp (r^2\cos^2\phi - r^2 + r_L^2)^{1/2}}{\sin\theta} \qquad ...(2.58)$$

$$\theta_1(\phi) = \tan^{-1}\left[\frac{r\cos\phi - (r^2\cos^2\phi - r^2 + r_L^2)^{1/2}}{L - z}\right] \qquad ...(2.59)$$

$$\theta_2(\phi) = \tan^{-1}\left[\frac{r\cos\phi - (r^2\cos^2\phi - r^2 + r_L^2)^{1/2}}{-z}\right] \qquad ...(2.60)$$

$$-\phi_1 = \phi_2 = \cos^{-1}\left[\frac{\left(r^2 - r_L^2\right)^{1/2}}{r}\right] \qquad ...(2.61)$$

where r_L is the lamp radius. Integrating Eqn.2.57 with respect to ρ gives

$$q_\lambda = 2\kappa \int_\phi \int_\theta \sin\theta \cos\phi \left[r^2 \cos^2\phi - r^2 + r_L^2\right]^{1/2} d\theta\, d\phi \qquad ...(2.62)$$

Eqn.2.62 is valid for an empty reactor. If an absorbing medium is present, the rays will be attenuated according to Lambert's equation. Hence for an annular reactor filled with absorbing medium the energy flux density vector becomes

$$q_\lambda = 2\kappa \int_\phi \int_\theta \sin\theta \cos\phi \left[r^2 \cos^2\phi - r^2 + r_L^2\right]^{1/2} \left[\exp(-\mu\rho)\right] d\theta\, d\phi \qquad ...(2.63)$$

And applying Eqn.2.48 the LVREA is then calculated by :

$$e^a = \int_\lambda \mu_\lambda q_\lambda \qquad ...(2.64)$$

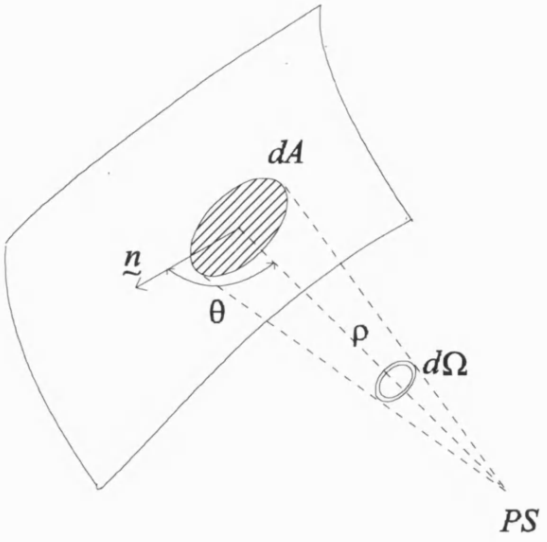

Fig. 2.6 Geometric Representation of the Point Source Model

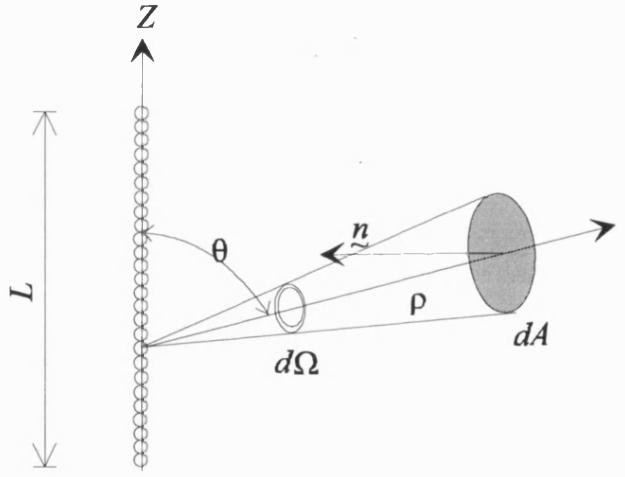

Fig. 2.7 Geometric Representation of the LSSE Model

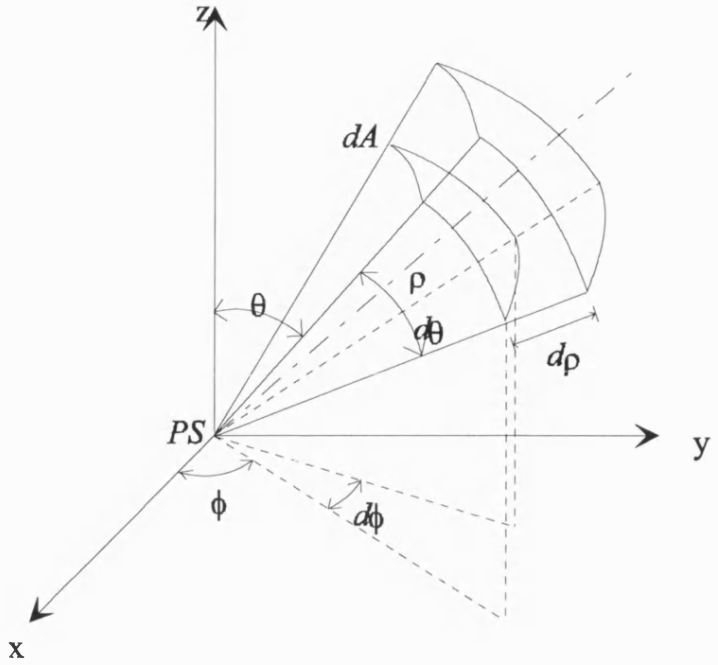

Fig. 2.8 Radiation Balance for Point Sources

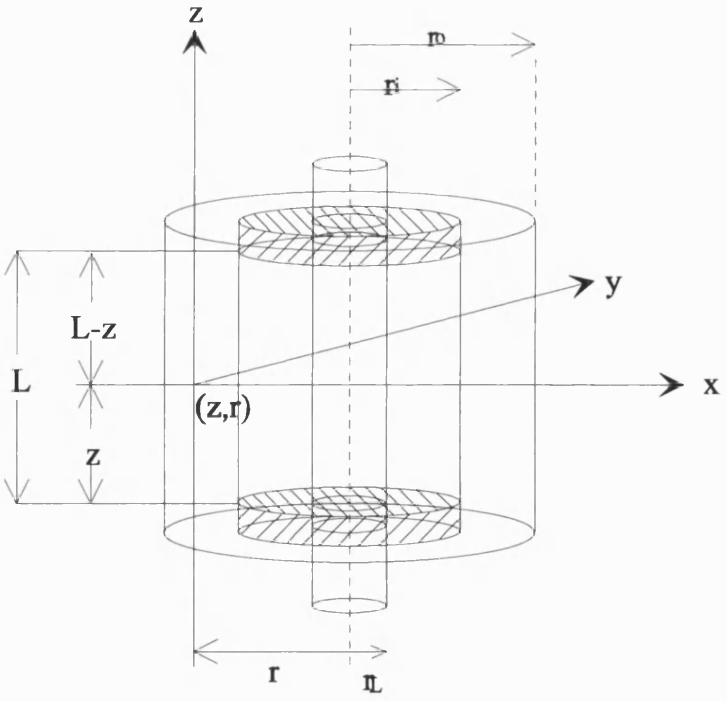

Fig.2.9 Photoreactor Geometry

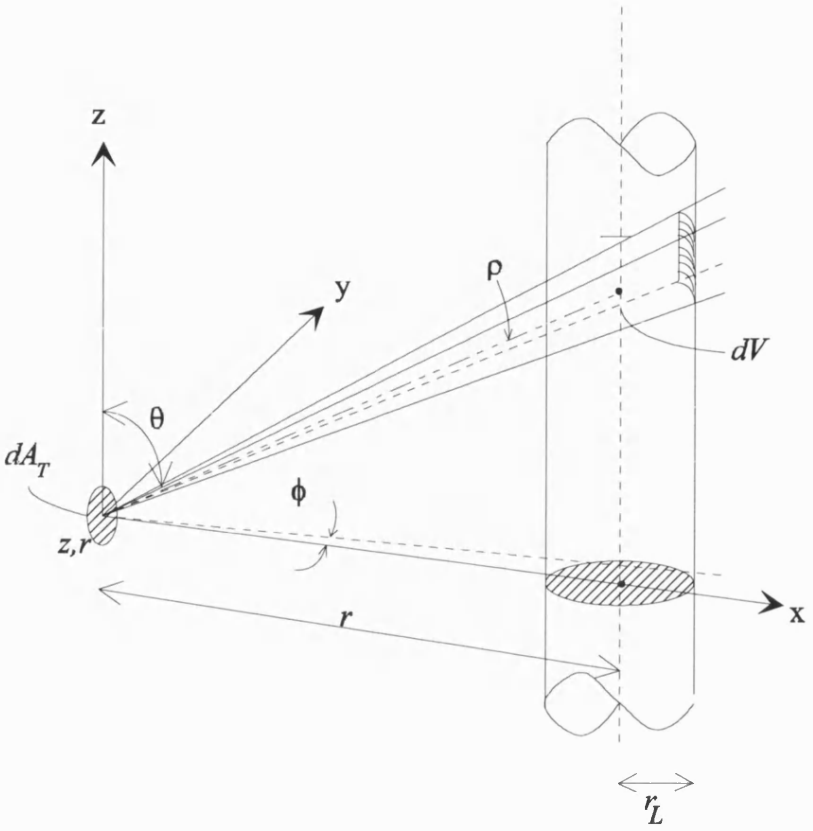

Fig. 2.10 Variables Involved in the Theoretical Analysis

CHAPTER 3
PHOTOCHEMICAL REACTORS AND EXPERIMENTAL PROCEDURES

Many types of photochemical reactors have been used in industry and for research. The main differences are in the geometry with relation to the light source. The geometrical configuration of a photoreactor is usually chosen to maximise the benefits of the pattern of irradiation from the UV lamp. The photoreactors can be categorised into three main types : cylindrical (or tubular), parallel plate and annular. Of these three classes, annular photoreactors are an excellent approach to what is, perhaps, the most practical type of photochemical reactor to be used for commercial purposes (Cassano et al, 1986). The utilisation of energy can be the maximised and, moreover, they accurately represent the common case of a reaction vessel with a tubular lamp placed at its axis by means of an immersion well. Therefore the annular photoreactor was the natural choice to be used in this research project. This chapter will described all the photoreactors and the procedures used in this research.

3.1 Low Pressure UV Lamp Batch Reactor

In the early stages of the research a low pressure UV lamp batch reactor was used to study the photo-degradation of citric acid. It is shown in Fig.3.1 with its dimensions.

The batch reactor is made from Pyrex with a quartz immersion well mounted coaxially for the low pressure UV lamp. It has a volume of 2.5 litres and is 0.74 m long with outer diameter of 0.1 m. While the immersion well has a length of 0.615 m and diameter of 0.035 m. There are 2 ports on the top of the reactor to remove waste gases for incineration and introducing reactant solution into the reactor. Another port

is present on the side of the reactor for withdrawing samples. In addition, there is a sparging disc at the base of the reactor for sparging ozone or helium into the reactor, to create a well mixed environment.

The low pressure UV lamp is rated at 16 W power consumption with UV output at 254 nm. The lamp is 43 cm long with an arc length of 41 cm. From the results of actinometric experiments, the photon energy emitted by the lamp was found to be 10 μein/s. To minimise operator exposure to the UV light, the reactor was wrapped up with a sheet of aluminium foil.

All citric acid solutions used in the experiments were prepared from analytical grade reagent from Merck Ltd, UK. and ultra high quality (UHQ) water. Where ferric salt was to be used in the experiments, it was introduced into the reactor together with the citric acid solution. A stream of nitrogen gas was sparged for about 5 seconds into the reactor and a sample was taken from the homogenised solution in the reactor. The low pressure UV lamp was switched on. After 5 minutes, another sample was taken as hydrogen peroxide solution was introduced into the reactor or as the ozone generator was switched on and was sparged into the reactor. If both hydrogen peroxide and ozone were to be used in the experiment then the ozone generator was switched on after hydrogen peroxide solution was introduced into the reactor. Samples were then withdrawn from the reactor every 10 minutes, for run time of one hour. All the samples were immediately filtered into vials for HPLC analysis of citric acid, while the rest were used for analysis of TOC content.

3.2 Medium Pressure UV Lamp Batch Reactor

The shape and dimension of the reactor are as shown in Fig.3.2. The reactor has a quartz immersion well with a cooling jacket mounted coaxially along the axis of the reactor. The total reactor volume of about 1.25 litres and it is 25 cm long with an outer diameter of 10 cm. The immersion well with cooling jacket has an internal

diameter of 3.5 cm and outer diameter of 5.5 cm. There is a port near the middle of the reactor for withdrawing samples, and 2 further ports at the top to remove waste gases for incineration or for introducing solutions. In addition inert gases such as nitrogen can be introduced into the reactor via a fritted disc sparger at the bottom of the reactor. The medium pressure mercury arc lamp is 16 cm long with an arc length of 11 cm. It has a nominal power rating of 250 W. When UV lamp of higher power rating of 475W and 600W are used, the cooling jacket is used for more efficient cooling of the lamp and the reacting medium.

The procedures for carrying out experiments in this reactor are almost identical to those for the low pressure UV lamp batch reactor. Citric acid solutions were prepared from UHQ water and introduced into the reactor before the UV lamp is switched on. Nitrogen gas was then sparged into the reactor, followed by the simultaneous introduction of ready weighed ferric salt, and a measured volume of hydrogen peroxide. As soon as the solution in the reactor was well mixed and homogenised (in about 5 seconds) the nitrogen gas was turned off. Samples were withdrawn from the reactor every 2 minutes for the first 10 minutes and then every 10 minutes until the end of the experiment. All samples were immediately prepared for HPLC analysis of citric acid and determination of TOC and hydrogen peroxide content, to minimise the effects of any continued decomposition.

3.3 Pilot Plant Reactor

Several experiments were carried out on the pilot plant reactor for the purpose of testing the accuracy of the model produce by the medium and high pressure UV lamp batch reactors. The pilot plant reactor consists of an immersion well mounted coaxially along the axis of the reactor, a reservoir, a reverse osmosis (ROS) unit, a softener and pumps. The reactor has a diameter of 15.92 cm and a height of 113 cm. The immersion well has an internal diameter of 4.2 cm and has a small glass tube

running along its length for introducing nitrogen-air gas to cool the UV lamp. The reservoir has the same diameter as the reactor and a height of 210 cm. The high pressure UV lamp is 116 cm long with an arc length of 106 cm. The lamp has a nominal power rating of 3 kW. A schematic diagram of this plant is as shown in Fig.3.3. The reactor, reservoir and the piping are made of thick pyrex glass, while the gas cooled inner tube of the reactor is made of quartz. The total volume of the pilot plant is about 268 litres. However only 138 litres of the volume is used due to the limited budget available for the chemicals required.

The procedures for experiments with this reactor are as follows. The valve leading to the reactor is closed before purified water from ROS unit is pumped into the reservoir tank. Citric acid is prepared with UHQ water and introduced through an opening on the top of the tank. The flow is stopped once the water level in the reservoir has reached the desired level. The pump is switched on to mix well the citric acid solution and recycle through the reactor. The valve is adjusted to desired flow rate and the UV lamp is switched on. Ferric salt and hydrogen peroxide solution are then introduced simultaneously through the top of the reservoir tank. A stop clock is started and the first sample is taken. Consecutive samples are taken every minute for the first 10 minutes and then every 2 minutes for the next 10 minutes. All the samples were immediately prepared for TOC analysis and hydrogen peroxide determination to minimise the effects of any continued decomposition. After every experiment, the contents in the plant are drained out and purified water from the ROS unit is pumped into the system to clean the plant at least twice.

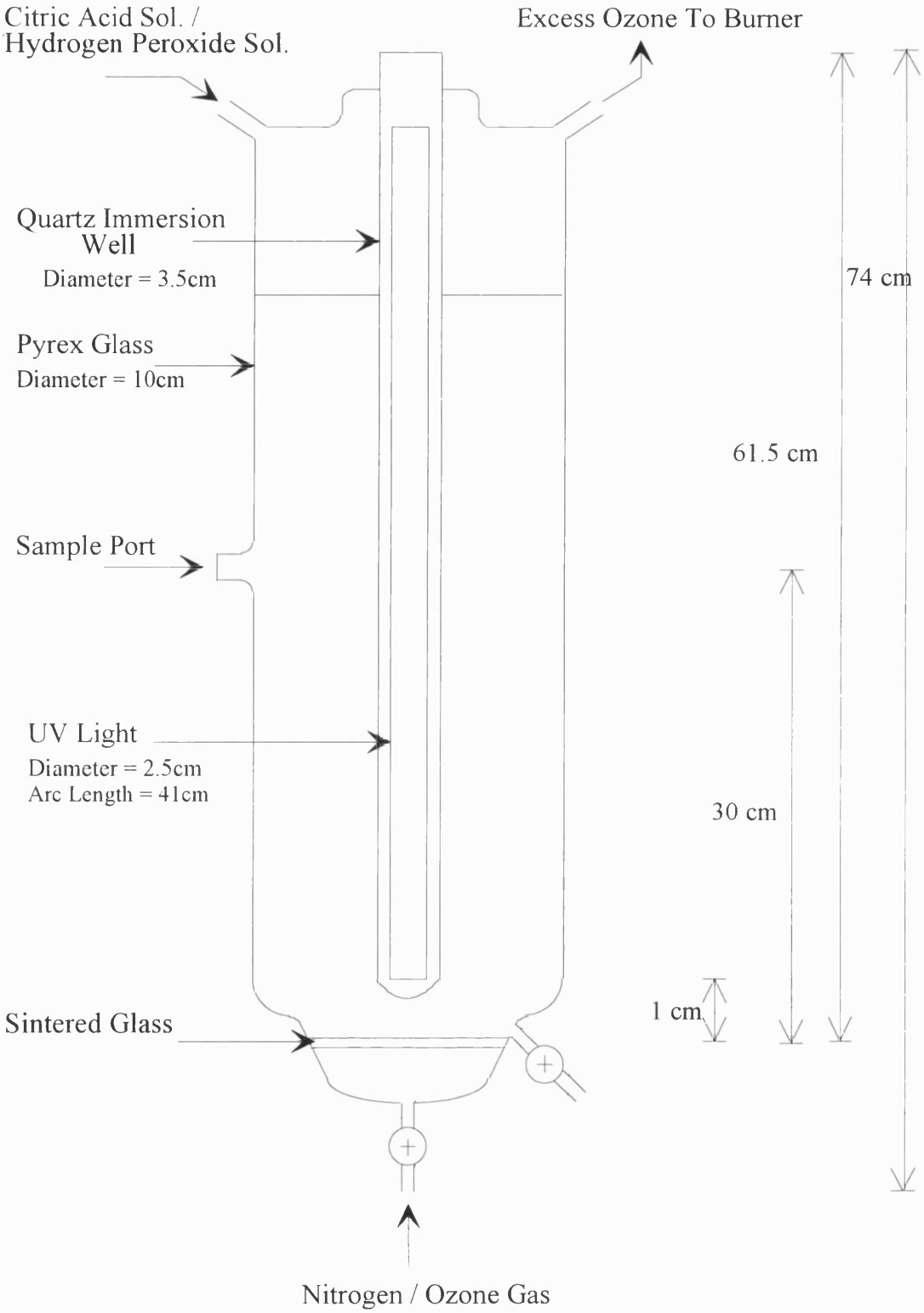

Fig. 3.1 Low Pressure UV Lamp Batch Reactor

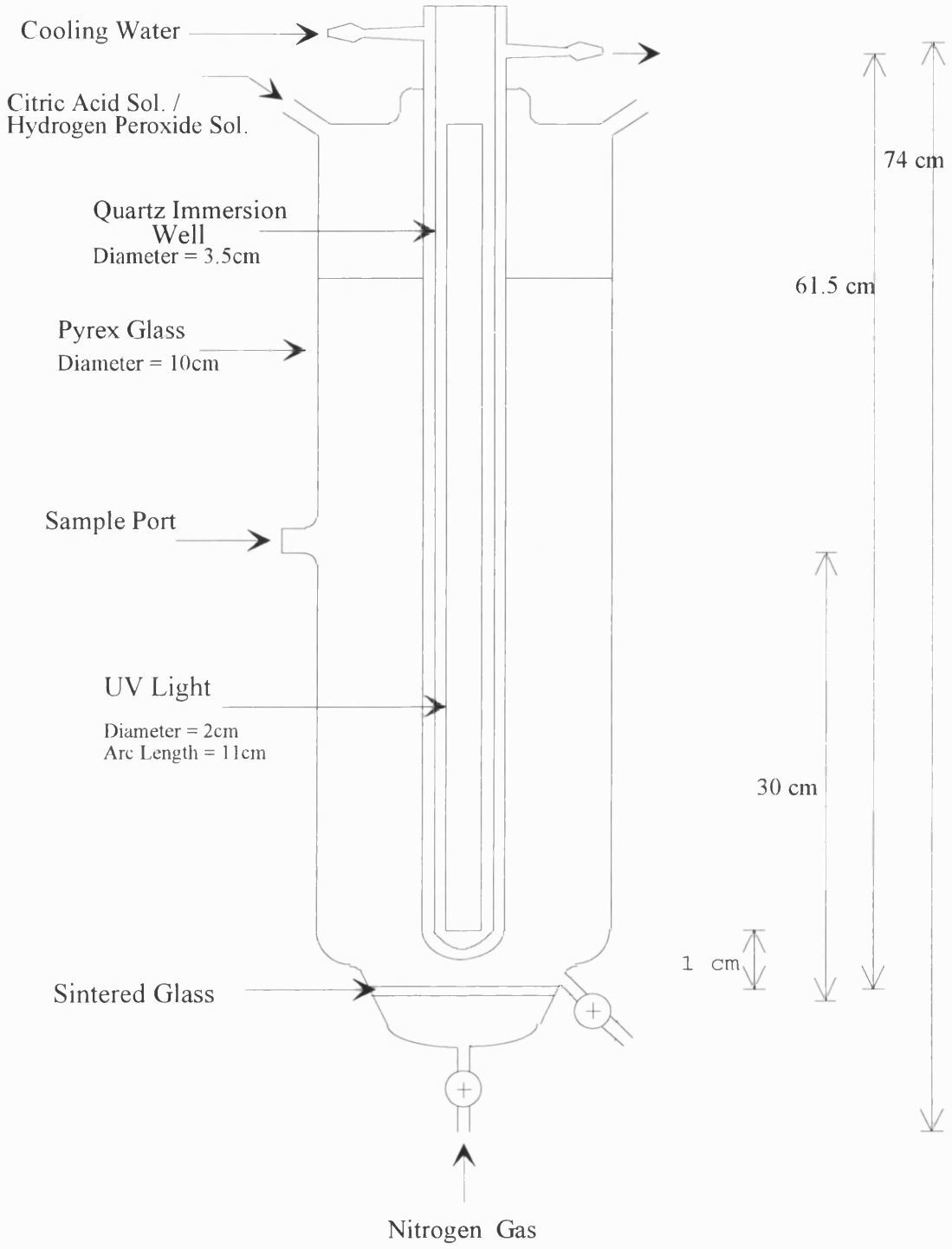

Fig. 3.2 Medium Pressure UV Lamp Batch Reactor

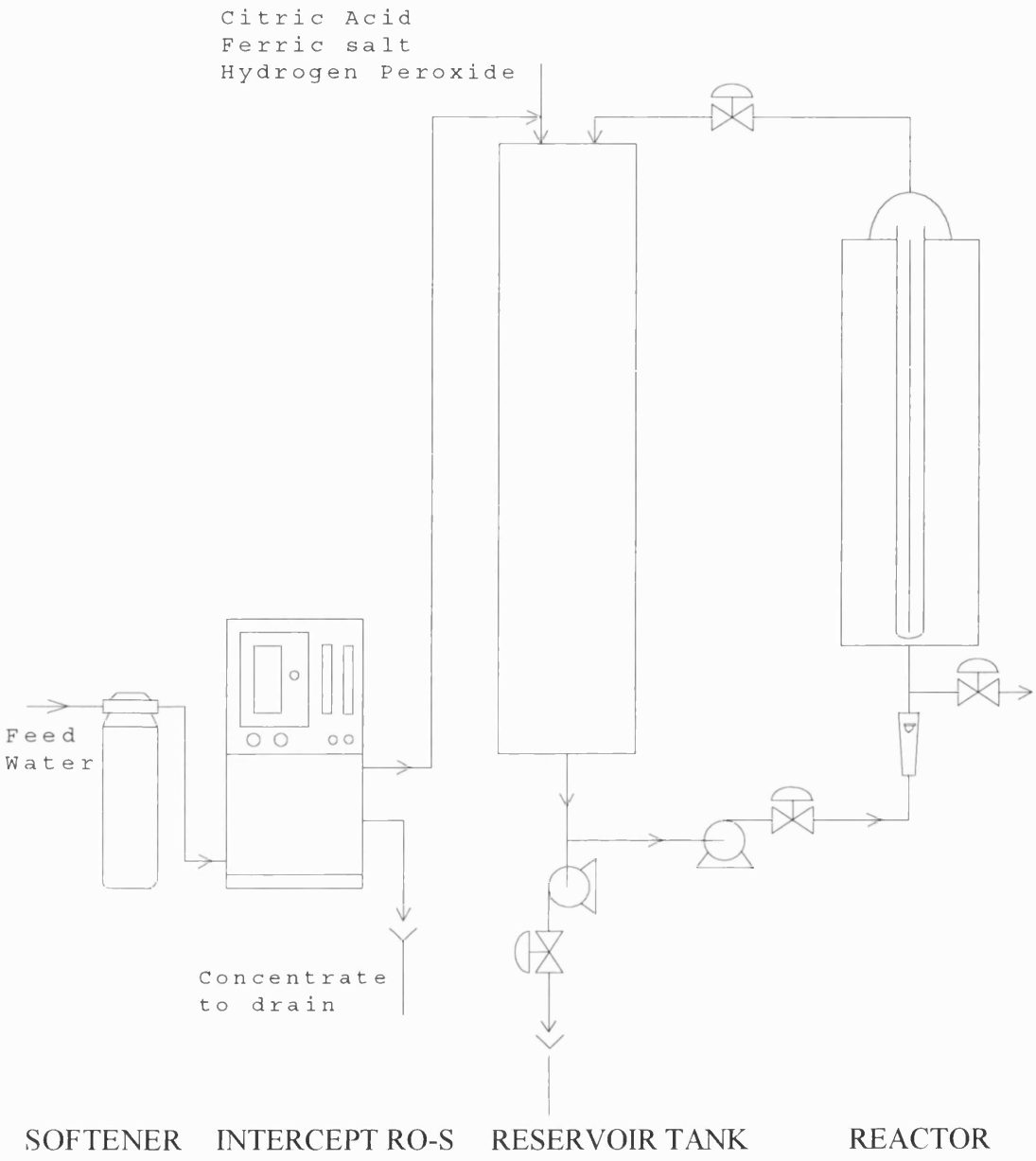

Fig. 3.3 Pilot Plant Reactor

CHAPTER 4
ANALYTICAL METHODS, APPARATUS AND PROCEDURES

This chapter is mainly concerned with the methods used in the determination of citric acid, total organic carbon concentrations and the photon rate in the reactor. The apparatus used and the procedures involved are also described. The determination of the degree of degradation of citric acid and total organic carbon (TOC) were made easier with the help of HPLC and TOC analyzer respectively. An alternative method is described for the determination of citric acid concentration involving gas-liquid chromatography. However this method was not used due to its complexity and time-consuming procedures. The photon rate was determined by actinometric experiment. The specifications of ozone generator, UHQ unit and scanning spectrophotometer are stated. Finally the sources of all the chemicals used are given.

4.1 Determination of Citric Acid

This section will show the two mehods which can be used to analyse and quantify citric acid concentration : the HPLC and GLC method. However only one of them is suitable for the purpose in this research.

4.1.1 HPLC Method

High performance liquid chromatography (HPLC) has been used for separations and determinations of numerous organic compounds, macromolecules and ionic species of biomedical interest, labile natural products and stable compounds. It has many advantages as compared with gas chromatography (GC) : simple operation,

convenient, high precision and high speed analysis. In addition, the reactant and a number of intermediate products can be determined both quantitatively and qualitatively.

Apparatus and Operating Conditions

Gilson Gradient HPLC System is used with a Gilson System Controller. The Gilson HPLC System Controller Software analyzes chromatographic data and controls modules (i.e. pumps, sample injector,injection valve etc) that are connected to the controller by contact input/output. The chromatography was equipped with a 20 µl sample loop, a variable wavelength 116 UV detector and two reciprocating 302' pumps. In addition a microprocessor driven LS-3200 autosampler from SGE is used for repetitive analysis. Column effluents were monitored at detector wavelength of 210 nm for citric acid. Analysis was performed isocratically at room temperature, and quantisation was based on peak height measurements since the peak height is proportional to the concentration of citric acid.

Column

a).A 220 x 4.6 mm i.d. HPLC Polypore H Column (Anachem, U.K.) was used. The column contains macroprous styrene divinylbenzene, an anion exchange resin (10 µm diameter) which separates organic acids by ion exclusion partition chromatography. The mobile phase used was 0.01 N H_2SO_4 and at a flow rate of 0.2 ml/min.

b).A 250 x 4.6 mm i.d. HPLC Sperisorb C_8 Column (Fisions, U.K.) was also used. The column contained porous, bonded spherical silica (5 µm diameter) with a 6% carbon load. It is a reversed phased column suitable for separation of compounds of high and low polarity. The mobile phase used was 0.2 M H_3PO_4 at 0.8 ml/min.

Reagents

The mobile phase 0.01 N H_2SO_4 is prepared by diluting analytical grade 1 N sulphuric acid (Merck Ltd, U.K.) with ultra high quality water. The mobile phase is then filtered through a 0.2 μm membrane filter (Millipore, U.K.) and degassed thoroughly with helium. The mobile phase of 0.2 M H_3PO_4 is prepared by diluting analytical grade concentrated orthophosphoric acid (Merck, U.K.) with ultra high quality water. It is then filtered and degassed as above.

Sample Preparation

Samples collected from the experiments were properly filtered through 0.2 μm membrane filter (Aerodisc 13 CR PTFE, Fisions, U.K.). High concentration samples were first diluted accordingly before introduction into vial bottles for analysis.

4.1.2 Gas-Liquid Chromatography (GLC) (Yue, 1991)

An alternative for determination of citric acid involves gas-liquid chromatography (GLC) after its conversion to the methyl ester with boron trifluoride in methyl alcohol. However this method was not used because of the complexity and time-consuming of the procedures involved. This is a major disadvantage over HPLC which can analyse the experimental samples almost immediately and thus give more accurate result of the actual concentrations of the desire compounds.

This method is applicable over the range 10^{-2} to 10^{-5} M citrate. First of all the acid samples must be neutralised before esterification. Citric acid is then determined by GLC.

Esterification Procedure

1.0 ml of sample is placed into a culture tube. To this, 1.0 ml of internal standard solution[a] and 0.2 ml of 1.0 M sodium hydroxide solution are added. The contents of the tube are mixed by swirling. The tube is then placed in the "Reacti-therm" heating block. The thermostat is then set to 95°C and evaporator needle placed in position over the uncapped tube. A stream of air is passed through the needle and solution in the tube is evaporated to dryness. The tube is removed from the block and cooled to room temperature. 1.0 ml of boron trifluoride-methanol reagent is added and the tube capped tightly. The tube is placed in the heating block and the esterification reaction is allowed to proceed for not less than 90 minutes. The tube is removed from the block and allowed to cool to room temperature. 3.0 ml of 1.0 M phosphate buffer is added along with 1.0 ml of solvent mixture (1:1 mixture of chloroform and dichloromethane). The tube is recapped and the two liquid layers mixed by shaking vigorously. The layers are allowed to separate and the upper aqueous layer is removed and discarded using a pasteur pipette. The tube is recapped and the solvent layer containing the ester is retained for analysis by gas chromatography. The solution is stable for at least one week.

Chromatography

A 10 m long 530 μm diameter HP5 capillary column was used in the oven of HP5890 chromatography. The following parameters were used :

Column flow	:	10 ml / min helium
Split vent flow	:	100 ml / min helium
Detector make up gas flow	:	25 ml / min helium
Detector hydrogen flow	:	35 ml / min
Detector air flow	:	150 ml / min
Oven temperature	:	150°C

[a] Weigh 0.2 g nitrilotriacetic acid (NTA) into a 250 ml beaker. Add 200 ml demin water and a magnetic stirrer bar. Heat and stir the mixture until the NTA dissolves.

Injector temperature	:	220°C
Detector temperature	:	220°C

When conditions are stable, detector flame is lighted. A 10 μm syringe is used to inject about 2 μl of the solvent containing the esterified citric acid into the chromatography. The chromatogram reading on the integrator is then recorded.

Calculation of Results

Calibration graphs were prepared by plotting area ratios for standards against citrate concentrations of the standards. Graphs were then used to calculate citrate concentrations in the samples.

4.2 Determination of TOC

TOC measurements are necessary in environmental monitoring processes as they include all the organic carbon contents present in samples, i.e. parent organics and all intermediate organic carbons formed. This can be done with the help of TOC Analyser or DC-180 Analyser.

TOC Analyser

This is a carbon in water analyser manufactured by Dohrmann to analyse samples for Total Organic Carbon (TOC), Total Carbon (TC), Purgeable Organic Carbon (POC), Non-purgeable Organic Carbon (NPOC), and Inorganic Carbon (IC). It employs an externally linearized non-dispersive infrared detector (Fuji Model 3300 NDIR) for detection of CO_2 products. It is sensitive from 10 ppb through 30000 ppm. A typical sequence involves processing of a sample, delivery to the UV reactor for oxidation and then to the NDIR for measurement of the CO_2 product. The operational procedures are described in the manual.

4.3 Determination of Photon Rate

Actinometry allows determination of the incident photon rate for a system of specific geometry and in a well-defined spectral domain. There are numerous chemical actinomers employed in gaseous and solution phase and the most frequently used actinomers are uranyl oxalate and potassium ferrioxalate (Calvert and Pitts, 1966; Murov, 1973; Rabeck, 1982) for ultraviolet and visible domains.

4.3.1 Uranyl Oxalate Actinometer

Mixing solutions of uranyl sulphate and of oxalic acid produces uranyl oxalate complexes : $UO_2(C_2O_4)_2^{2-}$ and $UO_2C_2O_4$ (Calvert and Pitts, 1966; Heidt et al, 1970; Murov, 1973; Rabeck, 1982). These complexes absorb light in the ultraviolet and they sensitise the decomposition of the oxalate ions according to the overall reaction :

$$H_2C_2O_4 \xrightarrow{h\upsilon} H_2O + CO_2 + CO \qquad ...(4.1)$$

The quantum yield of disappearance of the oxalate ions is of the order of 0.6 between 254 nm and 436 nm (Leigton and Forbes, 1930; Discher et al, 1963). The number of moles of oxalate transformed during the irradiation period is determined by titrating the oxalate actinometric solution before and after irradiation with potassium permanganate :

$$5H_2C_2O_4 + 2KMnO_4 \rightarrow 10CO_2 + 8H_2O + K_2SO_4 + 2MnSO_4 \qquad ...(4.2)$$

4.3.2 Experimental Method

A solution of 10 mol l^{-1} in uranyl sulfate and 5x10 mol l^{-1} oxalic acid is prepared. This solution may be kept for several days under total darkness. Identical

volumes of solution are irradiated for various periods. After irradiation, a 1 cm^3 aliquot from each sample is taken and is treated with a few drops of concentrated H_2SO_4, and titrated with a standard $KMnO_4$ solution (10 mol l^{-1}) until the appearance of the persistent rose-violet colour of the MnO_4^- ions is seen (Braun et al, 1991).

4.3.3 Calculation

The line slope a, which represents the variation of the volume of the added $KMnO_4$ solution as a function time, is determined. The number of molecules of oxalate transformed per unit time is given by (Braun et al, 1991) :

$$\Delta n_{Ac} = \frac{N\,a\,\mathrm{N}}{2}$$

where N is the normality of the titrated $KMnO_4$ solution ($2x10^{-3}$ mol l^{-1}). The incident photon rate is calculated according to :

$$P_{0,\lambda} = \frac{\Delta n_{Ac}}{\phi_{Ac,\lambda}\, t}$$

4.4 The Elgastat UHQ (Ultra High Quality) Unit

All the standard solutions, the mobile phase for high performance liquid chromatography etc., used in the experiments are produced by this unit. It involves five purification technologies : reverse osmosis, adsorption, deionisation, microfiltration and photo-oxidation. The contents of the reservoir (feedwater) are 'processed' up to the 'ultra high quality' level during the course of a pretimed period (approximately 30 minutes) of continuous recirculation.

The purity of the water is as follows :

Internal Standards	ASTM, CAP and NCCLS Type 1
Inorganics	18 megaohm - cm Resistivity at 25°C
Organics	< 0.0001 Au at 254 nm

T.O.C	20 - 50 ppb
Bacteria	< 1 CFU / ml
Particles	0.2 μm absolute filtration

4.5 Ozone Generator

Ozone is generated by a Triozgen Ozone 2 Generator (Barr & Wray Ltd). It is able to produce ozone in high concentrations and volume by utilising the high voltage corona discharge method. The generator has been calibrated using different oxygen feedrates as shown below :

TABLE 4.1 Ozone Rate Produced by Corresponding Oxygen Feedrate Into the Generator.

Oxygen / l min^{-1}	Ozone / mg min^{-1}
2	38.81
4	64.50
6	92.82
8	111.27
10	130.00

4.6 UV Scanning Spectrophotometer

The UV scanning spectrophotometer CE3040, 3000 series (Cecil, U.K.) is used to determine the absorbances of solution at different wavelength of UV light. It can also produce a scan of the absorbance of a solution over a range of wavelength of UV light. It has the following specification :

-wavelength precision of 0.1 nm

-less than 0.01% straylight

-allowing measurements up to 3 Absorbance

-a stability of ±0.001A per hour

-scan speed up to 4000 nm/min

4.7 Chemical Reagents

All chemicals used were of analytical reagent grade. Citric acid, sulphuric acid (1 N), hydrogen peroxide (30% w/v), ferric nitrate, ferric sulphate pentahydrate, potassium permanganate and ortho-phosphoric acid were obtained from Merck Ltd. Organic solvents required for solid phase extraction and GC-MS analysis, i.e. n-butanol, formic acid, ethyl acetate, bis(trimethylsilyl) trifluoracetamide, and trimethylchlorosilane, were obtained from Sigma Chemical Company Ltd., U. K.

CHAPTER 5
CHOICE OF SYSTEM

From this point onwards all experimental, computational and analytical work carried out in this research is presented in systematical order, showing all the procedures and methods used to achieve the objectives set out in the introduction.

The literature has shown that different organic compounds are best degraded by specific AOPs. So a section of this research work is the determination of the most efficient AOPs in photo-degradation of citric acid, i.e. the process that could reduce TOC and citric acid concentration to the lowest level in the shortest time. Information from the literature (see Sec.2.1.4) has indicated the 'superiority' of UV/H_2O_2/Fe^{3+} type of process over the others AOPs in degrading some organic compounds. This chapter will show that this is also true when applied to citric acid.

The following sections will show preliminary studies carried out using a low pressure UV lamp to determine the effectiveness of different AOPs in degrading citric acid. The results indicate that the UV/H_2O_2/Fe^{3+} process is more effective than other AOPs in degrading citric acid. A more detailed study is then presented using medium pressure lamp and different reaction conditions which confirm the results from the preliminary studies. An alternative Fe^{3+} salt is used to investigate any improvement in the degradation result. Specific problems encountered in these studies and the methods used to solve them are described. A conclusion was then made upon the results obtained from these studies. Finally, the last section will deal with the experimental strategy for the later chapters. The actual reaction conditions to be used in the future experiments are described.

5.1 Preliminary Studies

In the initial stage, experiments with a low pressure UV lamp batch reactor were used to study the photo-degradation of citric acid before proceeding into a more detailed study using a medium pressure UV lamp batch reactor. Ferric nitrate is used as the Fe^{3+} salt.

5.1.1 Aims

All the AOPs mentioned in Chapter 2, i.e. UV/O_3, UV/H_2O_2, O_3/H_2O_2 and $UV/H_2O_2/Fe^{3+}$, are used in photo-degradation of citric acid to determine the most effective AOPs for this application.

5.1.2 Reaction Conditions

The concentration of citric acid used throughout the experiments was 6000 ppm. This was chosen to reflect the concentration of citric acid apparent in the effluent discharge from industry (Yue, 1991). The concentrations of hydrogen peroxide used were 1.0% and 5%v/v and that of ferric nitrate were 0.001 and 0.01 mol/l. Concentrations lower than these would incur measurements errors while the upper limit on concentration was purely a convenient choice. The amount of ozone used was kept at 38.81 mg/min (corresponding to an oxygen flowrate of 2 l/min into the ozone reactor, see Table 4.1), since a previous worker in Bath University, Chemical Engineering Department (Pervez, 1992) has shown that increasing the flowrate of ozone does not further affect its mass transfer rate since water is saturated with ozone.

All the experiments were carried out for an hour and sample were taken every 10 minutes.

5.1.3 Experimental Results

The results are plotted in Fig.5.1 to Fig.5.9 corresponding to Exp.5.1 to Exp.5.9 and are summarised in Table 5.1. The figures are plotted in terms of initial concentrations of TOC and citric acid.

As can be seen from the results, among the AOPs (UV/O_3, UV/H_2O_2 and O_3/H_2O_2), UV/H_2O_2 and O_3/H_2O_2 processes showed promising results. Results are not improved when more oxidants are used as can be seen in the $UV/O_3/H_2O_2$ process. However the efficiency of the UV/H_2O_2 process is greatly improved by the addition of a small amount of ferric nitrate ($Fe(NO_3)_3.9H_2O$), as can be seen in Table 5.1 between Exp.5.2 and Exp.5.9. The percentage of TOC degradation doubled, and that of citric acid increased approximately seven fold.

Exp.5.7 shows that UV and ferric nitrate by themselves are insufficient to have any significant effect on the degradation of TOC and citric acid. Exp.5.9a proved that the nitrogen gas used for sparging the reactor has no effect on the process at all.

5.2 More Detailed Study With Medium Pressure UV Lamp

5.2.1 Aims

To use higher UV intensity to verify results in the preliminary studies and to study $UV/H_2O_2/Fe^{3+}$ process in more detail. Concentrations of reactants are varied to determine their effect on the degradation of citric acid. Alternative Fe^{3+} salt is used to investigate any improvement in the degradation result. Ferric sulphate pentahydrate ($Fe_2(SO_4)_3.5H_2O$) was tried as the alternative Fe^{3+} salt.

5.2.2 Reaction Conditions

It was decided to increase the concentration of citric acid to 60000 ppm which is a value comparable to certain industrial effluents (Yue, 1991). Also 300 ppm and 2300 ppm of citric acid were specifically used to compared UV/H_2O_2 and UV/H_2O_2/Fe^{3+} processes. Concentrations of hydrogen peroxide, ferric nitrate and ferric sulphate pentahydrate were varied to determine their effect on the process. For hydrogen peroxide the concentrations used were 1.0, 5.0 and 10%v/v; and that of ferric nitrate were 0.001, 0.01, 0.05 and 0.1 mol/l; while ferric sulphate pentahydrate concentrations were 0.01, 0.02 and 0.05 mol/l.

The total reaction time was one hour for each experiments and samples were taken every 10 minutes.

5.2.3 Experimental Results

Results are as plotted in Fig.5.10 to Fig.5.30 corresponding to Exp.5.10 to Exp.5.30 as summarised in Table 5.2.

Again UV/O_3 and UV/H_2O_2 process were repeated to determine if there is any difference in result when UV light intensity is increased. Results from Exp.5.12 and 5.13 proved that UV/H_2O_2 process is still more efficient than UV/O_3 process in the degradation of citric acid. And Exp.5.10 showed that UV light by itself can only degrade a small percentage of the TOC and citric acid. However hydrogen peroxide alone is able to degrade a significant percentage of TOC and citric acid as shown in Exp.5.11.

In the previous section UV/H_2O_2/Ferric nitrate process was shown to be much more efficient than UV/H_2O_2 process. To verify this in medium pressure UV lamp reactor, Exp.5.14, 5.15, 5.16 and 5.17 were carried out. The results were as predicted: TOC and citric acid concentrations were greatly reduced when UV/H_2O_2/Ferric nitrate is used.

For UV/H_2O_2/Ferric nitrate process, Exp.5.18 to 5.22 showed that the efficiency of the process is improved when either or both hydrogen peroxide and ferric nitrate concentrations are increased. However, one cannot increase the amount of oxidant and ferric salt indefinitely as this will cause a sudden violent exothermic reaction, in addition to the large costs involved. Exp.5.22 shows that the concentration of hydrogen peroxide and ferric nitrate used should be less than 10%v/v and 0.1 mol/l respectively to avoid a violent reaction from occurring.

When ferric sulphate pentahydrate $Fe_2(SO_4)_3.5H_2O$ was used instead of ferric nitrate, the degradation proceeded at a greater rate and resulted in almost a doubling of the TOC and citric acid degradation (compare Exp.5.19 and Exp.5.23). Exp.5.24 shows that hydrogen peroxide and ferric sulphate pentahydrate are able to reduce the TOC and citric acid level significantly without the need for UV light.

As with the UV/H_2O_2/Ferric nitrate process increasing the concentration of hydrogen peroxide and/or ferric sulphate pentahydrate (see Exp.5.23, 5.25, 5.26) increases the degradation rate. However, the process also has its limitations; the amount of hydrogen peroxide used has to be less than 5%v/v and that of ferric sulphate pentahydrate is 0.05 mol/l. From personal observations, the reaction is much more exothermic in the $UV/H_2O_2/Fe_2(SO_4)_3.5H_2O$ process than that in the $UV/H_2O_2/Fe(NO_3)_3.9H_2O$ process. Both processes showed violent reactions after 10 to 15 minutes. During this period a large amount of heat is given off by the reaction; and the cooling jacket surrounding the immersion well is not sufficient to remove the heat fast enough. To keep the temperature in the reactor constant through out the experiment the cooling jacket was modified in such a way that the cooling water was able to remove the heat effectively. Another solution is to simply reduce the amount of chemicals used.

Exp.5.27 and Exp.5.28 showed that complete degradation of citric acid can be achieved within a short time for lower initial concentration of citric acid.

Exp.5.29 and Exp.5.30 showed that if hydrogen peroxide is replaced by ozone for the production of hydroxyl radicals, the process become less efficient in degradation of citric acid.

Lastly, all results showed that photo-oxidation of citric acid was found to be most effective, especially in the first 10 minutes, after which time the rate of TOC reduction dropped significantly. These observations suggest that the degradation of the parent organic, citric acid, probably occurred in the initial period of 10 minutes. The flatter part of the two oxidation curves is due to the presence of refractory intermediates. The results indicate that the intermediates produced were resistant to oxidation by hydrogen peroxide but were susceptible to oxidation by the hydroxyl radicals, formed by the photolytic process, at a slower rate.

5.3 Problems

Problems arise when one tries to analyse the samples for citric acid using HPLC with presence of ferric salts. In the case of UV/H_2O_2/Ferric nitrate problems arise when the citric acid concentration is low and the Fe^{3+} salt concentration is high (>0.05 mol/l). This is illustrated in Fig.5.31, 5.32, and 5.33. Fig.5.31 shows the HPLC chromatogram when citric acid alone is in the sample; and with the presence of ferric nitrate shown in Fig.5.32. When concentration of citric acid is decreased and/or concentration of ferric nitrate is increased, then the resultant chromatogram shown in Fig.5.33 is obtained, where the citric acid peak cannot be resolved and thus its concentration determined.

In the case of the UV/H_2O_2/$Fe_3(SO_4)_3.5H_2O$ process, the Fe^{3+} salt itself does not cause any analysis problem with the HPLC chromatogram. However one of the intermediate compounds formed during photo-oxidation of citric acid gives a peak that may interfere with that of the citric acid (see Fig.5.34, 5.35 and 5.36). This depends on the concentration of citric acid and the intermediate compounds formed in the sample.

After consultation with the technical experts from the HPLC suppliers, several methods were tried to solve the problems mentioned above. Firstly, an alternative HPLC column was tried in the hope that it will give better separation of the components in the samples. Secondly, mobile phase concentration was varied (0.01M to 0.1M), even pure UHQ water was tried, in the hope that by varying the pH and ionic strength of the mobile phase the retention time of the components would change, thus giving a better separation result. Thirdly, the temperature of the HPLC column was raised by immersion in a water bath. Temperatures of 35°, 45°, 55° and 65°C were used. In theory, an elevation of temperature leads to a reduction of adsorption and, therefore, to a shorter retention time. Lastly, a combination of the above methods were used. Unfortunately these measures did not give better results.

5.4 Conclusions

Mineralization of citric acid is most effective when a small amount of ferric salt is present in the UV/H_2O_2 process. Among the ferric salts tried, ferric sulphate pentahydrate produced the best results in photodegradation of citric acid. A better part of the photodegradation occurred in the first ten minutes. Since iron salts and hydrogen peroxide exists in the natural environment, the $UV/H_2O_2/Fe^{3+}$ process does not create any secondary pollution.

5.5 Experimental Strategy

An outline of the experimental strategy for the modelling of the kinetic rate expression in later chapters is described in this section. Since it is unlikely to solve the problems stated in Sec.5.3 in the foreseeable future, it was decided to proceed with the research as time constraints were present. As far as rate expression is concerned, the concentration of TOC will be used in its determination instead of citric acid concentration as the TOC is the more important parameter in indicating the 'purity' of

'purity' of the water. Since degradation of the parent organic often produces intermediates which may be very stable and refractory to further degradation. The TOC concentration includes all organic carbon species present in the sample and hence provided a measure of the degree of mineralization rather than the degradation of the parent organic. Thus the kinetic expression to be modelled is the mineralization rate of the process. The UV/H_2O_2/Ferric sulphate pentahydrate process is the natural choice for more detailed studies and modelling of the photo-oxidation of citric acid.

For the purposes of modelling the rate equation, experiments are planned with varying concentrations of parameters to show the effects of individual and the interaction between parameters. Since there are an excessive number of parameters involved, it was decided to fixed the concentration of the ferric salt and vary the concentrations of citric acid and hydrogen peroxide along with the intensity of the UV light.

The concentration of ferric sulphate pentahydrate was fixed at 0.01 mol/l since experiments in Sec.5.2 have shown it to be adequate and higher concentrations would involve too high a cost when used for pilot plant experiments. The other three parameters would be performed at three different levels. The concentrations of citric acid use are 1500, 2000 and 2500 ppm, since these are the typical concentrations in certain effluents in industry, e.g. nuclear power plant (Yue, 1991), and also because a higher concentration of citric acid (i.e. 60000 ppm) would require a higher amount of hydrogen peroxide, which is very costly. The nominal power of the UV lamps used were 250, 475 and 600W which are fixed at manufacture. The concentrations of hydrogen peroxide to be used are determined in further experiments. For modelling purposes the concentrations of hydrogen peroxide needs to be chosen to give a wide variation in reaction rates. Fig.5.37 and Fig.5.38 show the results of photo-oxidation of citric acid with different concentrations of hydrogen peroxide. The concentrations of hydrogen peroxide used were in term of moles with respect to citric acid. Thus hydrogen peroxide/citric acid moles ratio of 5, 10 and 30 are chosen.

Since most of the reactions occur in the first ten minutes, experiments are focussed on the first few minutes.

Table 5.1 Experimental Results From Low Pressure UV Lamp Batch Reactor

			% Degradation after 1 hour	
Exp.	Process	Initial Citric Acid Conc./ppm	TOC	Citric Acid
5.1	UV/H_2O_2[a]	6000	3	10
5.2	UV/H_2O_2[b]	6000	11	12
5.3	UV/O_3	6000	0	6
5.4	O_3/H_2O_2[b]	6000	18	19
5.5	$UV/O_3/H_2O_2$[a]	6000	4	18
5.6	$UV/O_3/H_2O_2$[b]	6000	9	11
5.7	UV/Ferric nitrate[c]	6000	5	6
5.8	UV/H_2O_2[a]/Ferric nitrate[c]	6000	2	20
5.9	UV/H_2O_2[b]/Ferric nitrate[d]	6000	24	85
5.9a	N_2	6000	0	0

N.B.

a. H_2O_2 ≈ 1.0%v/v
b. H_2O_2 ≈ 5.0%v/v
c. Ferric nitrate ≈ 0.001 mol/l
d. Ferric nitrate ≈ 0.01 mol/l

Table 5.2 Experimental Results From Medium Pressure UV Lamp Batch Reactor

			%Degradation after 1 hour	
Exp.	Process	Initial citric acid conc./ppm	TOC	Citric Acid
5.10	UV	60000	4	5
5.11	H_2O_2[a]	60000	14	14
5.12	UV/O_3	60000	8	10
5.13	UV/H_2O_2[a]	60000	14	20
5.14	UV/H_2O_2[a]	300	8	20
5.15	UV/H_2O_2[a]	2300	15	29
5.16	UV/H_2O_2[a]/Ferric nitrate[d]	300	98	≈100
5.17	UV/H_2O_2[a]/Ferric nitrate[d]	2300	≈100	≈100
5.18	UV/H_2O_2[a]/Ferric nitrate[c]	60000	17	28
5.19	UV/H_2O_2[a]/Ferric nitrate[d]	60000	18	26
5.20	UV/H_2O_2[a]/Ferric nitrate[e]	60000	34	32
5.21	UV/H_2O_2[b]/Ferric nitrate[e]	60000	34	57
5.22	UV/H_2O_2[b]/Ferric nitrate[f]	60000	49*	85*
5.23	UV/H_2O_2[a]/$Fe_2(SO_4)_3.5H_2O$[d]	60000	25	43
5.24	H_2O_2[a]/$Fe_2(SO_4)_3.5H_2O$[d]	60000	19	19
5.25	UV/H_2O_2[a]/$Fe_2(SO_4)_3.5H_2O$[g]	60000	41	50
5.26	UV/H_2O_2[b]/$Fe_2(SO_4)_3.5H_2O$[e]	60000	45*	66*
5.27	UV/H_2O_2[a]/$Fe_2(SO_4)_3.5H_2O$[d]	2300	90	50**
5.28	UV/H_2O_2[a]/$Fe_2(SO_4)_3.5H_2O$[d]	10000	61	67***
5.29	$UV/O_3/Fe_2(SO_4)_3.5H_2O$[d]	60000	8	20
5.30	UV/O_3[h]/$Fe_2(SO_4)_3.5H_2O$[d]	60000	10	20

N.B.

a H_2O_2 ≈ 5.0%v/v
b. H_2O_2 ≈ 10%v/v
c Fe^{3+} salt ≈ 0.001 mol/l
d. Fe^{3+} salt ≈ 0.01 mol/l
e. Fe^{3+} salt ≈ 0.05 mol/l
f. Fe^{3+} salt ≈ 0.1 mol/l
g. Fe^{3+} salt ≈ 0.02 mol/l
h O_3 ≈ 92.82 mol/l

* %Degradation after 20 mins. Experiments was not able to proceed due to run away exothermic reaction.

** %Degradation after 5 mins. Further analysis by HPLC was not possible due to interference from intermediate peak.

*** % Degradation after 40 mins. As **.

Fig 5.1 Photo-oxidation of Citric Acid
UV Light / Hydrogen peroxide (1.0 %v/v)

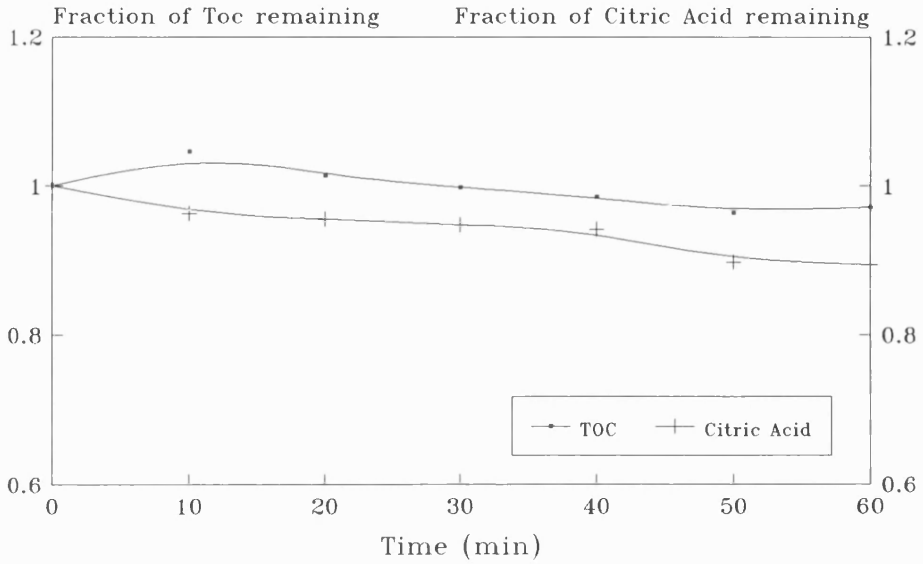

Low Pressure Lamp
Initial TOC ~ 3963 ppmC
Initial Citric Acid ~ 6000 ppm

Fig 5.2 Photo-oxidation of Citric Acid
UV Light / Hydrogen peroxide (5.0 %v/v)

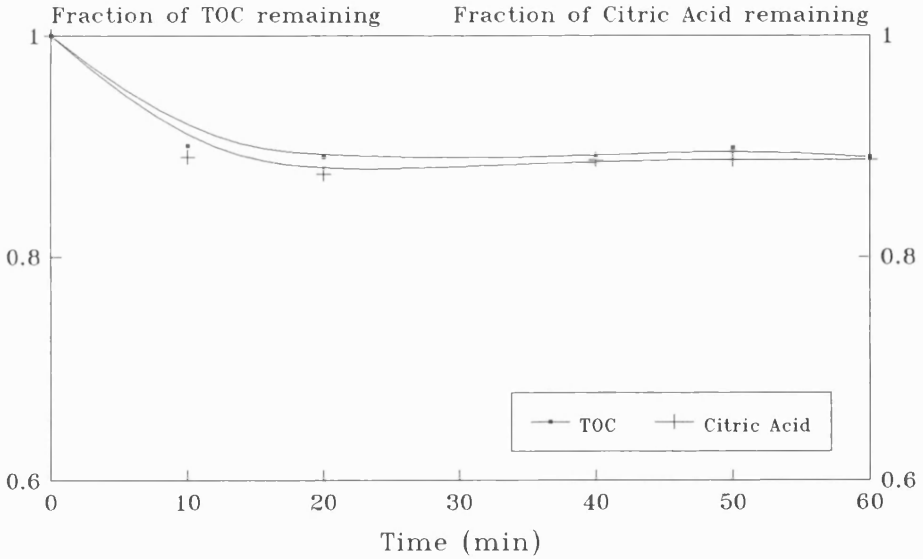

Low Pressure Lamp
Initial TOC ~ 2170 ppmC
Initial Citric Acid ~ 6000 ppm

Fig 5.3 Photo-oxidation of Citric Acid
UV Light / Ozone (38.81 mg/min)

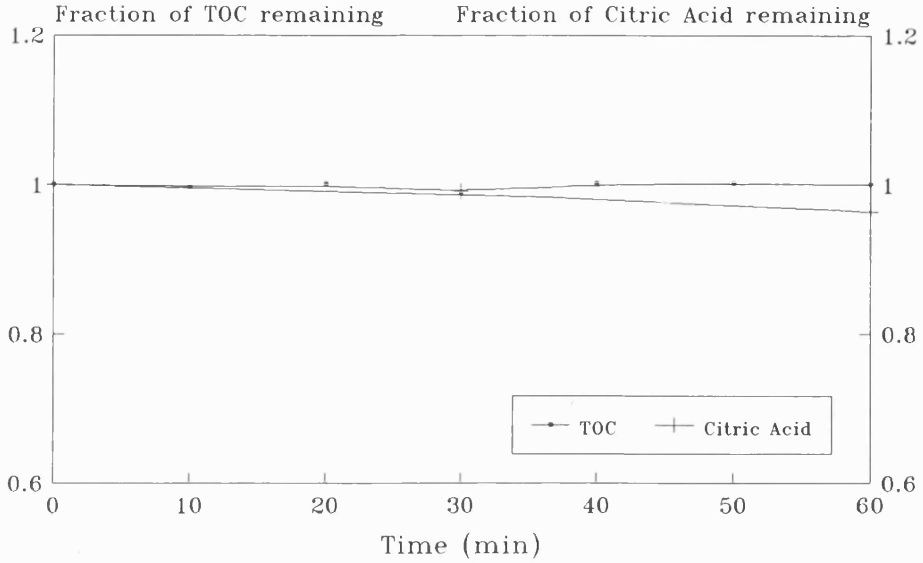

Low Pressure Lamp
Initial TOC ~ 2176 ppmC
Initial Citric Acid ~ 6000 ppm

Fig 5.4 Oxidation of Citric Acid
Ozone / Hydrogen Peroxide (5%v/v)

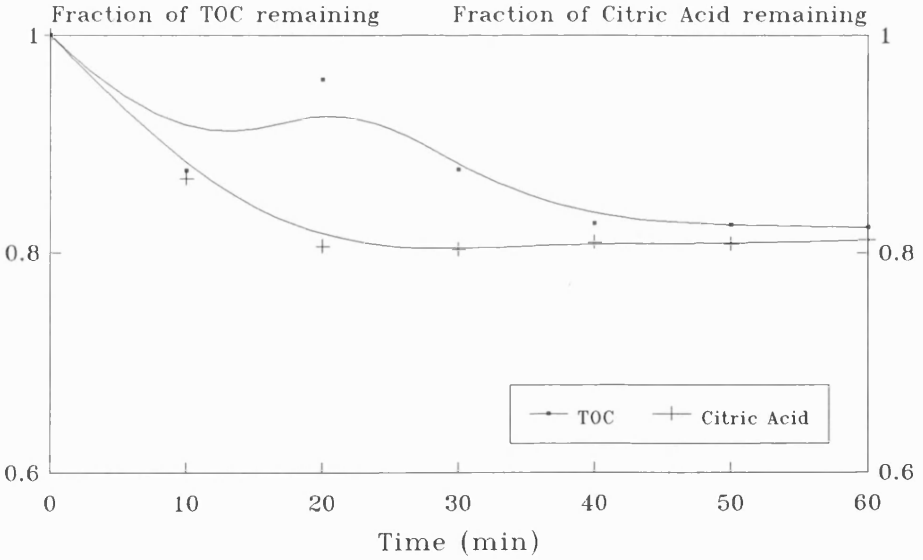

Low Pressure Lamp
Initial TOC ~ 2991 ppmC
Ozone ~ 38.81 mg/min

Fig 5.5 Photo-oxidation of Citric Acid
UV Light / Hydrogen peroxide (1%v/v) /
Ozone (38.81 mg/min)

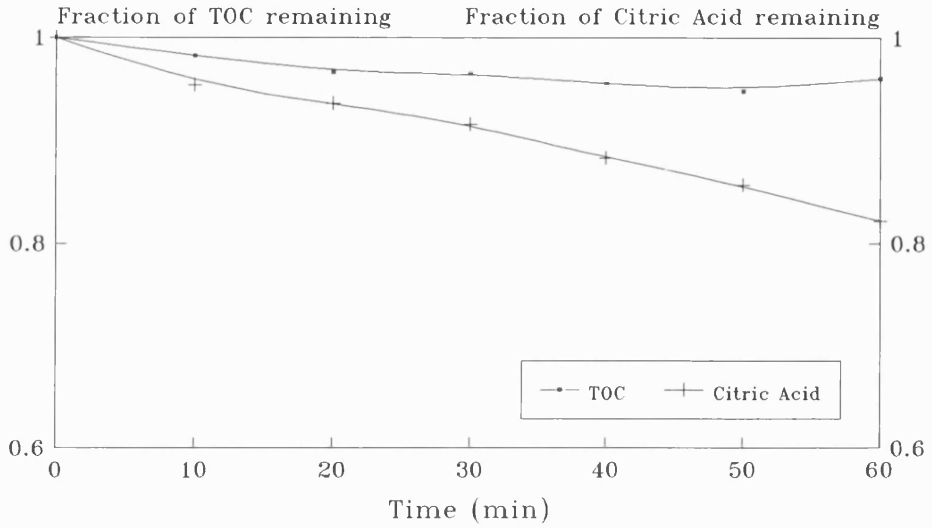

Low Pressure Lamp
Initial TOC ~ 2113 ppmC
Initial Citric Acid ~ 6000 ppm

Fig 5.6 Photo-oxidation of Citric Acid
UV Light/Hydrogen peroxide (5%v/v)/
Ozone (38.81 mg/min)

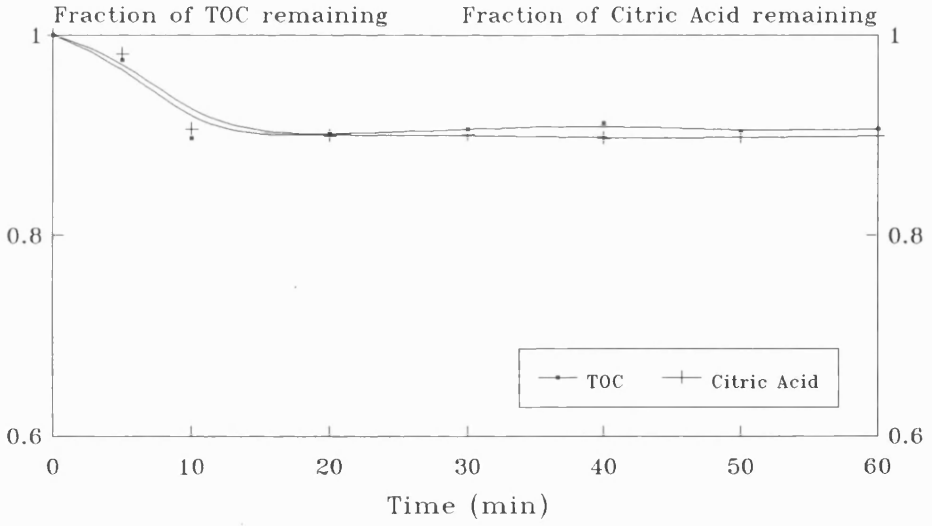

Low Pressure Lamp
Initial TOC ~ 2123 ppmC
Initial Citric Acid ~ 6000 ppm

Fig 5.7 Photo-degradation of Citric Acid
in Presence of Ferric Nitrate(.001mol/l)

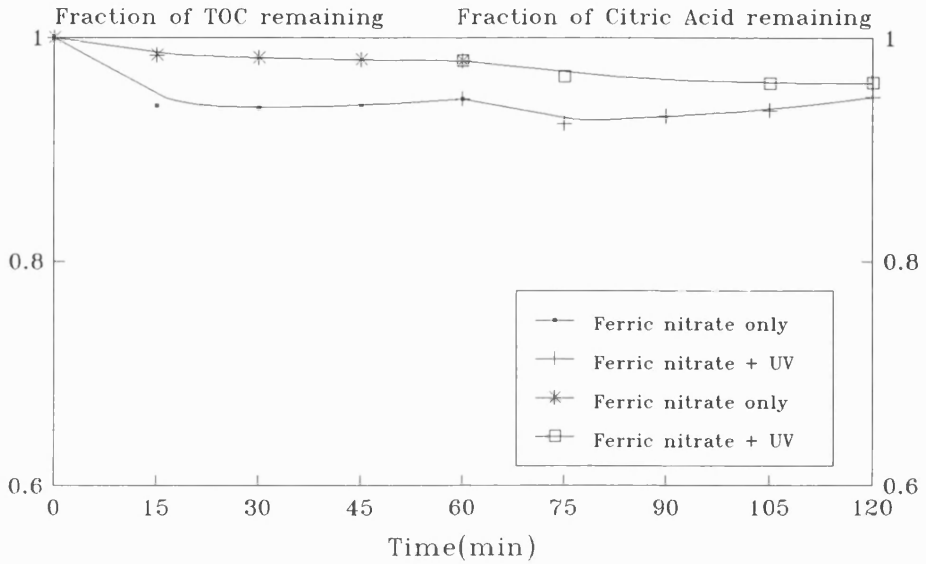

Low Pressure Lamp
Initial TOC ~ 2331 ppmC
Initial Citric Acid ~ 6000 ppm

Fig 5.8 Photo-oxidation of Citric Acid
UV Light/Hydrogen Peroxide (1 %v/v) in
presence of Ferric Nitrate (0.001 mol/l)

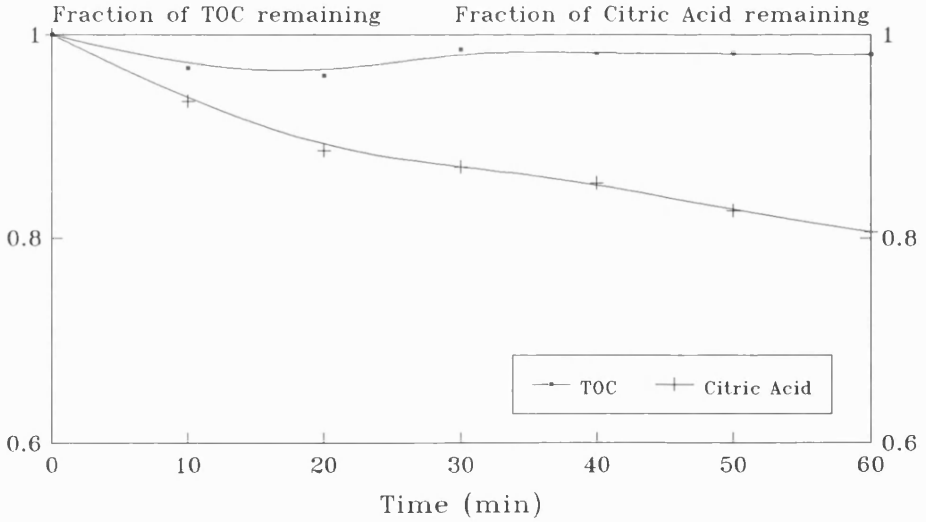

Low Pressure Lamp
Initial TOC ~ 2430 ppmC
Initial Citric Acid ~ 6000 ppm

Fig 5.9 Photo-oxidation of Citric Acid
UV Light/Hydrogen Peroxide (5 % v/v) in
Presence of Ferric Nitrate (0.01mol/l)

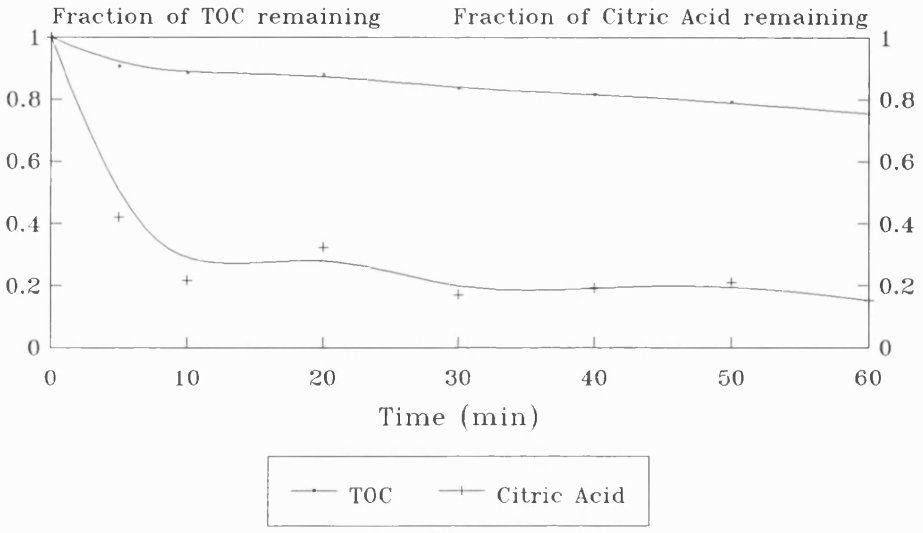

Low Pressure Lamp
Initial TOC ~ 1882 ppmC
Initial Citric Acid ~ 6000 ppm

Fig 5.10 Photo-Degradation of
Citric Acid (UV Light Only)

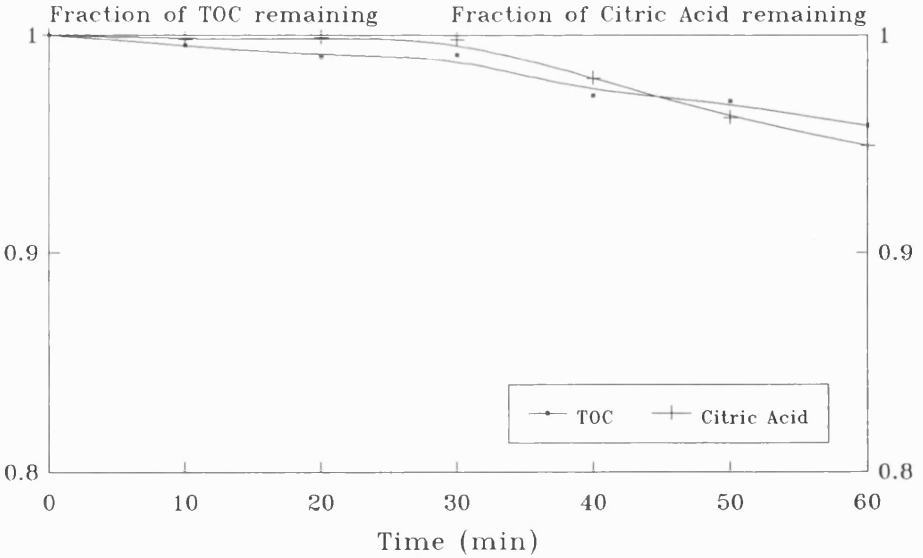

Medium Pressure Lamp
Initial TOC ~ 24528 ppmC
Initial Citric Acid ~ 60000 ppm

Fig 5.11 Oxidation of Citric Acid
Hydrogen Peroxide (5% v/v) only

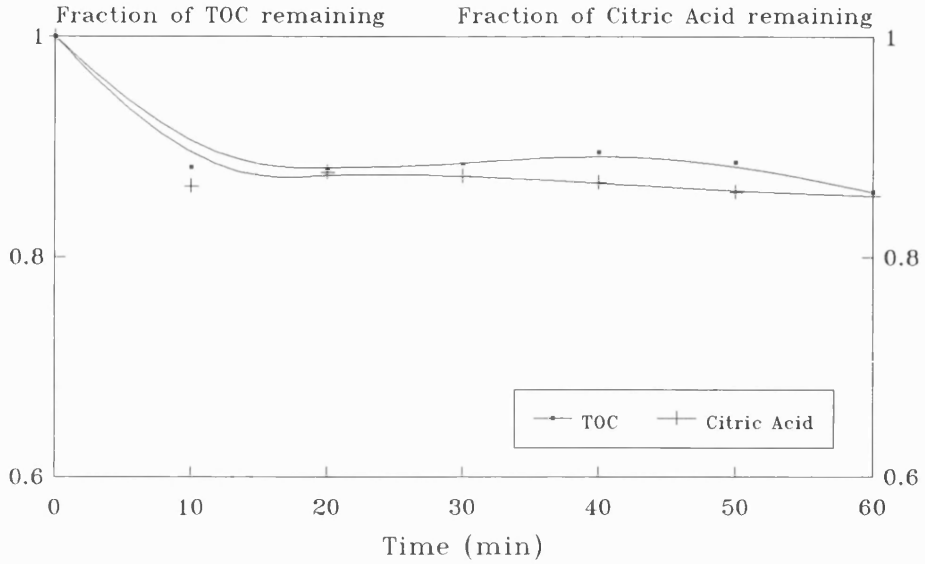

Medium Pressure Lamp
Initial TOC ~ 23352 ppmC
Initial Citric Acid ~ 60000 ppm

Fig 5.12 Photo-oxidation of Citric Acid
UV Light / Ozone (38.81 mg/min)

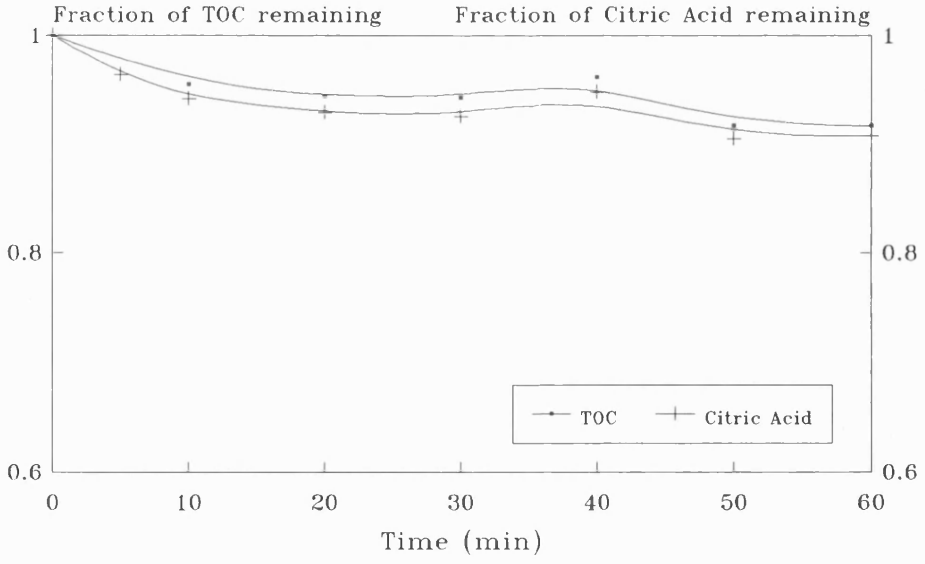

Medium Pressure Lamp
Initial TOC ~ 5982 ppmC
Initial Citric Acid ~ 60000 ppm

Fig 5.13 Photo-oxidation of Citric Acid
UV Light/Hydrogen Peroxide (5% v/v) only

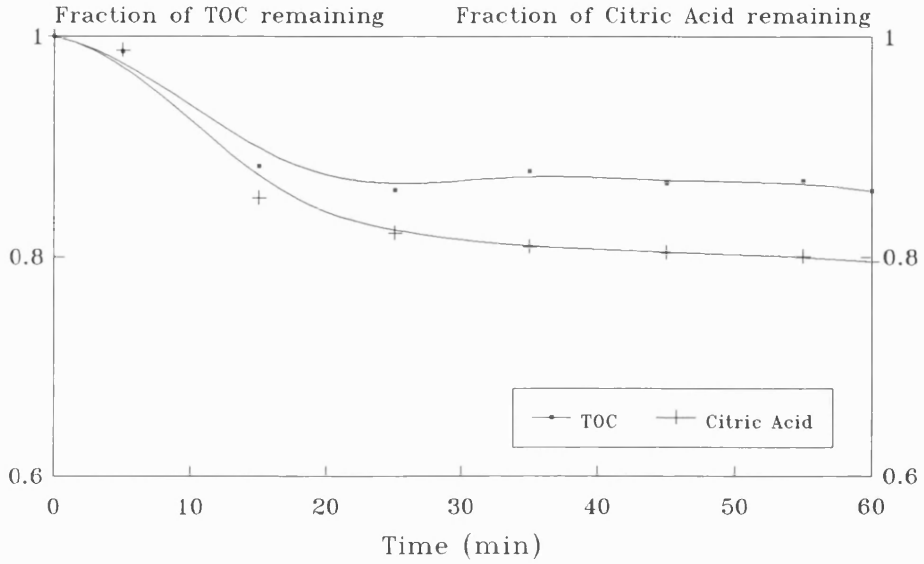

Medium Pressure Lamp
Initial TOC ~ 22032 ppmC
Initial Citric Acid ~ 60000 ppm

Fig 5.14 Photo-Oxidation of Citric Acid
UV Light/Hydrogen Peroxide (5% v/v) only

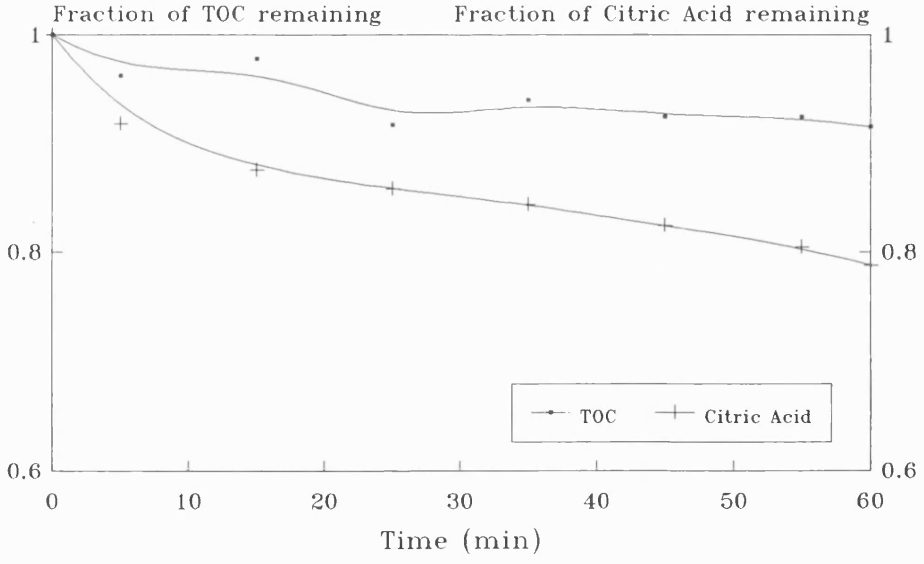

Medium Pressure Lamp
Initial TOC ~ 132 ppmC
Initial Citric Acid ~ 300 ppm

Fig 5.15 Photo-Oxidation of Citric Acid
UV Light/Hydrogen Peroxide (5% v/v) only

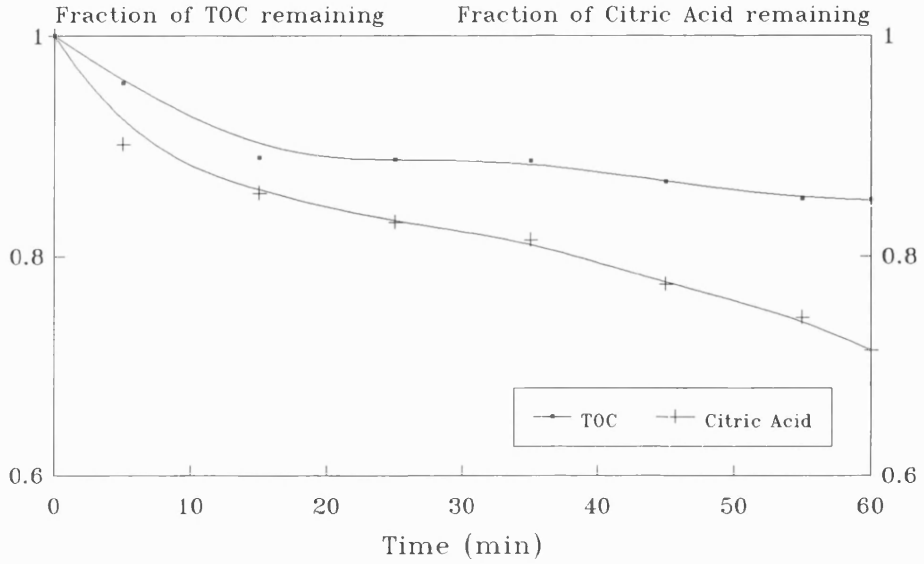

Medium Pressure Lamp
Initial TOC ~ 852 ppmC
Initial Citric Acid ~ 2300 ppm

Fig 5.16 Photo-oxidation of Citric Acid
UV Light / Hydrogen Peroxide (5% v/v) in
Presence of Ferric Nitrate (0.01 mol/l)

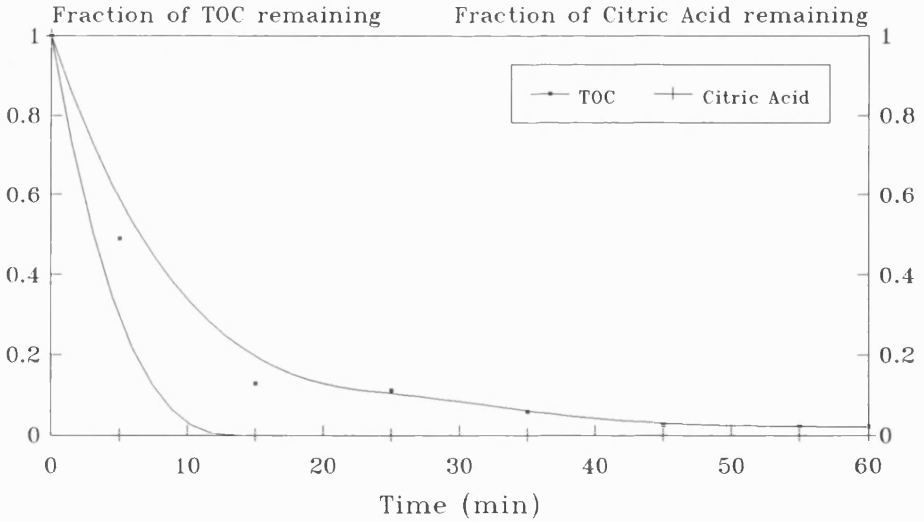

Medium Pressure Lamp
Initial TOC ~ 80.84 ppmC
Initial Citric Acid ~ 300 ppm

Fig 5.17 Photo-oxidation of Citric Acid
UV Light / Hydrogen Peroxide (5% v/v) in
Presence of Ferric Nitrate (0.01 mol/l)

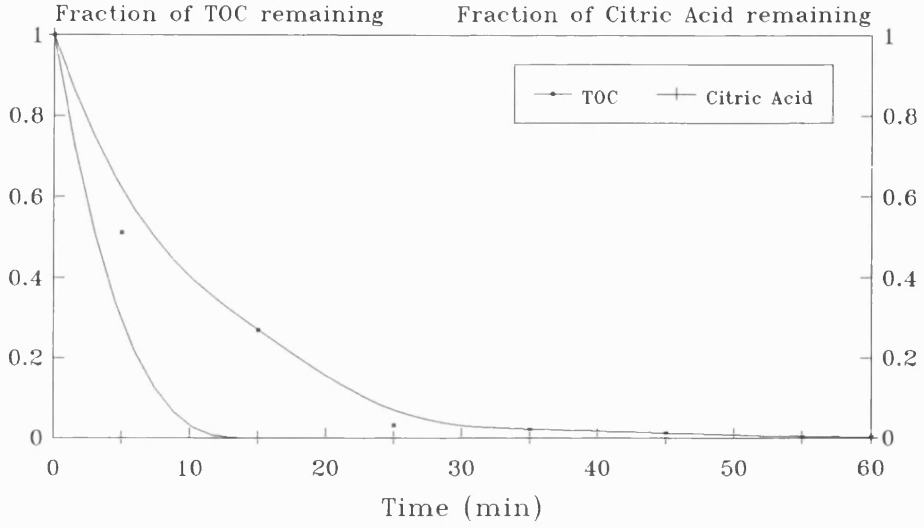

Medium Pressure Lamp
Initial TOC ~ 489.5 ppmC
Initial Citric Acid ~ 2300 ppm

Fig 5.18 Photo-oxidation of Citric Acid
UV Light / Hydrogen Peroxide (5% v/v) in
Presence of Ferric Nitrate (0.01 mol/l)

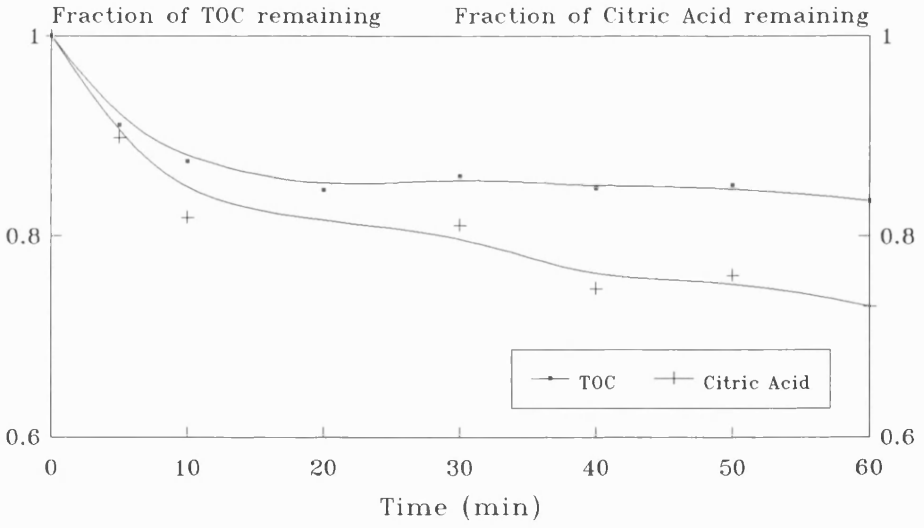

Medium Pressure Lamp
Initial TOC ~ 1216 ppmC
Initial Citric Acid ~ 60000 ppm

Fig 5.19 Photo-oxidation of Citric Acid
UV Light/Hydrogen Peroxide (5% v/v) in
Presence of Ferric Nitrate (0.01 mol/l)

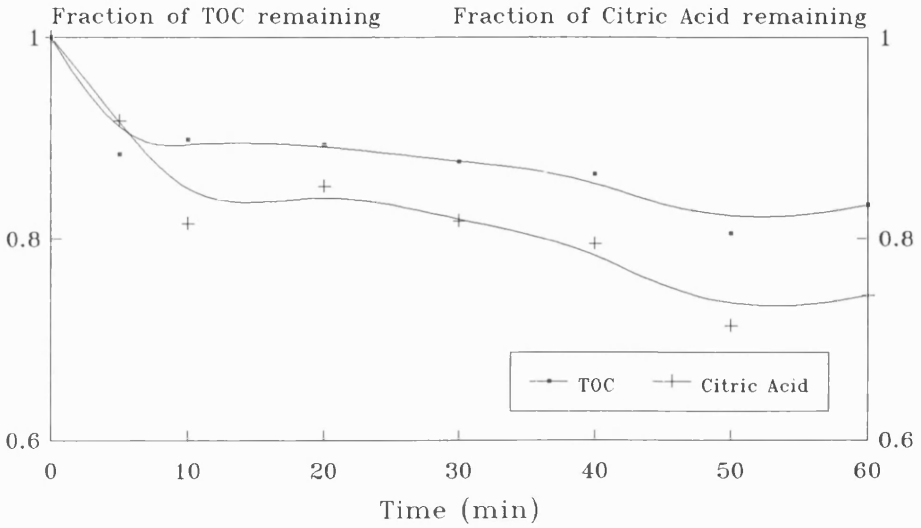

Medium Pressure Lamp
Initial TOC ~ 20624 ppmC
Initial Citric Acid ~ 60000 ppm

Fig 5.20 Photo-oxidation of Citric Acid
UV Light/ Hydrogen Peroxide(5% v/v) in
Presence of Ferric Nitrate (0.05 mol/l)

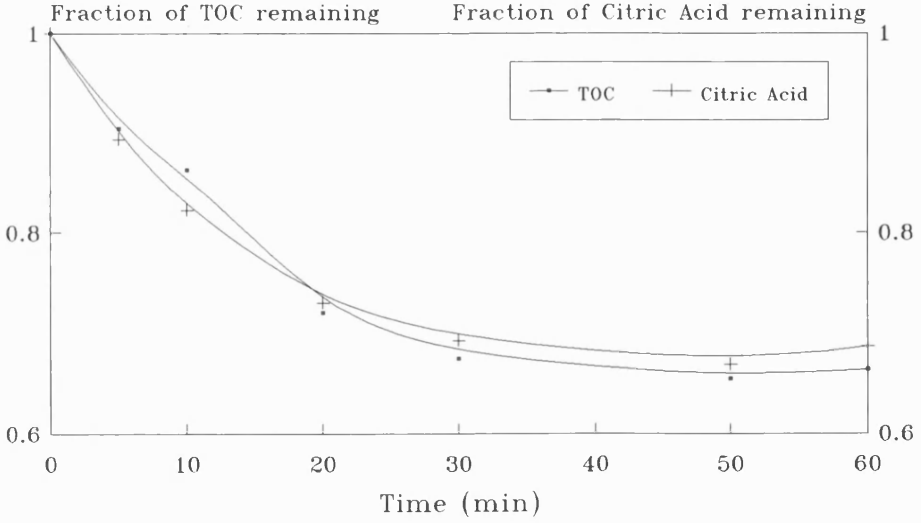

Medium Pressure Lamp
Initial TOC ~ 20336 ppmC
Initial Citric Acid ~ 60000 ppm

Fig 5.21 Photo-oxidation of Citric Acid
UV Light/Hydrogen Peroxide (10% v/v) in
Presence of Ferric Nitrate (0.05 mol/l)

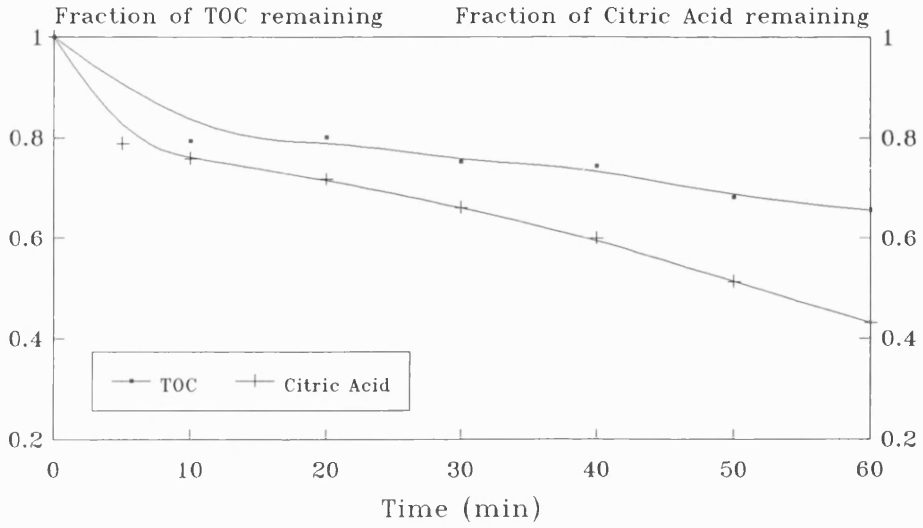

Medium Pressure Lamp
Initial TOC ~ 13577 ppmC
Initial Citric Acid ~ 60000 ppm

Fig 5.22 Photo-oxidation of Citric Acid
UV Light/Hydrogen Peroxide (10% v/v) in
Presence of Ferric Nitrate (0.1 mol/l)

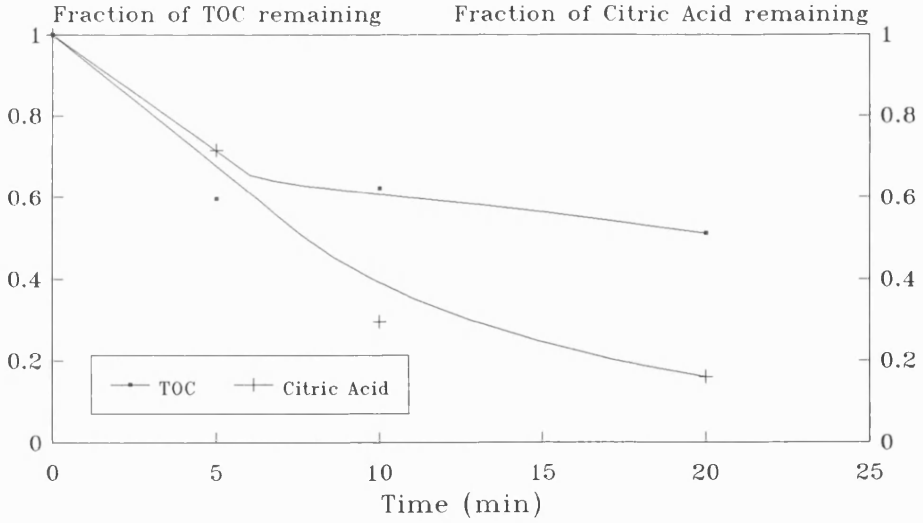

Medium Pressure Lamp
Initial TOC ~ 13302 ppmC
Initial Citric Acid ~ 60000 ppm

Fig 5.23 Photo-Oxidation of Citric Acid
UV Light / Hydrogen Peroxide (5% v/v) in
Presence of Fe2(SO4)3.5H2O (0.01mol/l)

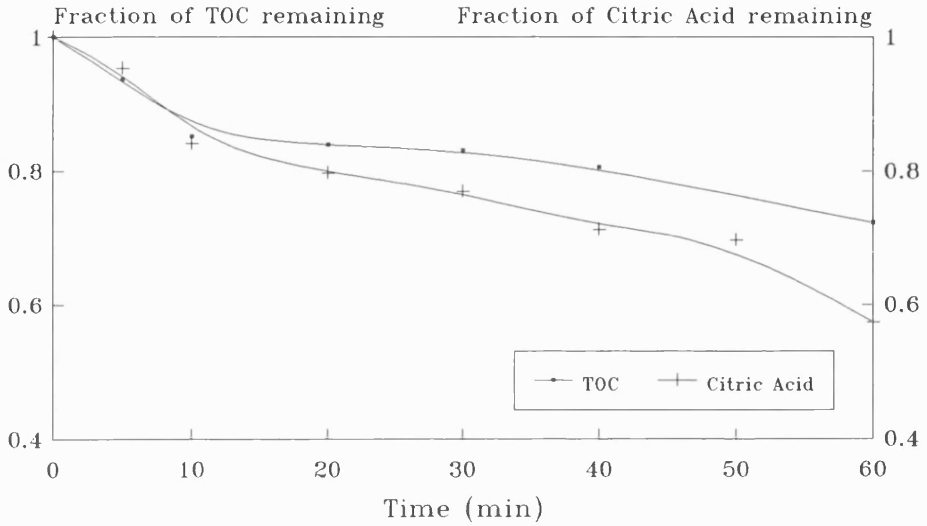

Medium Pressure Lamp
Initial TOC ~ 64902 ppmC
Initial Citric Acid ~ 60000 ppm

Fig 5.24 Oxidation of Citric Acid
Hydrogen Peroxide (5% v/v) only in
Presence of Fe2(SO4)3.5H2O (0.01mol/l)

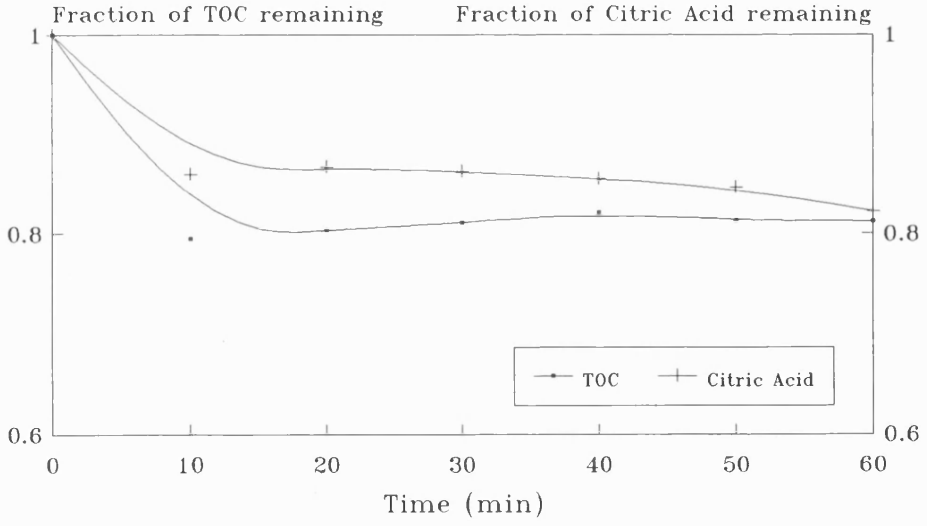

Medium Pressure Lamp
Initial TOC ~ 70200 ppmC
Initial Citric Acid ~ 60000 ppm

Fig 5.25 Photo-Oxidation of Citric Acid
UV Light/Hydrogen Peroxide (5 % v/v) in
Presence of Fe2(S04)3.5H20 (0.02 mol/l)

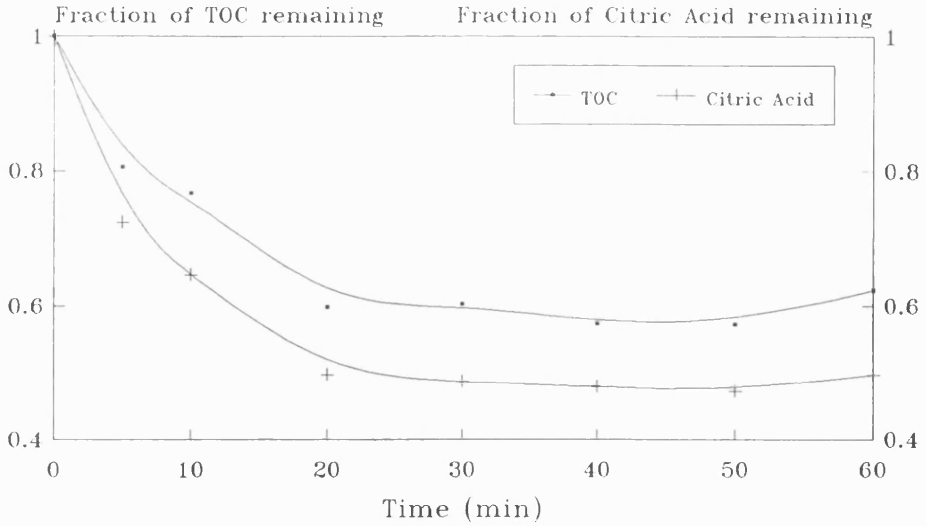

Medium Pressure Lamp
Initial TOC ~ 5982 ppmC
Initial Citric Acid ~ 60000 ppm

Fig 5.26 Photo-Oxidation of Citric Acid
UV Light/Hydrogen Peroxide (10 %v/v) in
Presence of Fe2(S04)3.5H20 (0.05mol/l)

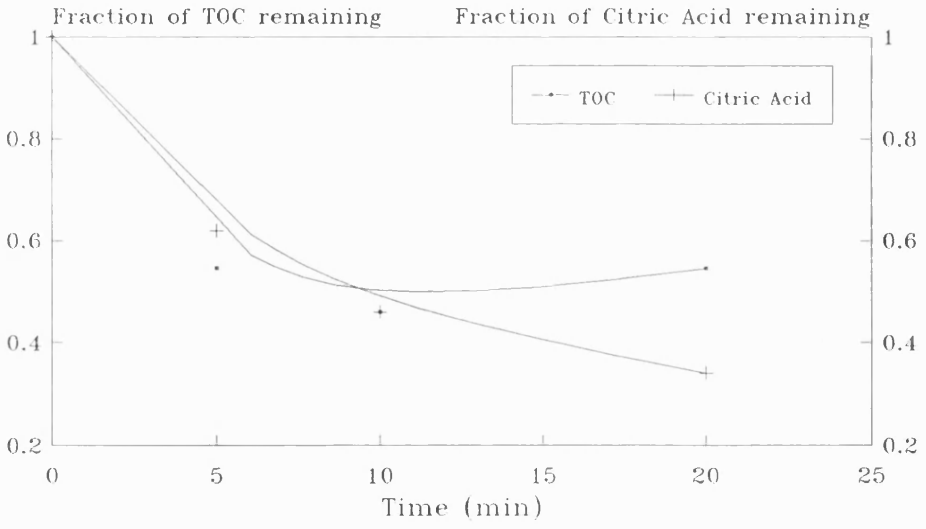

Medium Pressure Lamp
Initial TOC ~ 13644 ppmC
Initial Citric Acid ~ 60000 ppm

Fig 5.27 Photo-oxidation of Citric Acid
UV Light / Hydrogen Peroxide (5% v/v) in
Presence of Fe2(S04)3.5H20 (0.01mol/l)

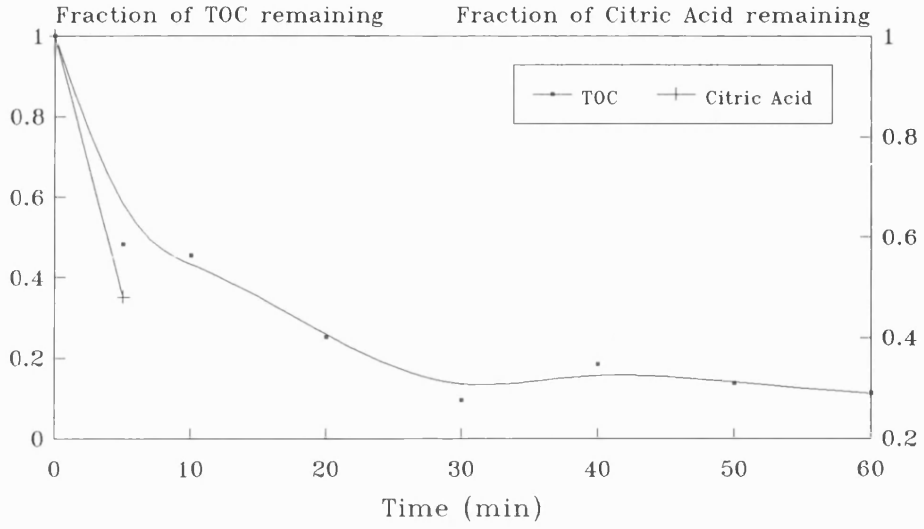

Medium Pressure Lamp
Initial TOC ~ 2296 ppmC
Initial Citric Acid ~ 2300 ppm

Fig 5.28 Photo-oxidation of Citric Acid
UV Light / Hydrogen Peroxide (5% v/v) in
Presence of Fe2(S04)3.5H20 (0.01mol/l)

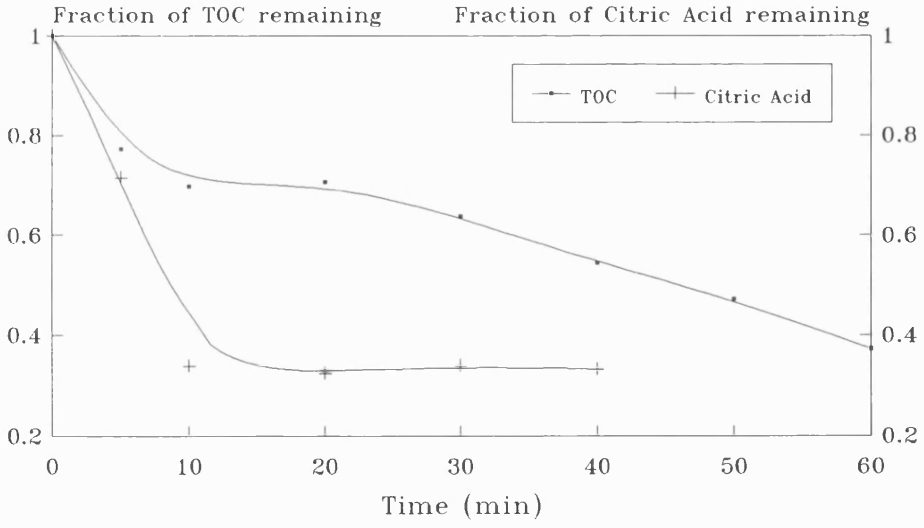

Medium Pressure Lamp
Initial TOC ~ 10960 ppmC
Initial Citric Acid ~ 10000 ppm

Fig 5.29 Photo-Oxidation of Citric Acid
UV Light / Ozone (38.81mg/min) in
Presence of Fe2(SO4)3.5H2O (0.01 mol/l)

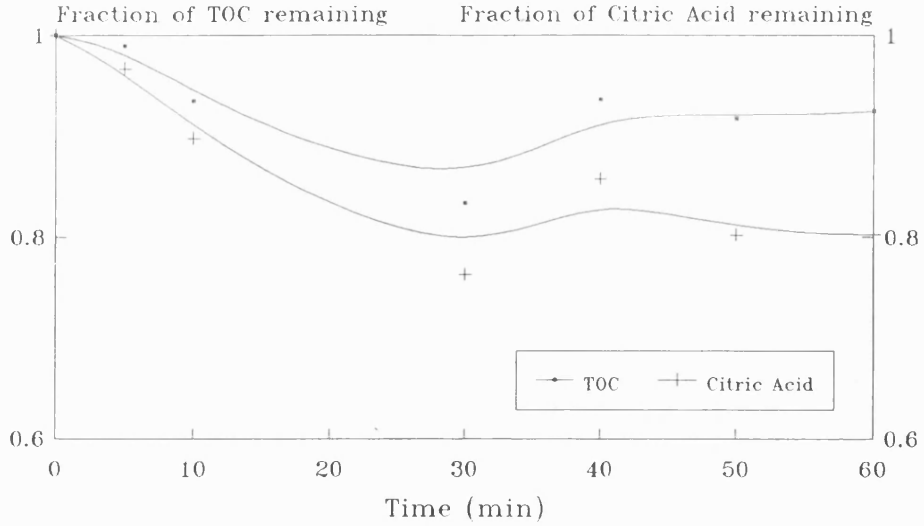

Medium Pressure Lamp
Initial TOC ~ 5982 ppmC
Initial Citric Acid ~ 60000 ppm

Fig 5.30 Photo-Oxidation of Citric Acid
UV Light / Ozone (92.82 mg/min) in
Presence of Fe2(SO4)3.5H2O (0.01 mol/l)

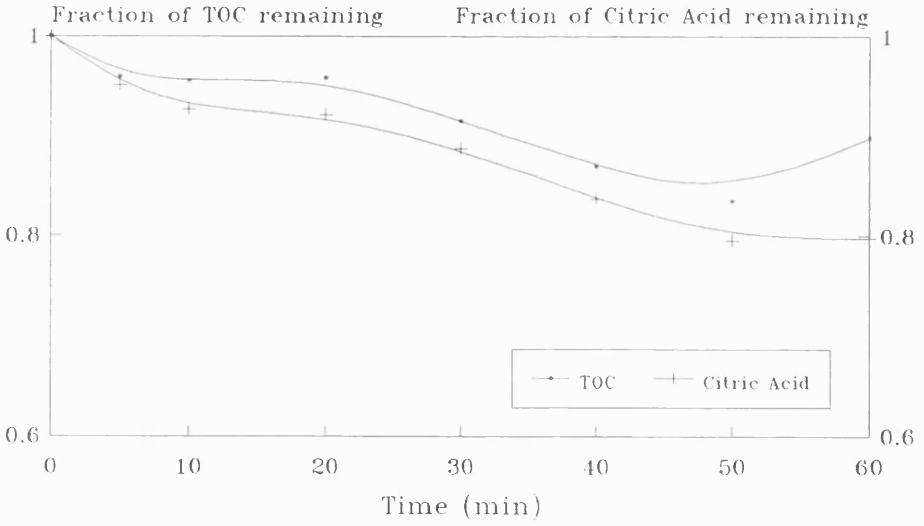

Medium Pressure Lamp
Initial TOC ~ 5982 ppmC
Initial Citric Acid ~ 60000ppm

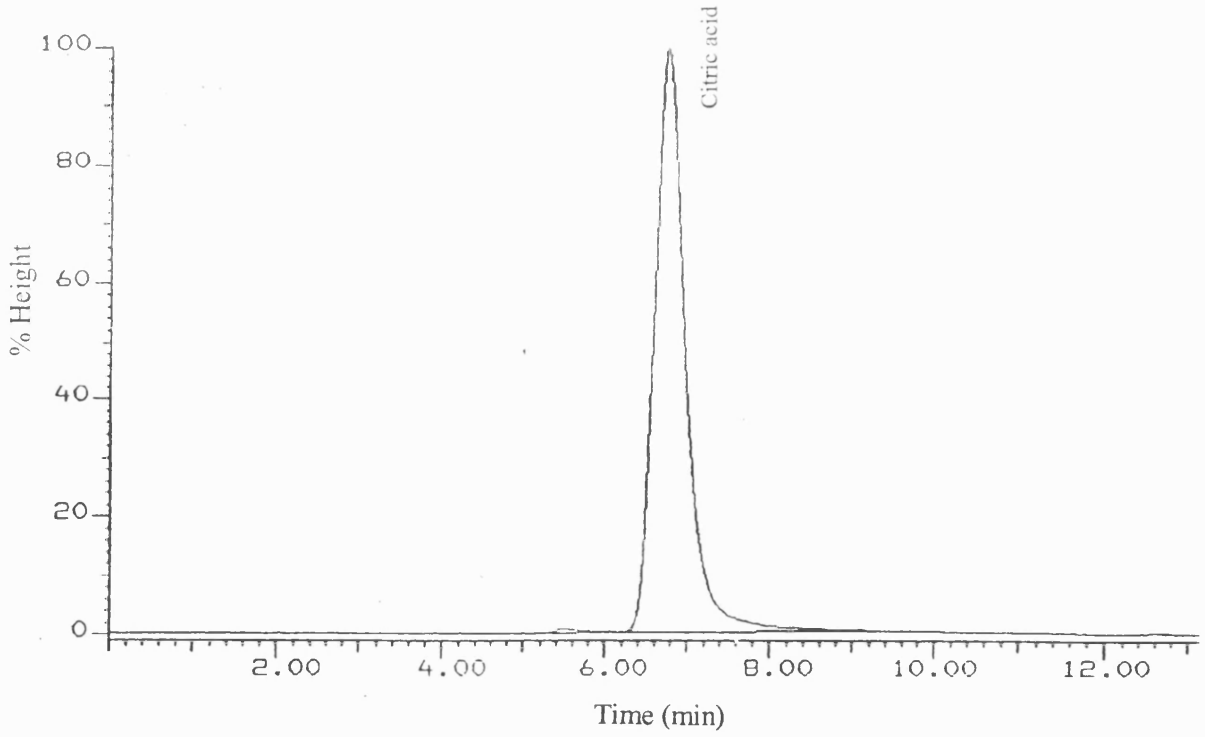

Fig.5.31 HPLC chromatogram : citric acid only

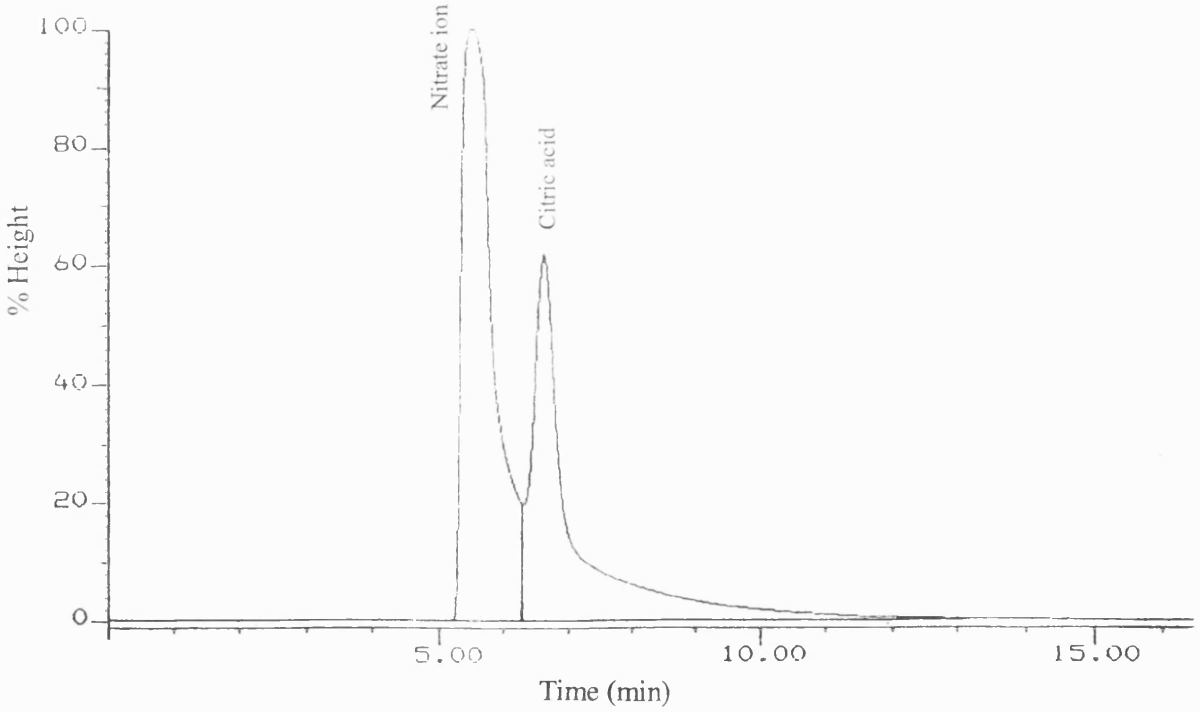

Fig.5.32 HPLC chromatogram : citric acid and ferric nitrate salt in sample

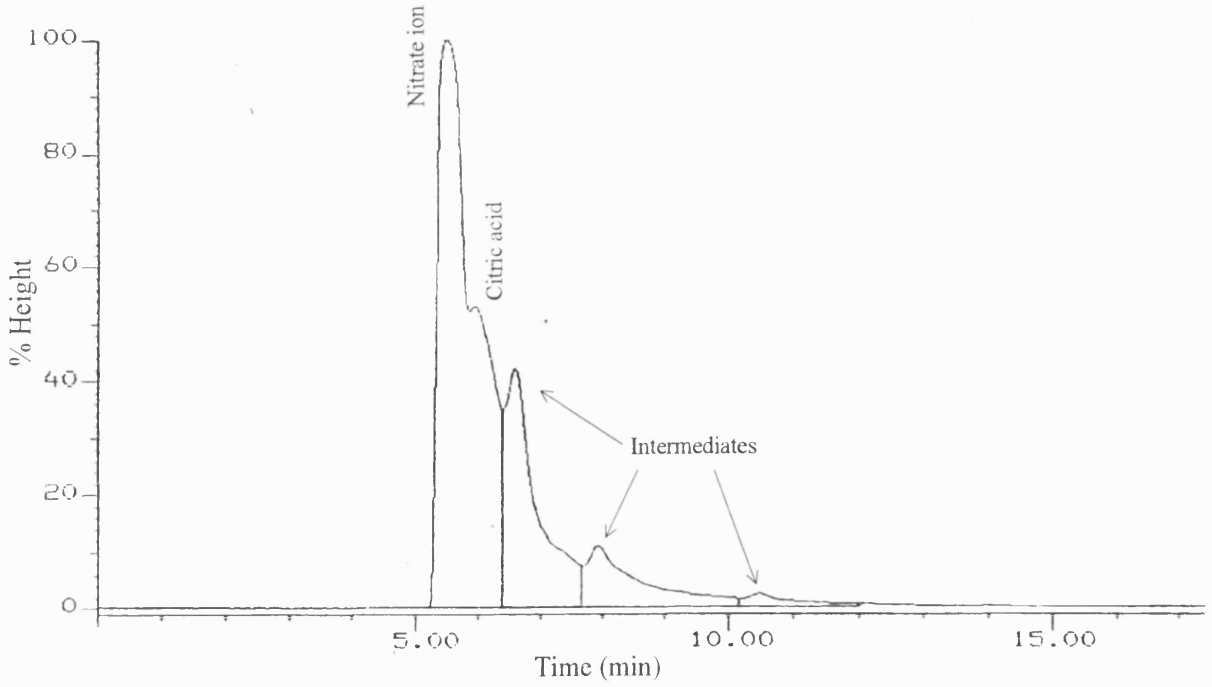

Fig.5.33 HPLC chromatogram : citric acid, ferric nitrate and intermediate compounds in sample

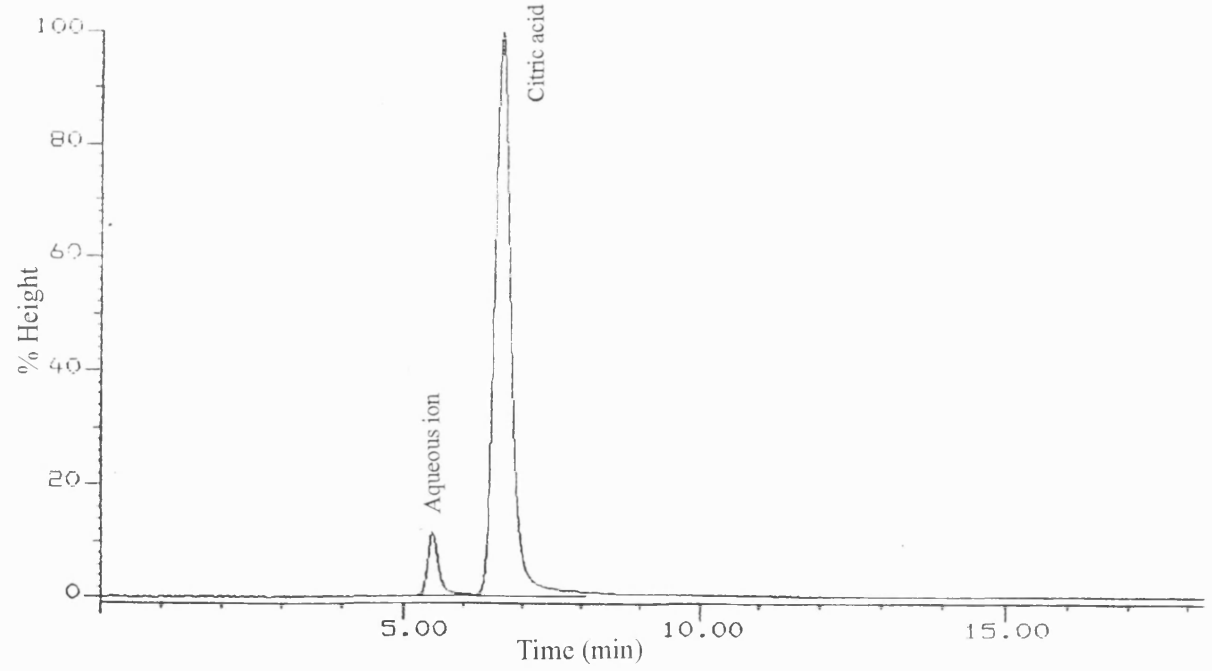

Fig.5.34 HPLC chromatogram : citric acid with ferric sulphate pentahydrate salt in sample

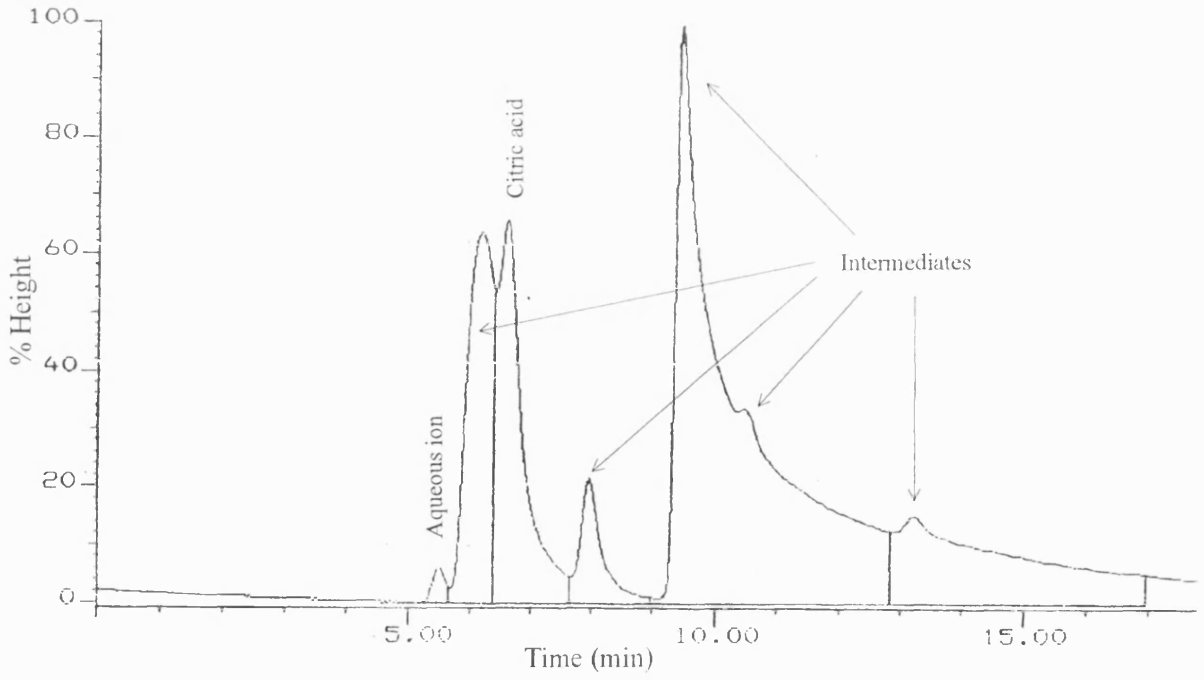

Fig.5.35 HPLC chromatogram : citric acid, ferric sulphate pentahydrate salt with intermediate compounds in sample

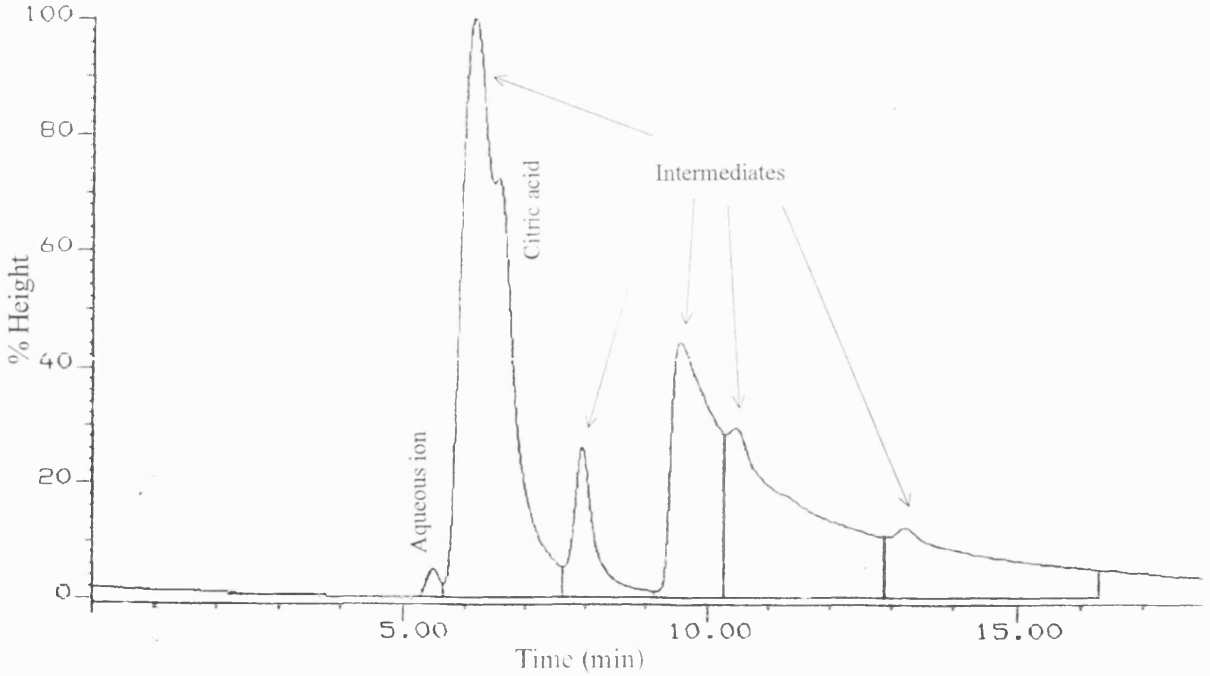

Fig.5.36 HPLC chromatogram : citric acid, ferric sulphate pentahydrate salt with intermediate compounds in sample

Fig 5.37 Photo-oxidation of Citric Acid
UV Light / Hydrogen Peroxide in
Presence of Fe2(SO4)3.5H20 (0.01mol/l)

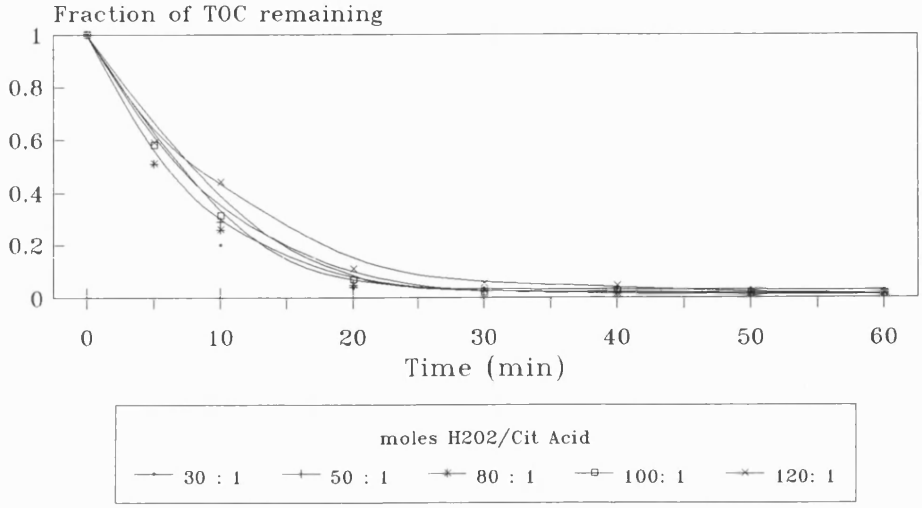

High Pressure Lamp I=600W
Initial TOC ~ 850ppmC
Initial Citric Acid ~ 2500 ppm

Fig 5.38 Photo-oxidation of Citric Acid
UV Light / Hydrogen Peroxide in
Presence of Fe2(SO4)3.5H20 (0.01mol/l)

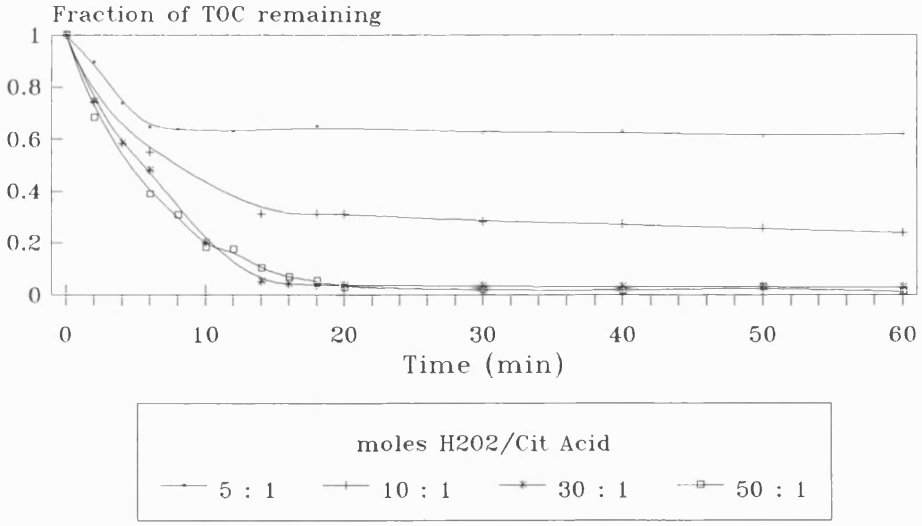

High pressure lamp I=600W
Initial TOC~850 ppmC
Initial Citric Acid~2500 ppm

CHAPTER 6
FACTORS AFFECTING THE PHOTO-OXIDATION PROCESS

The last chapter showed the results of different AOPs upon the degradation rate of citric acid. The effect of individual reactants on the degradation rate has not been studied. Also only the 'reactants' (hydrogen peroxide, light intensities and ferric sulphate pentahydrate) which are directly involved in the reaction were mentioned. Other factors such as pH, temperature and the presence of oxygen could alter the mineralization rate, are looked into as well. It is important to determine their effects (if any) on the system and hence determine if their role is important.

In this chapter the effect of reactants both individually and in combination are studied experimentally. A literature review is presented on the effect of pH, temperature and oxygen on the photooxidation process. The relevance of these parameters to the present work is then discussed and conclusions made.

6.1 Effect of Reactants

The 'reactants' were used individually and in combination to study their effects on the mineralization of citric acid. As a major part of reactions occur in the first ten minutes (see Sec.5.5), TOC and the mineralization rate (r) are determined in that time period. The concentrations of citric acid [C], hydrogen peroxide [H_2O_2], ferric sulphate pentahydrate [Fe^{3+}] and the nominal power output of UV light intensities [I] used are as specified in Sec.5.5.

6.1.1 Individual Reactants

The results are summarised in Table 6.1.

As can be seen, UV, H_2O_2 and Fe^{3+} alone have an insignificant effect on the degradation of citric acid.

TABLE 6.1 Results of the Effect of Individual Reactants on Photodegradation of Citric Acid

Reactants	Exp.	[C] /ppm	[I] /W	$\frac{[H_2O_2]}{[C]}$	$[Fe^{3+}]$/ mol l^{-1}	%TOC Degraded	r /ppm min^{-1}
UV	6.1	2500	600	0	0	1	<0.001
	6.2	1500	250	0	0	0	0
H_2O_2	6.3	1500	0	5	0	0	0
	6.4	1500	0	30	0	0	0
Fe^{3+}	6.5	1500	0	0	0.01	1	<0.001
	6.6	2500	0	0	0.01	0	0

6.1.2 Combination of Reactants

$UV+Fe^{3+}$, $UV+H_2O_2$ and $Fe^{3+}+H_2O_2$ are used to determine their effects on the degradation of citric acid. Results are summarised in Table 6.2.

Results show very clearly that while $UV+Fe^{3+}$ and $UV+H_2O_2$ combinations show a little improvement on the photodegradation of citric acid over the effects of individual reactants, the combined effect of $Fe^{3+}+H_2O_2$ is much more significant.

TABLE 6.2 Results of the Effect of Combinations of Reactants on the Photodegradation of Citric Acid

Reactants	Exp.	[C] /ppm	[I] /W	$\frac{[H_2O_2]}{[C]}$	$[Fe^{3+}]$ /mol l^{-1}	%TOC degraded	r /ppm min^{-1}
UV + Fe^{3+}	6.7	1500	250	0	0.01	1.25	<0.001
	6.8	2500	250	0	0.01	1.2	0.002
	6.9	2500	475	0	0.01	7.4	0.004
	6.10	1500	600	0	0.01	0.1	<0.001
	6.11	2500	600	0	0.01	7.1	0.008

TABLE 6.2 con't...

UV + H_2O_2	6.12	2500	600	5	0	1.8	0.005
	6.13	2500	600	30	0	1.0	0.006
	6.14	1500	600	5	0	1.0	0.001
	6.15	1500	600	30	0	1.2	0.006
Fe^{3+} + H_2O_2	6.16	2500	0	5	0.01	36	0.02
	6.17	2500	0	10	0.01	38	0.06
	6.18	2500	0	30	0.01	40	0.06
	6.19	1500	0	5	0.01	31	0.03
	6.20	1500	0	30	0.01	35	0.06

6.2 Effect of pH

pH is not a typical control variable for commercial applications of the photochemical oxidation process although a knowledge of it helps in exercising design on operational stage controls (Prengle, 1975).

Workers studying different photochemical oxidation processes have come to the conclusion that the efficiency of their processes are best in certain pH range. For example H_2O_2 and O_3/UV seems to favor high pH (Paul and Canter, 1990) while the Fe^{3+}/H_2O_2 process is highly sensitive to pH with an optimum at 2.7-2.8 (Pignetello, 1992). Fenton's reaction was most effective in the range 3-5 (Bishop et al, 1968).

Larson et al (1991) investigated the photodegradation rates of triazines with salts of ferric iron. They found out that the pH of their system was highly dependent on the iron concentration; increasing the iron concentration by a factor of 10 increased $[H^+]$ by a factor of 10 and a decreased in the pH by 1 unit. Thus for the Fe^{3+}/H_2O_2/UV system, the pH, $[Fe^{3+}]$ and $[H^+]$ are inter-related. An increase or a reduction of $[Fe^{3+}]$ affects the pH of the system and thus its efficiency.

In this work, however, the effect of pH on the system can be ignored since the concentration of the ferric salt is fixed at 0.01 mol/l for the experiments presented (Sec.5.5). Attempts to study the effect of varying pH on photodegradation using buffered solutions will fail, as the presence of inorganic or organic compounds can

influence the rate of photodegradation of the pollutants (Farhataziz and Ross, 1977; Simons and Zepp, 1986; Zepp et al, 1988; Kochany et al, 1990; Larson et al; 1991). Moreover since acids and alcohols are important intermediate products in the course of the chain of photochemical oxidation reactions it is generally concluded that pH control is not desirable (Prengle, 1975).

6.3 Effect of Temperature

Little detailed study of the effect of temperature on UV/H_2O_2/Fe^{3+} or other photooxidation processes has been carried out. This is mainly because industrially photo-oxidation processes are 'ambient' processes, operating at low temperatures. Also, photochemically initiated reactions have low activation energies, hence temperature has no direct effect on photochemical oxidation processes (Calvert and Pitts, 1966; Mukherjee, 1978). Even when a higher temperature improves the photochemical oxidation rate, as a general practice, increased reaction rates are obtained by increasing the UV dosage instead of increasing the temperature of the system. This is because of the higher costs involved in installing a heat exchanger in comparison to increasing UV wattage by incorporating additional or more powerful lamps (Paul and Canter, 1990). Furthermore, Sundstrom et al (1986) showed that higher temperature increased the rate of reaction substantially but at the expense of larger peroxide consumption in UV/H_2O_2 process.

Experiments carried out so far in this research have showed only a maximum increased in temperature of 7.5°C due to the exothermic reaction. The temperature profile of the experiments are as shown in Fig.6.1 to 6.8. It also shows that the temperature increase last only a few minutes. The activation energy of the reaction cannot be determined as the intermediate final products are unknown. Since Sec.6.1 has shown clearly that the process is photochemically initiated, it is reasonable to ignore the effect of temperature as suggested in the literature. Furthermore, means to control the process temperature are both impractical and uneconomical.

6.4 Effect of Oxygen

The role of oxygen in the photo-oxidation processes has seldom been studied or exploited. This is regrettable since it could form one of the most reactive radicals and improve the efficiency of the photo-oxidation process.

Mansour et al (1984) studied the influence of oxygen and nitrogen on the photodecomposition rates of some organic compounds using UV/H_2O_2 process. They found that increasing the concentration of oxygen accelerated the H_2O_2 breakdown and hence the photodecomposition rates.

Larson et al (1991) also showed that oxygen had a significant effect on UV/H_2O_2/Fe^{3+} process in photodecomposition of triazines. It is known that oxygen will react with Fe^{2+} in the dark to produce $O_2\cdot^-$ (reaction 6.1).

$$Fe^{2+} + O_2 \rightarrow Fe^{3+} + O_2\cdot^- \qquad ...(6.1)$$

Although the reaction is slow at low pH, it is reportedly promoted at interfaces and by light (Stumm and Morgan, 1981). Therefore, oxidation of ferrous ion (in the presence of reasonable concentration of oxygen) would generate superoxide ($O_2\cdot^-$), which as its conjugate acid HOO· is susceptible to disproportionate to hydrogen peroxide and oxygen (Bielski, 1978).

$$2O_2\cdot^- + 2H^+ \rightarrow H_2O_2 + O_2 \qquad ...(6.2)$$

Ultimately, additional HO· could be produced by the Fenton reaction of H_2O_2 with Fe^{2+}.

$$Fe^{2+} + H_2O_2 \rightarrow HO\cdot + HO^- + Fe^{3+} \qquad ...(6.3)$$

However, in the present research the effect of changing oxygen concentration will not be considered as there are already numerous parameters involved. More detailed studies could be carried out in future on the effect of oxygen on Fe^{3+}/H_2O_2/UV process or any other photo-oxidation processes as this could prove beneficial.

6.5 Conclusions

The results discussed previously show that the individual reactants (UV, H_2O_2 and Fe^{3+}) do not show any significant effect in the mineralization of citric acid. Results improved somewhat when the reactants were used in combination. The UV/Fe^{3+} and UV/H_2O_2 combinations show little improvement in the amount of TOC being degraded due to a very slow rate of mineralization. In contrast Fe^{3+}/H_2O_2 combine effectively to show a significant reduction in TOC content due to a higher rate of mineralization of citric acid.

Study of the effect of pH and temperature were considered to be unnecessary. The literature has reported that pH is directly related to the concentration of Fe^{3+}, and since this value will be the same for all experiments, its effect can be ignored. Attempts to vary the pH using buffer solutions have been shown to be undesirable.

In the case of temperature, for practical and economical reasons, its effect will not be studied. Experiments are done at ambient temperature and the increase in temperature due to exothermic reaction is not great. The average ambient temperature in the lab is 16-17°C.

In the literature, oxygen has shown great promise in improving the efficiency of the UV/H_2O_2/Fe^{3+} process. However due to the number of parameters involved, its effect was not studied.

Fig.6.1 Temperature Profile (Batch)
Photo-oxidation of Citric Acid
UV/H202/Fe2(S04)3.5H20 Process

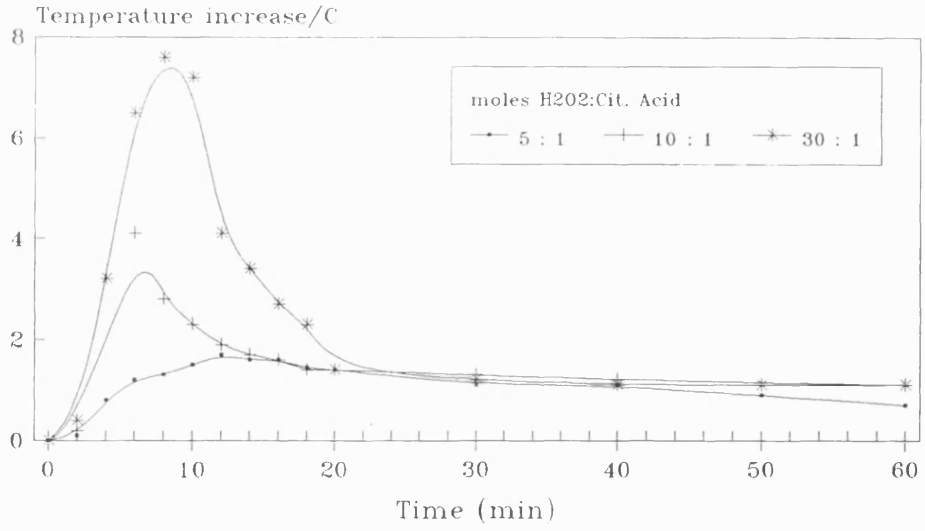

Medium Pressure Lamp(Nominal Power=600W)
Initial Citric Acid =2500 ppm
Ferric Sulphate=0.01 mol/l

Fig.6.2 Temperature Profile (Batch)
Photo-oxidation of Citric Acid
UV/H202/Fe2(S04)3.5H20 Process

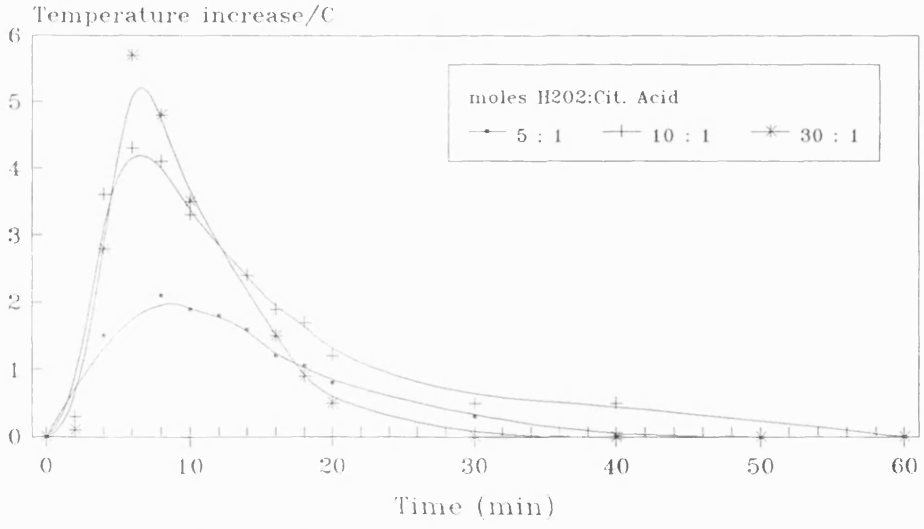

Medium Pressure Lamp(Nominal Power=600W)
Initial Citric Acid =2000 ppm
Ferric Sulphate=0.01 mol/l

Fig.6.3 Temperature Profile (Batch)
Photo-oxidation of Citric Acid
UV/H202/Fe2(S04)3.5H20 Process

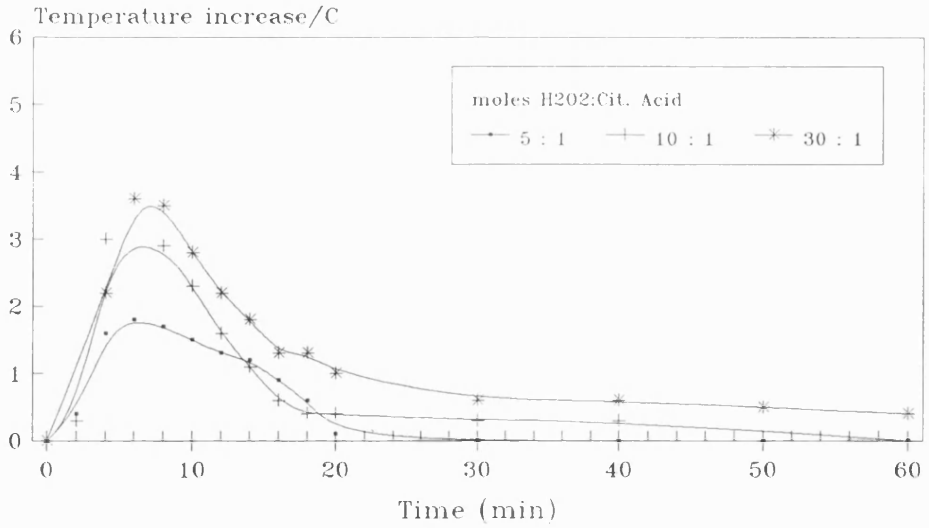

Medium Pressure Lamp(Nominal Power=600W)
Initial Citric Acid =1500 ppm
Ferric Sulphate=0.01 mol/l

Fig.6.4 Temperature Profile (Batch)
Photo-oxidation of Citric Acid
UV/H202/Fe2(S04)3.5H20 Process

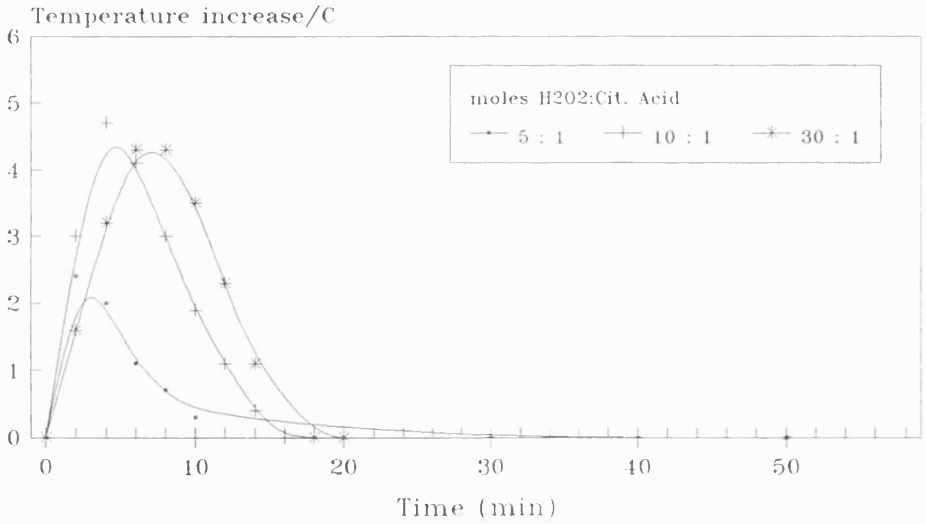

Medium Pressure Lamp(Nominal Power=475W)
Initial Citric Acid =2500 ppm
Ferric Sulphate=0.01 mol/l

Fig.6.5 Temperature Profile (Batch)
Photo-oxidation of Citric Acid
UV/H202/Fe2(S04)3.5H20 Process

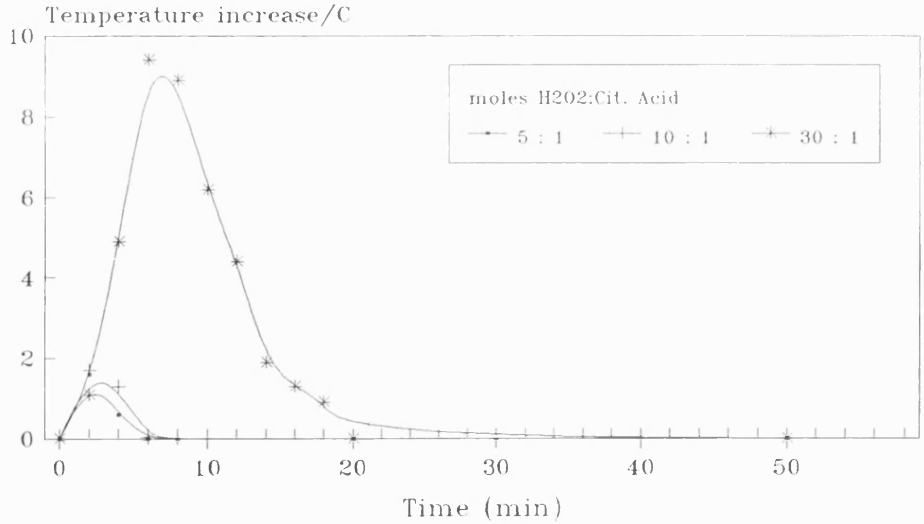

Medium Pressure Lamp(Nominal Power=475W)
Initial Citric Acid =2000 ppm
Ferric Sulphate=0.01 mol/l

Fig.6.6 Temperature Profile (Batch)
Photo-oxidation of Citric Acid
UV/H202/Fe2(S04)3.5H20 Process

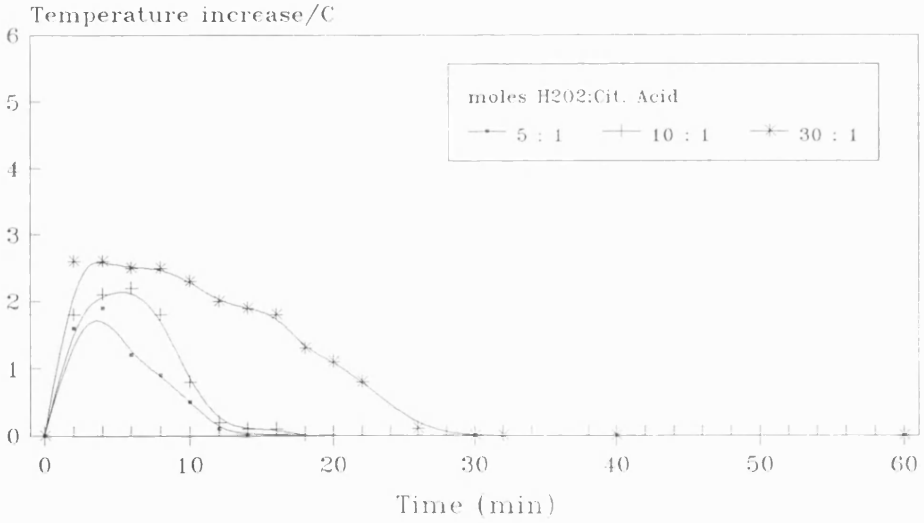

High Pressure Lamp I=475 W
Initial Citric Acid =1500 ppm
Ferric Sulphate=0.01 mol/l

Fig.6.7 Temperature Profile (Batch)
Photo-oxidation of Citric Acid
UV/H202/Fe2(S04)3.5H20 Process)

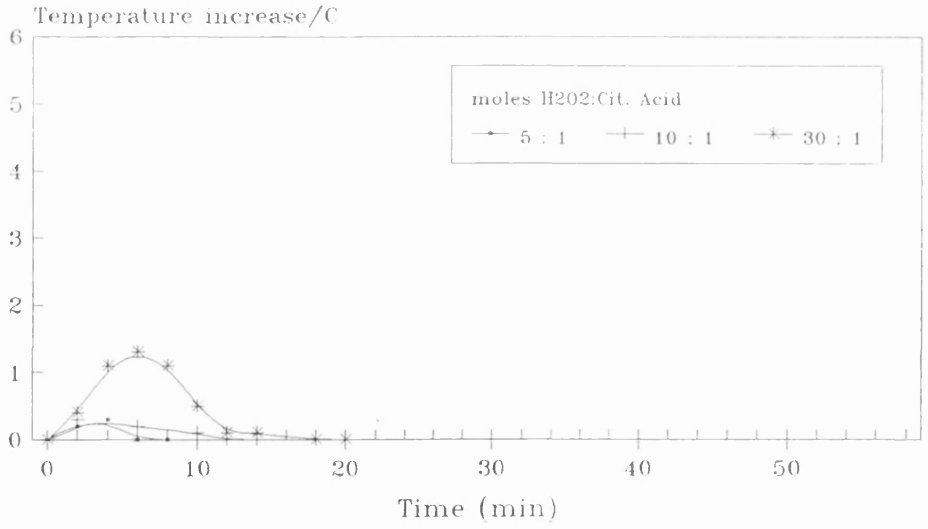

Medium Pressure Lamp(Nominal Power=250W)
Initial Citric Acid =2000 ppm
Ferric Sulphate=0.01 mol/l

Fig.6.8 Temperature Profile (Batch)
Photo-oxidation of Citric Acid
UV/H202/Fe2(S04)3.5H20 Process

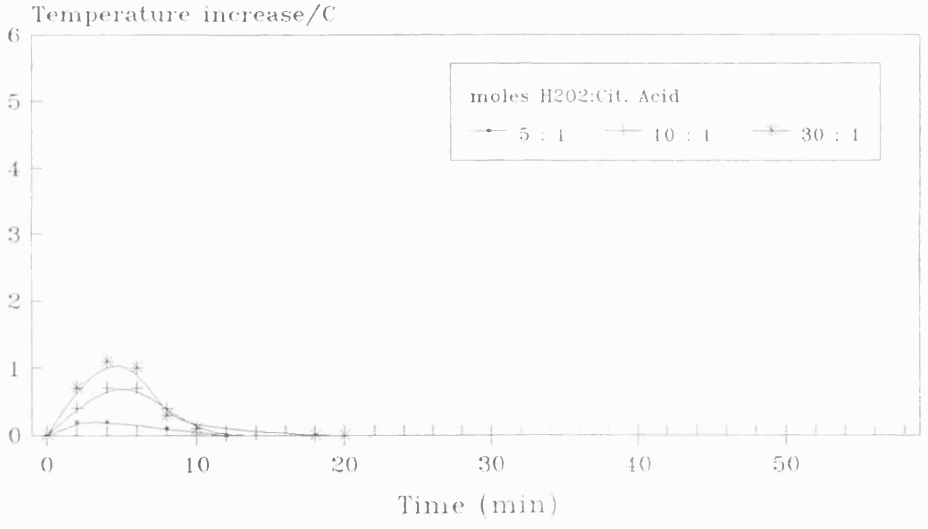

Medium Pressure Lamp(Nominal Power=250W)
Initial Citric Acid =1500 ppm
Ferric Sulphate=0.01 mol/l

CHAPTER 7
IDENTIFYING INTERMEDIATE COMPOUNDS

Efforts were made to understand the reactions that occurred in the photoreactor. To achieve this it was necessary to identify any intermediates compounds produced as a result of the photo-oxidation reaction. In so doing, this would also confirm whether there are any toxic by-products formed.

In this chapter three main sections are devoted to investigations related to intermediate compound identification. The first section will show author's search in the literature to find a method suitable for the analysis of the intermediates, as well the results of the attempts to use the method. An alternative method is also devised for this purpose. The second section gives a review of the reaction mechanisms proposed by some workers for the photo-oxidation of citric acid by $UV/H_2O_2/Fe^{3+}$, with the intermediates and final products determined. The product and possible intermediates are analysed by HPLC and their retention times is compared with those obtained in experiments. The last section will show some experimental observations and their interpretation, and finally conclusions are made.

7.1 Attempts to Isolate and Identify Intermediates

To determined accurately the intermediates present would required the use of GC-MS system. This constitutes a major obstacle as most organic acids are water soluble and hence not suitable for GC analysis. A tremendous amount of time and effort has been spent by workers to find a method to derivatised these acids so that they are volatile enough to be analysed by GC. However, more often than not, a method used for one acid can not be used for another, hence a trial and error method has to be used to find the exact conditions and procedures for different acids. This

problem is made worst because a lot of methods mentioned in the literature are not clear in stating the precise conditions and procedures involved. This section will provide a brief literature review of the work done to date in extracting and derivation of organic acids (particularly those acids closely related to citric acid) from aqueous phase and GC analysis. An alternative method has been devised using HPLC to collect pure fractions of intermediates for analysis, however this method has many problems and its use is not practical.

7.1.1 Solid Phase Extraction and GC-MS Analysis

Many analytical methods are reported in the literature for the separation of organic acids, and a number of these have been devoted to the determination of the acids of the citric acid cycle. These methods, unfortunately, involve either tedious extraction and concentration procedures to increase detection sensitivity in liquid chromatographic determinations or time consuming extraction and derivation to enhance volatization for gas chromatography (Turkelson and Richards, 1978). In many of these methods, complete separation of all the acids of interest is not achieved and in others quantitation is achieved through the subsequent titrimetric analysis of each fraction with dilute alkali to an indicator end point.

Since the citric acid cycle acids are not sufficiently volatile for GC analysis, the preparation of suitable volatile derivatives is required. Several procedures have been described for the preparation of derivatives of these acids, as well as their GC separation and flame ionisation detection. Those derivatives used most frequently rely on the conversion of carboxyl groups to methyl esters or trimethylsilyl esters and hydroxyl groups to trimethylsiyl ethers. The common esterifying agents used were diazomethane/ether or boron trifluoride/methanol for the methyl esters and trimethyl chlorosilane and hexamethyldisilazone in pyridine for the other derivatives (Dalgleish et al, 1966; Alcock, 1969; Harmon and Doella, 1969).

However, numerous reports exist of unstable components resulting in multiple peaks, indicating difficulties which have been encountered with the derivative preparation procedures mentioned above (Turkelson and Richards, 1978). Some of these problems were resolved by Horning et al (1968). The best general procedure is that involving the preparation of methaxime-trimethylsilyl (MO-TMSi) derivatives. Mixtures of simple acids, hydroxy acids and keto acids were treated with methoxylamide hydrochloride in pyridine followed by silylation with bis(trimethylsilyl) trifluoracetamide. The samples is isolated by an ion exchange procedure using diethylaminoethyl-Sephadex (DEAE-Sephadex) column since solvent extraction methods are not satisfactory (Horning and Horning, 1971a). This is first described by Horning and Horning (1971b) and Jaakonmaki et al (1967) and further developed by others (Chalmers and Watts, 1972; Thompson and Markey, 1975; Horrocks et al, 1976; Sims et al, 1981). The principal advantage is its specificity and a high and reproducible extraction recovery of polar and non-polar acids. However, this method also has considerable disadvantages : it is a laborious and complex procedure and the profile may be obscured by dominant peaks of some polar acids and inorganic sulphate and phosphate trimethylsilyl derivatives (Thompson and Markey, 1975; Fitch et al, 1979; Williams et al, 1979; Greter and Jacobson, 1987).

Various alternative methods have been published, but none of them thus far have found widespread use : solid phase extraction on a cellulose matrix (Anderson et al, 1978) or Extrelut columns (Pinkston et al, 1981), on columns with a mixture of Porapak Q and Porapak T (Greter and Jacobson, 1987). A relatively new method for isolating and concentrating organic acids before gas-chromatography-mass spectrometry is used by Verhaegle et al (1988) and is by far the most comprehensive among the literature. Sulphate and phosphate anions are removed by precipitation with $Ba(OH)_2$, and the pH is adjusted to 8-8.5. The sample is then applied onto small, disposable, strong anion-exchange columns. Neutral and basic compounds are washed out with water, which is then removed by centrifugation and by rinsing the column

with methanol and diethyl ether. The organic acids are eluted with a 4/6 (by vol) mixture of an organic solvent-esther (n-butanol or ethyl acetate) and for nitric acid containing HSO_4^- (0.1 mol/l) as a highly selective counter-ion, and finally with methanol alone. Sulfate ions are retained, and the eluate is evaporated before trimethylsilyl derivatization. The derivatized sample is then injected into GC-MS system for analysis.

When the comprehensive methods and procedures published by Verhaegle et al (1988) are used to determine the intermediate compounds of the photo-oxidation of citric acid, the actual fractional groups or acids being derived cannot be determined. GC-MS analysis results showed only the peaks for trimethyl silyl derivation of citric acid and acetic acid, with a lot of noisy background and several peaks by chemicals used for the derivatization. (see Fig.7.1). Hence apart from acetic acid as one of the intermediates, concrete prove of other compound being formed as a result of degradation of citric acid cannot be established. Whether or not acetic acid is one of the intermediates is investigated further using HPLC in Sec.7.2.3.

7.1.2 HPLC Method

After a discussion with Dr T M Jefferies (School of Pharmacy and Pharmacology, University of Bath) the following method was devised in order to get a conclusive results. The procedures are as follows : fractions of HPLC effluents are collected and then freeze-dried. They are then dissolved in a small volume of water and passed through a reverse-phase cartridge to remove any inorganic compounds. The organic acids retained in the cartridge are then washed with water. Spectroscopic analysis can then be carried out with the samples obtained. The analysis equipment involved is mass-spectrometry (molecular weight determination), NMR (structure determination) and infra-red (functional group determination). However a major difficulty is foreseen, as only 20 μl of sample can be injected into the HPLC column, the fractions collected for each run would be extremely small. Thus, it would require

a tremendous number of runs and experiments to acquire the minimum amount of sample required for the analysis. Also because most of the fractions interlap with each other, collecting pure individual intermediates samples would be quite impossible.

7.2 Verifying Intermediates in the Literature

Two possible mechanisms are discussed in the literature to explain the photo-oxidation of citric acid in the presence of ferric salt. In each case the same conclusion was drawn that one mole of citric acid is degraded by two moles of iron (III). The intermediates are further degraded into final products of acetone and carbon dioxide. Thus the overall reaction is one mole of citric acid photodegraded to one mole of acetone and three moles of carbon dioxide. However when acetone is analysed using HPLC, its retention time does not correspond to any of the intermediates.

7.2.1 Mechanism A

Benrath (1911, 1912, 1917) studied the photochemical decomposition of citric acid in the presence of ferric ion by ultraviolet light and by sunlight had shown that formation of acetone and carbon dioxide as the final products. Ciamician and Silber (1913) found that the same final products result also from the prolonged exposure of citric acid to light in the absence of ferric iron. Benrath (1911) reported that acetonedicarboxylic acid is probably an intermediate product in the decomposition catalysed by ferric iron. The ferric iron is simultaneously reduced to the ferrous state during the initial photochemical change which has been formulated (Benrath, 1911; Fry and Gerwe, 1928; Rao and Aravamudan, 1955) as follows :

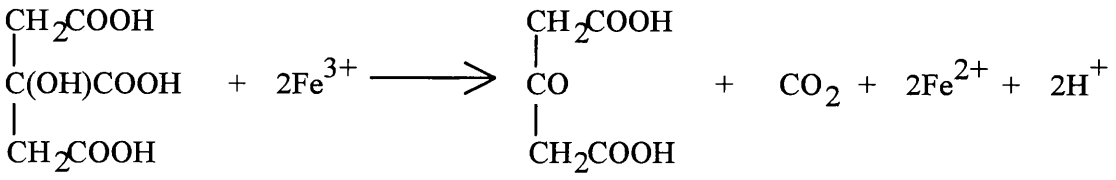

...(7.1)

The unstable acetonedicarboxylic acid would then decompose spontaneously to acetoacetic acid and carbon dioxide according to the equation :

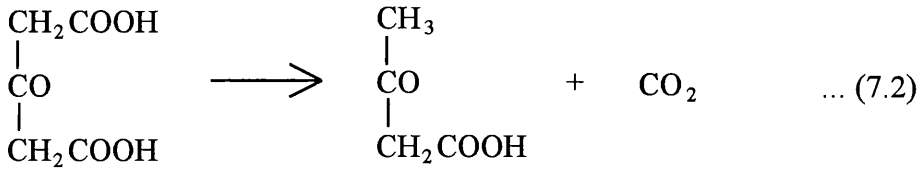

... (7.2)

Then the acetoacetic acid would break down to acetone and carbon dioxide as follows :

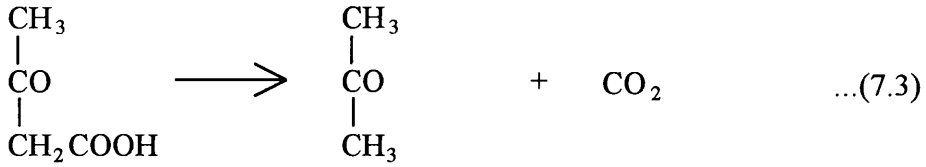

...(7.3)

Frahn (1958) was able to confirm that the photochemical oxidation of citric acid by sunlight in the presence of ferric ion proceeds according to the above formulation. Separation of the intermediate products of the reaction was achieved by means of paper ionophoresis using 0.05M sodium chloride as the electrolyte.

7.2.2 Mechanism B

It is known that the introduction of iron salts into solutions of many hydroxyl acids leads to the formation of complexes with various compositions. At the same time the sensitivity of the system to light is greatly increased. The action of light on

these complexes leads to decarboxylation of the acids, which arises as a result of intracomplex electron transfer (Glikman et al, 1965).

Hamm et al (1954) had shown that ferric and ferrous iron form series of complexes with citrate. And it has been established that citrate and the metal ion exist in these complexes in the ratio of 1:1 (Lanford and Quinan, 1948; Warner and Weber, 1953).

In a private communication (Yue, 1991), two possible reaction paths are possible when the ferric-citrate complex is irradiated. Both paths involved ligand to metal charge transfer. On irradiation, an electron is transfer from the citrate molecule to the co-ordinated iron (III) yielding iron (II) and a citrate radical.

Reaction Path 1

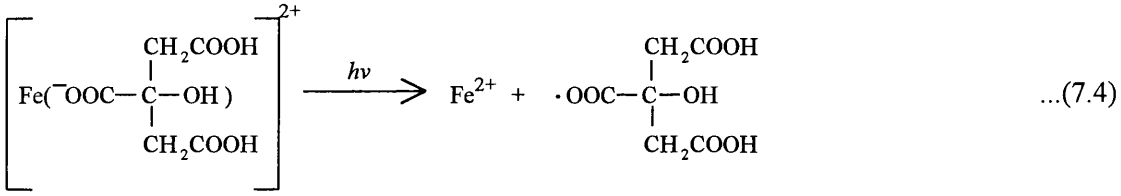

...(7.4)

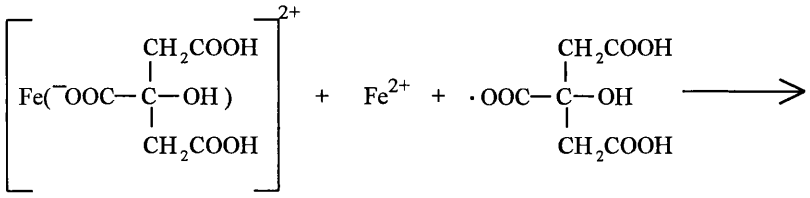

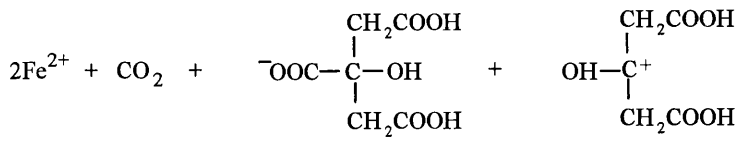

...(7.5)

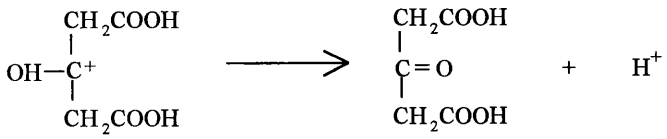

acetonedicarboxylic acid

...(7.6)

The acetonedicarboxylic acid is then spontaneously decomposed to acetoacetic acid and then degraded further to acetone and carbon dioxide as in Mechanism A.

Reaction Path 2

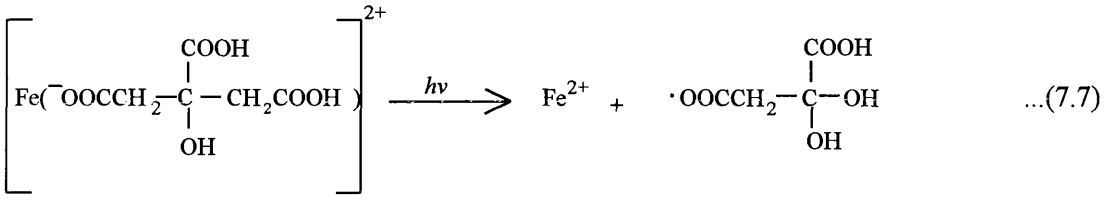

...(7.7)

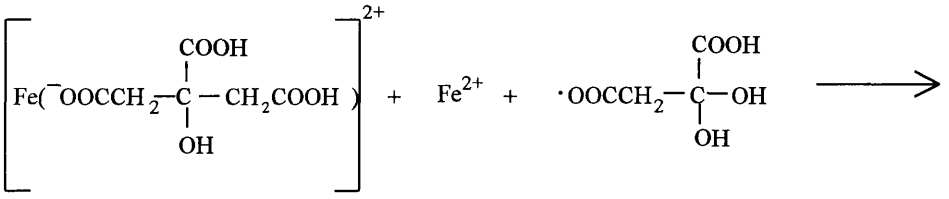

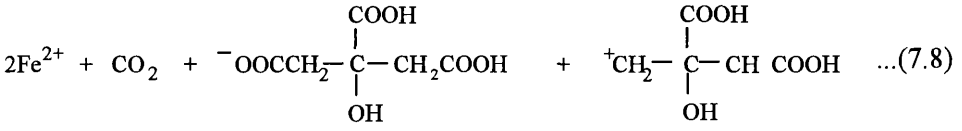

...(7.8)

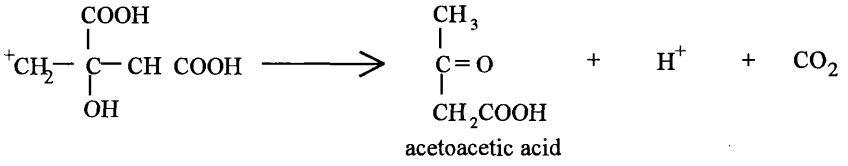

acetoacetic acid

...(7.9)

Acetoacetic acid is then broken down to acetone and carbon dioxide as in Mechanism A.

7.2.3 Experimental Verification

One way to determine if the acids and products mentioned in previous sections are one of the unknown intermediates is to compare their retention times in HPLC. Pure acids or compounds must be used or the HPLC chromatogram will show more than one peak.

When pure acetone and acetic acid were analysed using HPLC, their retention times are 16.70 and 11.52 minutes respectively (see Fig.7.2 and Fig.7.3). However the unknown intermediates have retention times of 5.95, 7.92, 9.34, 10.48 and 13.25 minutes. The results, though not conclusive, showed that acetone and acetic acids are not one of the intermediates or products formed in the experiments.

7.3 Experimental Observations

It has been observed that during the course of the experiments (photo-oxidation of citric acid using UV/H_2O_2/Fe^{3+} process), there is a change in the colour of the reacting solution. The solution was yellowish brown in colour at the beginning of the experiment. As the solution becomes exposed to UV light its colour gradually deepens and becomes reddish brown. The colour reaches a maximum intensity and then slowly fades until a colourless solution remains. If additional citric acid or hydrogen peroxide (or both) is added to the system, the reddish brown colour reappears and subsequently fades away until it became colourless once more.

Frahn (1958) explained that the solution turning from yellowish to reddish brown is due to the reaction of residual ferric iron with the intermediate products of the photochemical change. The fading away of the reddish brown colour until a colourless solution results indicates that ferric iron has been reduced completely to the ferrous state.

7.4 Conclusions

Experimental observations described in Sec.7.3 seem to indicate that the $UV/H_2O_2/Fe^{3+}$ process involves iron complexes. Thus the reaction mechanisms proposed in Sec.7.2.2 are highly probable since they explain the observations discussed in Sec.7.3 and they gave the same intermediates and products found by other workers (Sec.7.2.1). However the product acetone does not correspond to any unknown peaks in the HPLC chromatogram. Thus the system studied seems to be more complex than initially thought. Attempts to determine the intermediates using GC-MS was not successful as the method used for extraction and derivation of the intermediates was not suitable.

In conclusion, a method to derivatize the intermediates needs to be found for GC-MS analysis if the identities of the intermediates are to be known.

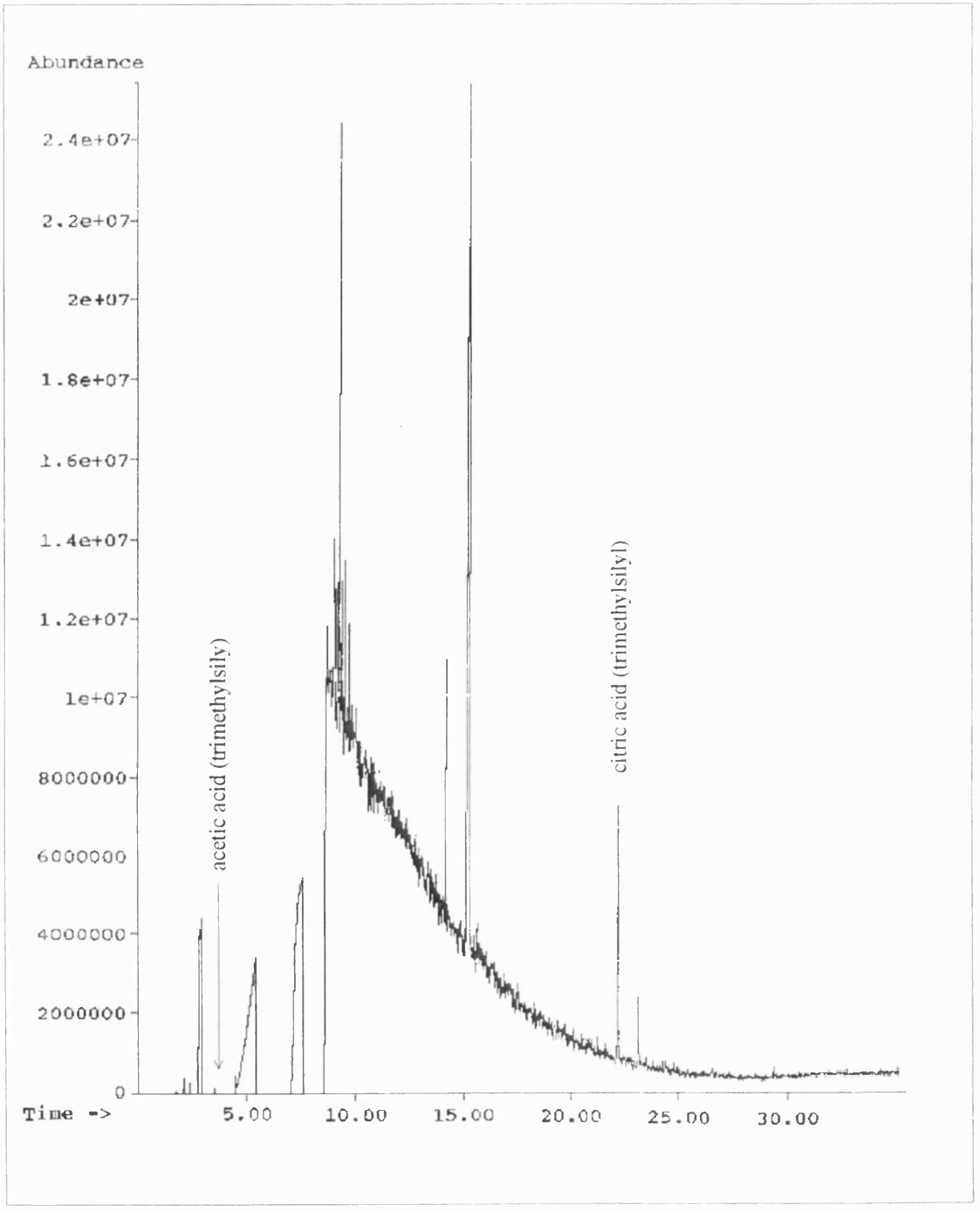

Fig.7.1 GC-MS chromatogram : result of derivation of citric acid and intermediates

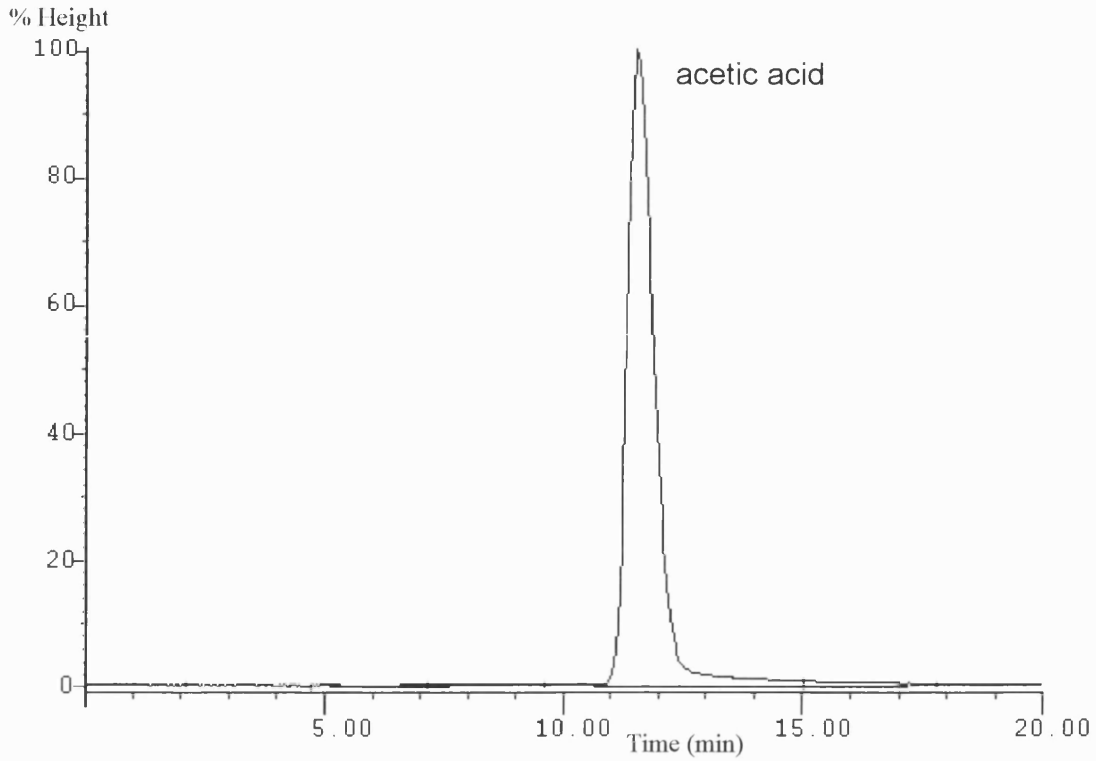

Fig 7.2 HPLC Chromatogram :Acetic Acid Only (retention time=11.52 min)

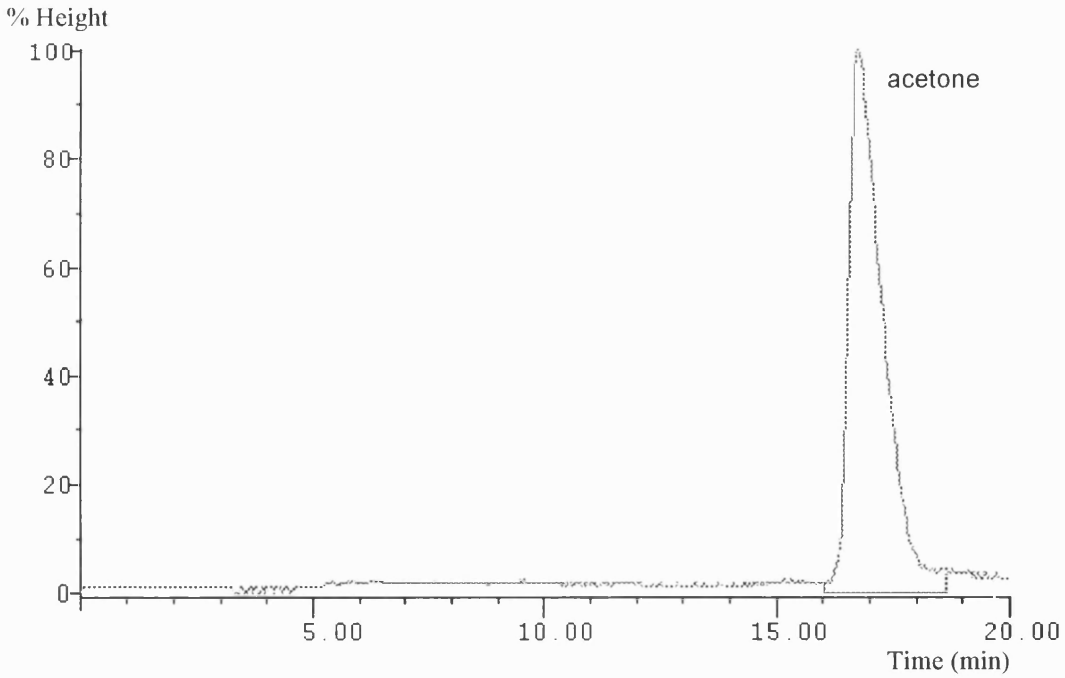

Fig 7.3 HPLC Chromatogram :Acetone Only (retention time=16.75min)

CHAPTER 8
PHOTON FLUX DETERMINATION

In Chapter 5 the most effective AOP process for the degradation of citric acid was determined and the reaction conditions to be used in later experiments for the purpose of kinetic modelling were isolated. In Chapter 6 the conclusion was drawn that only the combined effect of all reactants were significant; and that the effect of individual reactants and in combination, the pH, temperature and the presence of oxygen can be ignored. Therefore a set of experiments can now be designed for the purpose of kinetic modelling; the results of which are presented in the next chapter. This chapter will show how the photon flux used in kinetic modelling was determined. Knowledge of the local distribution of the light energy in a photochemical reactor in the presence of an absorbing substance is important in calculating the mean rate of reaction and also in determining the design of the reactor.

The following sections will firstly review relevant literature on the methods used to determined the photon flux absorbed by the reaction medium, I_{abs} (or LVREA in Sec.2.2). As discussed in Chapter 2, two radiation field models, LSSE and ESVE, were used to determine the radiation flux density vector (q_λ) which in turn were used to find I_{abs}. However, the literature also showed that when the absorbance of the reaction medium is high, a much simpler method can be used without involving the radiation field models.

The literature review was followed by sections showing the results of applying the methods proposed in the literature to current work in this research. To be absolutely sure two approaches were used to determine the photon flux absorbed by the reaction medium. Approach A will assume that all the photon flux emitted by the lamp was absorbed by the reaction medium as it was found that the absorbance of the reaction medium is very high. Approach B will use the radiation field models

mentioned previously to facilitate determination of the photon flux in the reactor. The results obtained are compared and used for the kinetic modelling described later in the chapter. The method selected was then used to calculate the photon flux produced in the pilot plant which had a 3 kW UV lamp. Finally conclusions are drawn from the results obtained.

8.1 Literature Review

For the purposes of kinetic modelling it is necessary to know the actual intensity of the UV light used and the actual intensity absorbed by the reaction solution. In physics and engineering terms, this would mean determining the photon flux produced by the UV lamp (I_e) and absorbed by the reacting solution (I_{abs}) in the reactor. The former can be easily determined as the spectral characteristic of the lamp is provided by the manufacturer. The photon flux emitted by the different power rating of the UV lamp were calculated using Eqn.8.1 and Eqn.8.2 (Li-Puma, 1994), and are as shown in Table 8.1.

$$\text{Energy (kcal/ein)} = 2.8591 \times 10^4 / \text{wavelength (nm)} \quad \ldots(8.1)$$

$$\text{Photon flux emitted by lamp, } I_e = \text{Power (watts)}/4184 \times \text{Energy (kcal/ein)} \quad \ldots(8.2)$$

Calculation of the actual photon flux absorbed by the reacting solution is more complicated. Actinometry gives the flux of photon energy emitted by the lamp and transferred into the lamp over the entire emission spectrum of the lamp (i.e. 230 to 580 nm). However the actual photon flux absorbed by the reacting solution is obtained by Eqn.8.3 (Cassano et al, 1986; Esplugas et al, 1994). This is where the radiation field models come into play.

$$I_{abs} = \Sigma_\lambda \int_V \mu_\lambda [q_\lambda] dV \quad \ldots(8.3)$$

where I_{abs} = photon flux absorbed by the reaction medium, ein s^{-1}

V = reaction volume, cm^3

μ_λ = absorbance (or coefficient of absorption) of reacting medium, cm^{-1}

q_λ = radiant energy flux density vector, ein cm^{-2} s^{-1}

The product $\mu_\lambda[q_\lambda]$ is the volumetric flux of energy absorption at the wavelength λ and depends on the concentration of the components which absorb radiation (Irazoqui et al, 1976). μ_λ is the coefficient of absorption of light by reacting medium at wavelength λ and is assumed not to vary with time.

The evaluation of q_λ and I_{abs} requires the determination of the coefficient of absorption of the individual components and of the reacting medium. The absorbances of reactants are individually determined and the absorbance of the reacting medium is taken to be the sum of the absorbances of the individual reactants, neglecting the absorbances of the photodegradated products (Esplugas et al, 1994).

$[q_\lambda]$ is the modulus of the radiation flux density vector, a function which depends on the radial and axial position in the reactor. Several models have been developed to describe the radiation field inside the photoreactor (Cassano et al, 1986; Alfano et al, 1986). Two particular models, LSSE and ESVE (see Sec.2.2), were found to be adequate in describing the radiation field inside the annular reactor. The later model is especially complex since three dimensional spherical co-ordinates are involved and both models can only be solved numerically.

However, Esplugas et al (1987) has showed that when the light absorption in the reaction chamber is high, or the width (difference between the outer and inner radii, r_o and r_i) of the reactor is large, the radiation absorption flux, I_{abs}, will tend towards the flow rate of photons entering the reactor, I_e. Thus it is not necessary in this case to solve the radiation balance (Eqn.8.3) in the reaction chamber. The authors also found that I_e could be used as a good approximation to I_{abs} when the dimensionless absorbance $\mu(r_o-r_i)$ is greater than 5.

Thus the actual values of I_{abs} can be determined with the help of actinometry (Sec.4.3). Actinometric experiments gave the decomposition rate of oxalic acid R at different UV intensities which are used to determined the photon flux emitted by the

lamp and passed into the reactor. The photon flux in the reactor is obtained by the following equation (Braun et al, 1991):

$$I_{abs} = R / \Phi_{ave} \quad ...(8.4)$$

where R = decomposition flux of oxalic acid, mol/s

Φ_{ave} = quantum yield of uranyl oxalate disappearance over the entire emission spectrum of the lamp

and Φ_{ave} is can be determined by (Li-Puma, 1995) :

$$\Phi_{ave} = \Sigma (\Phi_\lambda I_{e,\lambda} / \Sigma_\lambda I_{e,\lambda}) \quad ...(8.5)$$

where $I_{e,\lambda}$ = photon flux emitted from the lamp at wavelength λ

Φ_λ = quantum yield of uranyl oxalate at wavelength λ

The quantum yields Φ_λ of uranyl oxalate for the range of wavelength used can be obtained from the literature (Cassano et al, 1986) and are tabulated in Table 8.2.

8.2 Approach A

This section will show the high absorbance of the reacting medium which leads to the assumption that I_{abs} can be approximated by I_e as proposed by Esplugas et al (1987).

Table 8.3a, b and c showed the absorbances of individual reactants and of the reaction medium as determined by scanning photospectrometer. Since the exact wavelength of the emission spectrum of the UV lamp is known (Table 8.1) the absorbance of the reactants were determined at these wavelength. Results showed that absorbance of citric acid is zero over the emission range of the UV lamp. Table 8.3a gives the absorbances of the ferric salt in different concentration of citric acid solutions and Table 8.3b showed the absorbances of different concentration of hydrogen peroxide solution. The absorbance of the reaction medium is taken to be the sum of the individual reactants as shown in Table 8.3c. Since the differences in absorbances of the reaction medium with different concentration of hydrogen

peroxide are not great, an average of these absorbances was used in calculations. As can be seen from Table 8.3d, the high absorbance of the reaction medium gives value of $\mu(r_o-r_i)$ greater than 5 over most of the emission range of the UV lamp except at wavelength longer than 435 nm.

The results from actinometry experiments are tabulated in Table 8.4a, b, c. The decomposition rates of oxalic acid R were found for the three lamp powers used. Using Eqn.8.4 and 8.5 gives the photon flux absorbed by the reaction medium at different nominal power are obtained as shown in Table 8.5.

8.3 Approach B

This section discusses the results obtained when radiation field models are used to calculate the radiation flux absorbed by the reactor. Computer programmes written in Fortran for the two models were used to evaluate numerically the values of $\int_V[q_\lambda]dV$ and hence obtained values of I_{abs} for different power rating of the UV lamp and reaction medium.

8.3.1 LSSE Model

The derivation of and the assumptions made for the model were described in Sec.2.2.1 where I_{abs} was written as e^a, the local volumetric rate of energy absorption (LVREA). The radiant energy flux density vector q_λ in Eqn.2.45 can be written in terms of radial and axial co-ordinates (Jacob and Dranoff, 1970; Esplugas et al, 1987) :

$$q_\lambda = \frac{W_{L,\lambda}}{4\pi L}\int_x^{L+x}\frac{\exp(-\mu_{m,\lambda}a)dz'}{r^2+(z-z')^2} \qquad ...(8.4)$$

and

$$a = \left[r^2+(z-z')^2\right]^{1/2}\frac{r-r_i}{r} \qquad ...(8.5)$$

where $W_{L,\lambda}$ = photon flux emitted by the lamp at the wavelength λ, ein s^{-1}

L = length of the lamp, cm

x = axis position of the interior edge of the lamp, cm

r_i = inner radius of the reactor, cm

$\mu_{m,\lambda}$ = absorbance of the reacting medium at wavelength λ, cm^{-1}

The values of L, H, x, and r_i were determined from the geometry of the lamp and reactor and they are 14, 30, 8 and 1.75 cm respectively These fixed values and the variables, z, z' and r, are represented in Fig.8.1. The radiant energy flux density vector over the whole reactor $\int_V[q_\lambda]dV$ for the emission wavelength of the UV lamp was calculated by a computer programme complied in Fortran (included in Appendix A) and the results are tabulated in Table 8.6. The 'goodness' of the computer programme was checked with a spreadsheet using arbitrary variables. The increment dr, dz and dz' used in the calculation are 0.05, 0.05 and 0.1 respectively as smaller increments did not improved the results.

A closer inspection of the values shown in Table 8.6 reveals that they appear identical due to rounding off error. Hence the values of $\int_V[q_\lambda]dV$ from one reaction media were sufficient to be used for the calculation of I_{abs}. Using Eqn.8.3 values of I_{abs} for different lamp power were obtained and are shown in Table 8.7.

Comparing the values of I_{abs} obtained with that of I_e in Table 8.1, it will be seen that I_{abs} is greater than I_e over the major wavelength range, which clearly is not possible. However, I_{abs} for wavelengths greater than 435 nm, where the absorbance were low, provided reasonable values. The only conclusion that can be drawn is that this model cannot be applied to reaction medium which has this high absorbance. The other possibility is that the experimental data obtained is inaccurate. However this is unlikely as rigorous checks on experimental accuracy were applied. I therefore conclude that this model and its results are not applicable to the present work.

8.3.2 ESVE Model

This is a three dimensional emission model proposed by Irazoqui et al (1973) which described more accurately the radiation field in the reactor. Unlike the previous model, this model takes into account the dimension of the UV lamp. The actual derivation and assumptions made for this model were described in Sec.2.2.2. The energy flux density vector in this case is :

$$q_\lambda = \frac{W_{L,\lambda}}{2\pi V_L} \int_\phi \int_\theta \sin\theta \cos\phi (r^2 \cos^2\phi - r^2 + r_L^{\,2})^{1/2} \exp(-\mu\rho)\, d\theta\, d\phi \quad ...(8.6)$$

and

$$\rho = \frac{r\cos\phi \mp (r^2 \cos\phi - r^2 + r_L^{\,2})^{1/2}}{\sin\theta} \quad ...(8.7)$$

where ρ = the length inside the reactor travelled by the incident ray with direction (θ,ϕ), cm

r = radial co-ordinate, cm

r_L = radius of the UV lamp, cm

V_L = lamp volume, cm^3

θ,ϕ = spherical co-ordinates, rad

with the following limits :

$$\theta_1(\phi) = \tan^{-1}\left[\frac{r\cos\phi - \left(r^2\cos^2\phi - r^2 + r_L^2\right)^{1/2}}{L - z}\right] \quad ...(8.8)$$

$$\theta_2(\phi) = \tan^{-1}\left[\frac{r\cos\phi - \left(r^2\cos^2\phi - r^2 + r_L^2\right)^{1/2}}{-z}\right] \quad ...(8.9)$$

$$-\phi_1 = \phi_2 = \cos^{-1}\left[\frac{\left(r^2 - r_L^2\right)^{1/2}}{r}\right] \quad ...(8.10)$$

The average photon flux was again calculated by Eqn.8.1. Hence the final integration needs to performed is (Cerda et al, 1978) :

$$I_{abs} = \int_0^{L_R} \int_0^{2\pi} \int_{r_i}^{r_o} \mu_\lambda q_\lambda \, dr\, d\beta\, dz \quad ...(8.11)$$

Eqn.8.6 is a very complicated equation with double integration and variable limits, even with the help of computer required time consuming computational work (Cerda et al, 1978). To solve the equation numerically, help is available from NAG Fortran Library Routine Document. It was found out that D01DAF subroutine is the only one which is able to evaluate a double integral with variable limits to a specific absolute accuracy (NAG). A Fortran computer programme written to perform the integration in Eqn.8.11 is in Appendix B and the results are tabulated in Table 8.8. The increment dr and dz used in the computer programme are 0.5 as a smaller increment did not produce significant changes.

Power rating of 600W was used for the above calculations. The results showed the values of I_{abs} to be extremely small over major range of the wavelength, a very large difference compared to the values of I_e. This clearly did not reflect the actual I_{abs} in the reactor given the high absorbance of the reaction medium. Closer studied of the values in Table 8.8 between wavelength 254 and 404 nm revealed a significant contradiction in that the values of I_{abs} decreased sharply with increased absorbance of the reaction medium. This might be due to the exponential term in Eqn.8.6. However for wavelength greater than 404 nm where the absorbance is less than 2, the values of I_{abs} are reasonably good in comparision with I_e in Table 8.1.

In conclusion ESVE model can not be use when the absorbance of the reaction medium is high. Hence the values of I_{abs} from this model will not be use in the next chapter for kinetic modelling purposes.

8.4 Pilot Plant

Pilot plant experiments will be presented in Chapter 10. However as a matter of convenience, photon flux I_{abs} for the pilot plant will be presented in this section.

In Sec.8.2 and 8.3 it was shown that the only means to obtain I_{abs} for the pilot plant is by Approach A. The spectral characteristic of the 3kW lamp used in pilot plant provided by the manufacturer is presented in Table 8.1 and the actinometry done

in the pilot plant is as shown in Table 8.9. Using the values of absorbance in Table 8.3c and the procedures stated in Sec.8.1, I_{abs} for the 3kW lamp was easily calculated and was found to be $1.75*10^{-4}$ ein s^{-1}.

8.5 Conclusions

In this chapter two different approaches were used to evaluate the photon flux in the reactor. In Approach B, where radiation field models (ESVE and LSSE) were used to determine I_{abs}, the results obtained did not show the actual photon flux in the reactor. The LSSE model gave values of I_{abs} which were greater than the photon flux produced by the UV lamp I_e; while ESVE model predicted extremely small I_{abs} which did not correspond to the high absorbance of the reaction medium. The reason for this large deviation is not clear. In the literature the models were applied to empty reactor or to reaction medium of low absorbance e.g. Jacob and Dranoff (1970), Irazoqui et al (1973) and Esplugas et al (1994). Esplugas et al (1987) had shown that when $\mu(r_o-r_i)$ is greater than 5, then I_e can be used as an approximation to I_{abs} and hence the radiation field models are not necessary in the case reaction medium of high aborbance. The results in this chapter go some way to supporting the results obtained by Esplugas et al (1987). Thus only the photon flux obtained from Approach A can be used in later chapters.

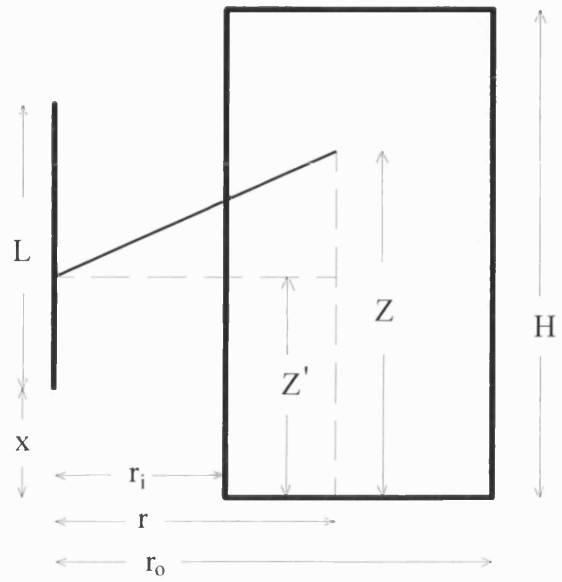

Fig. 8.1 Geometrical Diagram Showing the Variables of the Lamp and Reactor Used in LSSE Model

TABLE 8.1 Spectral Characteristic of the UV Lamp

λ nm	Nominal Power = 250W			Nominal Power = 475W		
	Power W	Energy kcal/ein	Photon flux I_e (ein/s)	Power W	Energy kcal/ein	Photon flux I_e (ein/s)
254	2.5	112.563	5.31E-06	4.75	112.563	1.01E-05
257	0.8	111.249	1.72E-06	1.52	111.249	3.27E-06
265	0.75	107.8906	1.66E-06	1.425	107.8906	3.16E-06
270	0.3	105.8926	6.77E-07	0.57	105.8926	1.29E-06
275	0.3	103.9673	6.9E-07	0.57	103.9673	1.31E-06
280	0.5	102.1107	1.17E-06	0.95	102.1107	2.22E-06
289	0.5	98.9308	1.21E-06	0.95	98.9308	2.3E-06
296	1.3	96.59122	3.22E-06	2.47	96.59122	6.11E-06
302	1.3	94.67219	3.28E-06	2.47	94.67219	6.24E-06
313	3.3	91.34505	8.63E-06	6.27	91.34505	1.64E-05
334	0.6	85.6018	1.68E-06	1.14	85.6018	3.18E-06
366	5.0	78.11749	1.53E-05	9.5	78.11749	2.91E-05
404	3.9	70.7698	1.32E-05	7.41	70.7698	2.5E-05
435	5.6	65.72644	2.04E-05	10.64	65.72644	3.87E-05
546	6.3	52.36447	2.88E-05	11.97	52.36447	5.46E-05
578	2.5	49.4654	1.21E-05	4.75	49.4654	2.3E-05
		Sum =	0.000119		Sum =	0.000226

λ nm	Nominal Power = 600W			Nominal Power = 3kW		
	Power W	Energy kcal/ein	Photon flux I_e (ein/s)	Power W	Energy kcal/ein	Photon flux I_e ein/s
254	6.0	112.563	1.27E-05	67	112.56	1.42E-04
257	1.92	111.249	4.12E-06	67	111.25	1.44E-04
265	1.8	107.8906	3.99E-06	52	107.89	1.15E-04
270	0.72	105.8926	1.63E-06	52	105.89	1.17E-04
275	0.72	103.9673	1.66E-06	55	103.97	1.26E-04
280	1.2	102.1107	2.81E-06	55	102.11	1.29E-04
289	1.2	98.9308	2.9E-06	55	101.75	1.29E-04
296	3.12	96.59122	7.72E-06	45	96.59	1.11E-04
302	3.12	94.67219	7.88E-06	71	94.67	1.79E-04
313	7.92	91.34505	2.07E-05	115	91.35	3.01E-04
334	1.44	85.6018	4.02E-06	31	85.60	8.66E-05
366	12.0	78.11749	3.67E-05	214	78.12	6.55E-04
404	9.36	70.7698	3.16E-05	91	70.77	3.07E-04
435	13.44	65.72644	4.89E-05	169	65.73	6.15E-04
546	15.12	52.36447	6.9E-05	201	52.36	9.17E-04
578	6.0	49.4654	2.9E-05	168	49.47	8.12E-04
		Sum =	0.000285		Sum =	4.89E-03

TABLE 8.2 Quantum Yields of Disappearance of Uranyl Oxalate

λ/nm	254	257	265	270	275	280	289	296
Φ_λ /mol ein^{-1}	0.6	0.6	0.59	0.58	0.58	0.58	0.58	0.57
λ/nm	302	313	334	366	404	435	546	578
Φ_λ/mol ein^{-1}	0.56	0.56	0.52	0.49	0.56	0.58	0	0

TABLE 8.3a Absorbances of Citric Acid Solution and Fe^{3+} Salt With Different Concentrations of Citric Acid

λ nm	Citric Acid only	Fe^{3+} in different citric acid concentrations		
		2500 ppm	2000 ppm	1500 ppm
254	0	82.9	75.7	67.3
257	0	81.1	74.3	65.7
265	0	77.3	71.4	63.1
270	0	75.1	69.6	61.9
275	0	72.2	67.5	60.3
280	0	69.1	65.2	58.7
289	0	62.5	60.0	56.0
296	0	56.2	54.4	50.7
302	0	51	49.8	46.65
313	0	42.7	42.05	39.55
334	0	29.6	28.1	26.25
366	0	15.9	13.8	12.35
404	0	6.7	3.95	2.8
435	0	1.634	1.442	1.134
546	0	0.041	0.035	0.033
578	0	0.029	0.026	0.026

TABLE 8.3b Absorbances of Hydrogen Peroxide With Different Concentrations of Citric Acid

λ	H_2O_2:2500ppm			H_2O_2:2000ppm			H_2O_2:1500ppm		
nm	30:1	10:1	5:1	30:1	10:1	5:1	30:1	10:1	5:1
254	6.8	2.245	1.03	5.28	1.774	0.939	3.476	1.368	0.669
257	5.824	1.922	0.878	4.62	1.52	0.807	2.92	1.176	0.573
265	3.748	1.242	0.564	2.96	0.976	0.515	2.2	0.755	0.364
270	2.776	0.919	0.416	2.204	0.721	0.382	1.636	0.562	0.273
275	2.036	0.676	0.123	1.61	0.53	0.28	1.24	0.412	0.198
280	1.488	0.493	0.224	1.176	0.387	0.203	0.907	0.302	0.145
289	0.800	0.300	0.100	0.600	0.200	0.100	0.450	0.210	0.09
296	0.512	0.168	0.075	0.398	0.131	0.069	0.308	0.105	0.048
302	0.336	0.11	0.05	0.266	0.086	0.046	0.202	0.07	0.032
313	0.152	0.05	0.022	0.12	0.04	0.022	0.1	0.034	0.014
334	0.024	0.007	0.004	0.018	0.006	0.005	0.014	0.005	0.001
366	0.008	0.001	0.003	0	0	0	0	0	0
404	0	0	0	0	0	0	0	0	0
435	0	0	0	0	0	0	0	0	0
546	0	0	0	0	0	0	0	0	0
578	0	0	0	0	0	0	0	0	0

TABLE 8.3c Absorbance of Reaction Medium

	Reaction Medium 1				Reaction Medium 2			
λ	H_2O_2 : 25000ppm Citric Acid				H_2O_2 : 20000ppm Citric Acid			
nm	30:1	10:1	5:1	Average	30:1	10:1	5:1	Average
254	89.7	85.145	83.93	86.26	80.98	77.474	76.639	78.36
257	86.924	83.022	81.978	83.97	78.92	75.82	75.107	76.62
265	81.048	78.542	77.864	79.15	74.36	72.376	71.915	72.88
270	77.876	76.019	75.516	76.47	71.804	70.321	69.982	70.70
275	74.236	72.876	72.323	73.15	69.11	68.03	67.78	68.31
280	70.588	69.593	69.324	69.84	66.376	65.587	65.403	65.79
289	63.30	62.80	62.60	62.90	60.60	60.20	60.10	60.30
296	56.712	56.368	56.275	56.45	54.798	54.531	54.469	54.60
302	51.336	51.11	51.05	51.17	50.066	49.886	49.846	49.93
313	42.852	42.75	42.722	42.77	42.17	42.09	42.072	42.11
334	29.624	29.607	29.604	29.62	28.118	28.106	28.105	28.11
366	15.908	15.901	15.903	15.90	13.8	13.8	13.8	13.80
404	6.70	6.70	6.70	6.70	3.95	3.95	3.95	3.95
435	1.634	1.634	1.634	1.63	1.442	1.442	1.442	1.44
546	0.041	0.041	0.041	0.04	0.035	0.035	0.035	0.04
578	0.029	0.029	0.029	0.03	0.026	0.026	0.026	0.03

TABLE 8.3c con't...

λ nm	Reaction Medium 3 H_2O_2 : 15000ppm Citric Acid			
	30:1	10:1	5:1	Average
254	70.776	68.668	67.969	69.14
257	68.62	66.876	66.273	67.26
265	65.3	63.855	63.464	64.21
270	63.536	62.462	62.173	62.72
275	61.54	60.712	60.498	60.92
280	59.607	59.002	58.845	59.15
289	56.45	56.21	56.09	56.25
296	51.008	50.805	50.748	50.85
302	46.852	46.72	46.682	46.75
313	39.65	39.584	39.564	39.60
334	26.264	26.255	26.251	26.26
366	12.35	12.35	12.35	12.35
404	2.80	2.80	2.80	2.80
435	1.134	1.134	1.134	1.13
546	0.033	0.033	0.033	0.03
578	0.026	0.026	0.026	0.03

TABLE 8.3d Values of $\mu(r_o-r_i)$ for Different Reaction Medium

λ nm	$\mu(r_o-r_i)$		
	1	2	3
254	280.34	254.68	224.69
257	272.92	249.00	218.58
265	257.24	236.87	208.67
270	248.53	229.78	203.85
275	237.72	222.00	197.97
280	226.96	213.81	192.24
289	204.43	195.98	182.81
296	183.47	177.45	165.27
302	166.29	162.28	151.94
313	139.02	136.86	128.70
334	96.24	91.36	85.33
366	51.69	44.85	40.14
404	21.78	12.84	9.10
435	5.31	4.69	3.69
546	0.13	0.11	0.11
578	0.09	0.08	0.08

TABLE 8.4a Results of Actinometry Experiments for Nominal Power of 250W

Time s	0.01M $KMnO_4$ used /ml	Oxalic Acid reacted /mol	Total Oxalic Acid Remained in reactor /mol
300	4.00	1.00E-04	1.55E-02
600	4.00	1.00E-04	1.55E-02
900	3.90	9.75E-05	1.51E-02
1200	3.60	9.00E-05	1.40E-02
1380	3.60	9.00E-05	1.40E-02
1560	3.60	9.00E-05	1.40E-02
1740	3.30	8.25E-05	1.28E-02
1920	3.10	7.75E-05	1.20E-02
2280	3.10	7.75E-05	1.20E-02
2460	2.60	6.50E-05	1.01E-02
2640	2.40	6.00E-05	9.30E-03
2820	2.30	5.75E-05	8.91E-03
3000	2.10	5.25E-05	8.14E-03
3180	1.90	4.75E-05	7.36E-03
3360	1.80	4.50E-05	6.98E-03
Decomposition rate of oxalic acid (mol/s) =			3.84425E-06

* Volume of reactor = 310ml, Volume of sample = 2ml

TABLE 8.4b Results of Actinometry Experiments for Nominal Power of 475W

Time s	0.01M $KMnO_4$ used /ml	Oxalic Acid reacted /mol	Total Oxalic Acid Remained in reactor /mol
0	4.00	1.00E-04	1.55E-02
60	3.90	9.75E-05	1.51E-02
120	3.90	9.75E-05	1.51E-02
180	3.80	9.50E-05	1.47E-02
240	3.60	9.00E-05	1.40E-02
300	3.60	9.00E-05	1.40E-02
360	3.30	8.25E-05	1.28E-02
420	2.90	7.25E-05	1.12E-02
480	2.00	5.00E-05	7.75E-03
540	1.30	3.25E-05	5.04E-03
600	1.30	3.25E-05	5.04E-03
660	0.90	2.25E-05	3.49E-03
720	0.90	2.25E-05	3.49E-03
780	0.80	2.00E-05	3.10E-03
840	0.70	1.75E-05	2.71E-03
900	0.80	2.00E-05	3.10E-03
Decomposition rate of oxalic acid (mol/s) =			2.10357E-05

* Volume of reactor = 310ml, Volume of sample = 2ml

TABLE 8.4c Results of Actinometry Experiments for Nominal Power of 600W

Time s	0.01M $KMnO_4$ used /ml	Oxalic Acid reacted /mol	Total Oxalic Acid Remained in reactor /mol
0	4.00	1.00E-04	1.55E-02
60	4.00	1.00E-04	1.55E-02
120	3.80	9.50E-05	1.47E-02
180	2.80	7.00E-05	1.09E-02
240	2.90	7.25E-05	1.12E-02
300	2.00	5.00E-05	7.75E-03
360	2.00	5.00E-05	7.75E-03
420	1.30	3.25E-05	5.04E-03
480	1.10	2.75E-05	4.26E-03
540	0.90	2.25E-05	3.49E-03
600	0.90	2.25E-05	3.49E-03
660	0.90	2.25E-05	3.49E-03
Decomposition rate of oxalic acid (mol/s) =			3.16458E-05

* Volume of reactor = 310ml, Volume of sample = 2ml

TABLE 8.5 Values of I_{abs} With Different Lamp Power

Nominal Power /W	I_{abs} /ein s^{-1}
250	1.05E-5
475	5.76E-5
600	8.66E-5

TABLE 8.6 Values of $\int_v q_\lambda dV$ With Different Reaction Medium and Lamp Power (LSSE Model)

λ	Reaction Medium 1			Reaction Medium 2		
nm	600W	475W	250W	600W	475W	250W
254	2.0E-05	1.6E-05	8.38E-06	2E-05	1.59E-05	8.38E-06
257	6.51E-06	5.16E-06	2.72E-06	6.51E-06	5.16E-06	2.72E-06
265	6.3E-06	4.99E-06	2.62E-06	6.3E-06	4.99E-06	2.62E-06
270	2.67E-06	2.04E-06	1.07E-06	2.67E-06	2.04E-07	1.07E-06
275	2.62E-06	2.07E-06	1.09E-06	2.62E-06	2.07E-07	1.09E-06
280	4.44E-06	3.51E-06	1.85E-06	4.44E-06	3.51E-06	1.85E-06
289	4.58E-06	3.63E-06	1.91E-06	4.58E-06	3.63E-06	1.91E-06
296	1.22E-05	9.65E-06	5.09E-06	1.22E-05	9.65E-06	5.09E-06
302	1.24E-05	9.86E-06	5.18E-06	1.24E-05	9.86E-06	5.18E-06
313	3.27E-05	2.59E-05	1.36E-05	3.27E-05	2.59E-06	1.36E-05
334	6.35E-06	5.02E-06	2.65E-06	6.35E-06	5.02E-06	2.65E-06
366	5.8E-05	4.6E-05	2.42E-05	5.8E-05	4.6E-05	2.42E-05
404	5E-05	3.96E-05	2.09E-05	5.02E-05	3.97E-05	2.1E-05
435	7.87E-05	6.23E-05	3.28E-05	7.89E-05	6.25E-05	3.29E-05
546	1.45E-04	1.15E-04	6.06E-05	1.45E-04	1.15E-04	6.06E-05
578	6.16E-05	4.89E-04	2.57E-05	6.16E-05	4.89E-05	2.57E-05

λ	Reaction Medium 3		
nm	600W	475W	250W
254	2.01E-05	1.6E-05	8.39E-06
257	6.51E-06	5.16E-06	2.72E-06
265	6.3E-06	4.99E-06	2.62E-06
270	2.57E-06	2.04E-06	1.07E-06
275	2.62E-06	2.07E-06	1.09E-06
280	4.44E-06	3.51E-06	1.85E-06
289	4.58E-06	3.63E-06	1.91E-06
296	1.22E-05	9.65E-06	5.09E-06
302	1.24E-05	9.86E-06	5.18E-06
313	3.27E-05	2.59E-05	1.36E-05
334	6.35E-06	5.02E-06	2.65E-06
366	5.8E-05	4.6E-05	2.42E-05
404	5.03E-05	3.98E-05	2.1E-05
435	7.96E-05	6.3E-05	3.32E-05
546	1.47E-04	1.16E-04	6.12E-05
578	6.16E-05	4.89E-05	2.57E-05

TABLE 8.7 Values of I_{abs} for Different Reaction Medium (LSSE Model)

λ	Reaction Medium		
nm	1	2	3
254	1.73E-03	1.25E-03	5.79E-04
257	5.46E-04	3.96E-04	1.83E-04
265	4.99E-04	3.64E-04	1.68E-04
270	2.04E-04	1.44E-05	6.71E-05
275	1.92E-04	1.41E-05	6.64E-05
280	3.10E-04	2.31E-04	1.09E-04
289	2.88E-04	2.19E-04	1.08E-04
296	6.88E-04	5.27E-04	2.59E-04
302	6.37E-04	4.92E-04	2.42E-04
313	1.40E-03	1.09E-04	5.40E-04
334	1.88E-04	1.41E-04	6.97E-05
366	9.22E-04	6.35E-04	2.99E-04
404	3.36E-04	1.57E-04	5.87E-05
435	1.29E-04	9.01E-05	3.73E-05
546	5.95E-06	4.02E-06	2.00E-06
578	1.79E-06	1.27E-06	6.68E-07
sum =	8.08E-03	4.64E-03	2.79E-03

TABLE 8.8 Values of I_{abs} With Different Reaction Medium and Lamp Power (ESVE Model)

λ	Reaction Medium		
nm	1	2	3
254	1.92E-156	9.74E-143	9.41E-127
257	5.85E-153	3.27E-140	5.55E-124
265	1.29E-144	9.68E-134	1.04E-118
270	2.35E-140	2.38E-130	1.63E-116
275	1.37E-134	3.38E-126	2.19E-113
280	1.27E-128	1.34E-121	4.33E-110
289	1.41E-116	4.54E-112	4.75E-105
296	5.69E-105	9.15E-102	2.877E-95
302	8.194E-96	1.153E-93	3.720E-88
313	7.634E-81	1.061E-79	2.351E-75
334	8.433E-59	3.438E-56	5.410E-53
366	3.678E-34	1.509E-30	4.688E-28
404	1.934E-18	9.143E-14	7.044E-12
435	9.351E-10	1.877E-09	5.685E-09
546	4.144E-08	4.144E-08	3.261E-08
578	3.743E-08	1.373E-08	1.373E-08

TABLE 8.9 Results of Actinometry Experiments for Nominal Power of 3kW

Time s	0.01M KMnO4 used /ml	Oxalic Acid reacted /mol	Total Oxalic Acid Remained in reactor* /mol
0	20.00	5.00E-04	4.83E-01
120	19.90	4.98E-04	4.80E-01
240	19.90	4.98E-04	4.80E-01
360	19.50	4.88E-04	4.70E-01
480	19.20	4.80E-04	4.63E-01
600	19.00	4.75E-04	4.58E-01
720	18.60	4.65E-04	4.49E-01
840	18.40	4.60E-04	4.44E-01
960	18.00	4.50E-04	4.34E-01
1080	17.80	4.45E-04	4.29E-01
1200	16.50	4.13E-04	3.98E-01
Decomposition rate of oxalic acid (mol/s) =			6.28712E-05

* Volume of reactor = 9.65l, Sample volume = 10ml

CHAPTER 9
MINERALIZATION RATE MODELLING

In the introduction to this thesis, the main aim of this research was highlighted : the prediction of the mineralization profile of citric acid in a pilot plant environment, and the subsequent comparison with actual experimental performance. To determine the mineralization profile of citric acid without first performing any experiments requires a knowledge of mineralization rate model which is applicable over a range of reaction conditions. Naturally, the model will work best within the concentration limits used in the modelling. The previous chapters have shown experiments carried out in batch reactor for this purpose : to determine the range of reaction conditions and to collect the necessary data for kinetic modelling of the mineralization of citric acid. This chapter will show the results of the experiments done at the range of reaction conditions mentioned above. The kinetic model is subsequently evaluated. The kinetic model obtained will be used in the next chapter to predict the performance of the pilot plant and subsequent comparison with the actual experimental results from the pilot plant. However, in this chapter, the model will first be tested by comparing it's prediction with that of actual experimental results from the batch reactor. Conclusions are then drawn.

9.1 Experimental Results

Using the reaction conditions set out in Sec.5.5, experiments were designed to cover a wide range of conditions. Since there were three different concentrations or intensity levels for each reactants, there are $3^3 = 27$ different experiments to carry out. In addition, each of the experiments was repeated three times which brought the total number of experiments to 81. The initial concentrations of citric acid used were 2500,

2000 and 1500 ppm (their respectively TOC concentrations were 834, 667 and 500). For hydrogen peroxide the concentrations used were in terms of molar ratio to that of citric acid, e.g. 30:1, 10:1 and 5:1, and they are as shown in Table 9.1. The actual radiation flux absorbed by the reactor for different power rating (250, 475 and 600W) of UV lamp had been determined in Chapter 8 and were as shown in Table 8.5. Experiments were carried out at the above conditions for 10 minutes (see Sec.5.5). Raw data from the experiments were plotted with the help of computer software Fit2 ver.1.17 (Shareware, UNIX) and the initial reaction rate for each experiments were determined and tabulated in Table 9.2. Average values of initial reaction rates from three experiments were used for the kinetic modelling in later sections of this chapter.

9.2 Mineralization Rate Model

In Sec.6.1 it was determined that the photochemical reaction was due to the combined effect of all the reactants. In the literature the only researchers who studied similar process and proposed a kinetic rate model for their system were Yue and Legrini (1989). They modelled the rate of TOC reduction for a UV/H_2O_2 system by a power law of the following forms:

$$r = k_1[H_2O_2]^a[TOC]^b \qquad ...(9.1)$$

$$r = k_2[TOC]^c \qquad ...(9.2)$$

Eqn.9.2 was found to be applicable when a large excess of hydrogen peroxide was used.

Francis (1987) who studied UV/ozone process proposed the overall rate of reduction of TOC concentration (rate of mineralization) for the process as :

$$-\frac{d[TOC]}{dt} = k_{TOC} I^a [O_3]^b [TOC]^d \qquad ...(9.3)$$

where $[O_3]$ = concentration of dissolved ozone

I = UV radiation intensity

k_{TOC} = constant

a, b, d = exponential constants

Hence a kinetic model for the mineralization rate of citric acid was proposed as :

$$r = -k[TOC]_o^a[H_2O_2]_o^b[I_{abs}]_o^c \quad ...(9.4)$$

where r = rate of mineralization, ppm s^{-1}

$[TOC]_o$ = initial total organic carbon concentration, ppm

$[H_2O_2]_o$ = initial hydrogen peroxide concentration, ppm

$[I_{abs}]_o$ = initial photon flux absorbed by the reactor, ein s^{-1}

k = reaction rate constant

a, b, c = exponential constants

Since the concentration of ferric sulphate pentahydrate was constant through out the experiments, any effect due to its presence will be accounted for in the reaction rate constant k. The negative sign in the model account for the decreasing TOC concentration.

Computer software Minsq (Micromath Inc., U.S.) was used to estimate the best values for the parameters k, a, b and c. A combination of Simplex and least square methods were used for this purpose. The Simplex method is an algorithm for fitting non-linear equations to data and it was used for an initial parameter estimation : to locate the point in the parameter space where the sum of squares is a minimum. This was followed by least squares parameter optimisation to find a local minimum, possibly the global minimum, of the sum of squared deviations between observed data and model calculations.

9.3 Mineralization Rate Equation

Results from the parameter estimator gave the values of k, a, b and c to be 1.0094×10^{-4}, 0.74, 0.39 and -0.11 respectively. Thus the model has the form :

$$r = -1.0094\text{x}10^{-4}[TOC]_o^{0.74}[H_2O_2]_o^{0.39}[I_{abs}]_o^{-0.11} \quad ...(9.5)$$

The statistical summary and the goodness of fit statistics for the data set is given in Table 9.3 and the residual analysis was tabulated in Table 9.4. They indicate that the data has a very good correlation of 93.5% and there was indication of a systematic non-random trend in the residuals.

The above model showed the mineralization rate to be proportional to the concentration of hydrogen peroxide and concentration of TOC, but inversely proportional to the intensity of the UV lamp. This result is significant and unusual since one would expect the reaction rate to be proportional to the UV light intensity. Double-checked with the raw data in Table 9.2 only reaffirm the above result : there seems to be a general trend of decreasing in r_0 with increasing I_{abs}. The literature does not showed any precedent cases or provide any clue to its explanation. One possible explanation is that higher UV light intensity produces rapidly much more radicals which have a higher chances of reacting with one another than with the organic acid and intermediate compounds.

9.4 Computer Simulation

Before the mineralization rate model obtained in the last section was used on pilot plant, it's 'reliability' was first tested against the experimental results from the batch reactor. A Fortran computer programme using the above model was written to simulate the mineralization profile of citric acid in batch reactor (Appendix C). The concentrations of reactants were chosen to represent both ends of the concentration spectrum. The concentration of citric acid chosen was 2500 and 1500 ppm with hydrogen peroxide concentration in molar ratio of 5 and 30 to 1 with respect to citric acid concentration. The nominal power of the UV lamps used were 250 and 600W.

Results from the computer simulation and the actual experimental results were compared graphically as shown in Fig.9.1 to Fig.9.8. Apart from one or two, the majority of the graphs showed a very good fit between the model and the actual

mineralization profiles. Calculations showed that at ten minutes the errors were well below 15%. The only large deviation was that shown by Fig.9.4 with an error of 55%. This appears to be an exceptional case, probably due to experimental error.

9.5 Conclusions

A mineralization rate model is proposed which has the form $r = -k[TOC]_o^a[H_2O_2]_o^b[I_{abs}]_o^c$ and the average initial rate data from a set of 81 experiments was used to determine the unknown parameters with the help of parameter estimator Minsq. The mineralization rate equation obtained was $r = -1.0094\text{x}10^{-4}[TOC]_o^{0.74}[H_2O_2]_o^{0.39}[I_{abs}]_o^{-0.11}$. The computer programme was written to simulate the mineralization profiles of citric acid using both ends of the concentration spectrum. Mineralization profiles compare very well with the actual experimental results from the batch reactor. This gave confidence that the model would work for the pilot plant as well.

TABLE 9.1 Concentration Of Hydrogen Peroxide With Respect To Citric Acid

Citric Acid /ppm	$\frac{[H_2O_2]}{[\text{Citric Acid}]}$	$[H_2O_2]$ /ppm
2500	30	12134.77
	10	4044.922
	5	2022.461
2000	30	9707.814
	10	3235.938
	5	1617.969
1500	30	7280.86
	10	2426.953
	5	1213.477

TABLE 9.2 Initial Rate Data From Experimental Results

$[TOC]_o$ /ppm	$[H_2O_2]_o$ /ppm	$[I_{abs}]_o$ /ein s^{-1}	r_o from experiments			Average r_o /ppm s^{-1}
			1	2	3	
834	2022.461	$1.05*10^{-5}$	1.68	1.70	2.70	2.03
667	1617.969		1.44	1.41	1.49	1.45
500	1213.477		1.01	0.91	0.99	0.97
834	4044.922		3.49	3.33	3.53	3.45
667	3235.938		3.03	2.93	2.73	2.90
500	2426.953		1.97	1.95	1.56	1.83
834	12134.77		4.36	4.23	3.84	4.14
667	9707.814		3.34	3.45	3.12	3.30
500	7280.86		1.91	1.99	1.84	1.91
834	2022.461	$5.76*10^{-5}$	2.15	1.48	1.49	1.71
667	1617.969		0.92	0.76	0.92	0.87
500	1213.477		0.85	0.82	0.71	0.79
834	4044.922		2.96	2.61	2.70	2.76
667	3235.953		2.39	2.20	3.04	2.54
500	2426.953		1.82	1.51	1.83	1.72
834	12134.77		3.79	3.55	4.39	3.91
667	9707.814		2.98	3.10	2.57	2.88
500	7280.86		2.68	2.41	2.50	2.53
834	2022.461	$8.66*10^{-5}$	1.14	1.22	1.27	1.21
667	1617.969		1.02	1.01	1.08	1.03
500	1213.477		0.69	0.77	0.69	0.71
834	4044.922		2.23	2.60	2.82	2.55
667	3235.938		2.92	2.07	2.05	2.35
500	2426.953		1.48	1.46	1.38	1.44
834	12134.77		3.84	3.20	3.12	3.38
667	9707.814		2.83	2.67	2.67	2.72
500	7280.86		1.76	1.79	1.92	1.82

TABLE 9.3 Statistical Summary And Goodness-of-fit Statistic For Data

Statistical Summary for Data		
For k :		
Estimate :	$1.0094*10^{-4}$	
Std Dev :	$1.2839*10^{-4}$	
95% Range (Univar) :	$-1.6466*10^{-4}$	$3.6654*10^{-4}$
95% Range (S-Plane) :	$-3.2841*10^{-4}$	$5.3028*10^{-4}$
For a :		
Estimate :	0.74217	
Std Dev :	0.16529	
95% Range (Univar) :	0.40025	1.0841
95% Range (S-Plane) :	0.18946	1.2949
For b :		
Estimate :	0.38720	
Std Dev :	0.042789	
95% Range (Univar) :	0.29868	0.47571
95% Range (S-Plane) :	0.24411	0.53028
For c :		
Estimate :	-0.10949	
Std Dev :	0.031424	
95% Range (Univar) :	-0.17449	0.044481
95% Range (S-Plane) :	-0.21457	0.0044057

Variance-CoVariance Matrix :

$1.2210*10^{-7}$			
$-1.4286*10^{-6}$	0.013561		
$7.6715*10^{-6}$	$-8.9340*10^{-10}$	0.0073141	
-0.0001452	-0.01353	$2.0555*10^{-9}$	0.20235

Correlation Matrix :

1.00000			
-0.035108	1.00000		
0.25671	$-8.9706*10^{-8}$	1.0000	
-0.92373	-0.25828	$5.343*10^{-8}$	1.0000

TABLE 9.3 con't...

Goodness-of -it Statistics		
	Weighted	Unweighted
Sum of square observations:	153.64	153.64
Sum of square deviations :	3.1052	3.1052
Standard deviation of data :	0.36744	0.36744
r-squared :	0.97879	0.97879
coeff of determination :	0.87344	0.87344
correlation :	0.93512	0.93512
Model selection criterion :	1.7708	1.7708

TABLE 9.4 Residual Analysis

The following are nomalized parameters with an expected value of 0.0. Values are in units of standard deviations from the expected value.

The serial correlation is 3.57 which indicates a systematic non-random trend in the residuals.

Skewness is -1.71 indicating the likelihood of a few large negative residual having an unduly large effect on the fit.

Kurtosis is 0.02 which is probably not significant.

The weighting factor used was 0.00 leading to a heteroscedacticity of -0.08 which suggests an optimal weight factor for this fit of about -0.08.

Fig 9.1 Photo-oxidation of Citric Acid
Mineralization Profile in Batch Reactor
Model vs Experimental Result

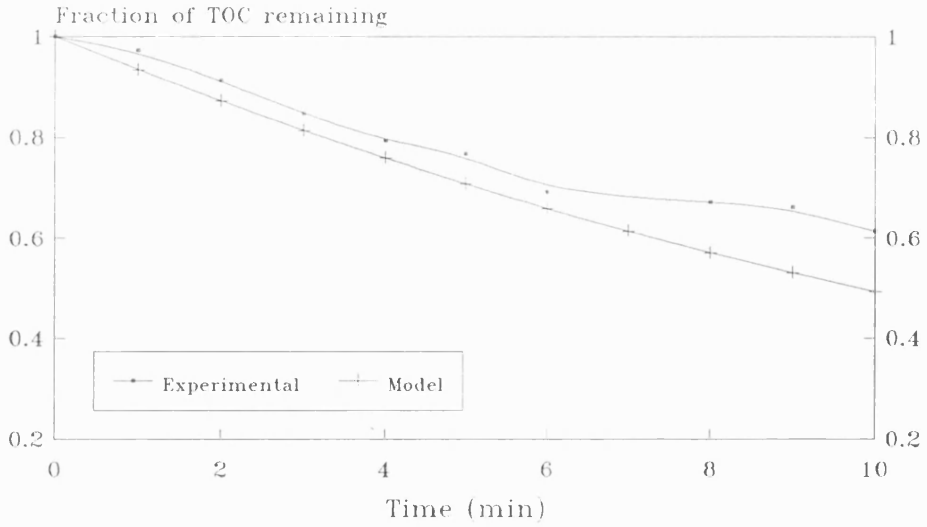

Medium Pressure Lamp(Nominal Power=250W)
Moles H2O2:Citric Acid=5
Initial TOC = 500ppm

Fig 9.2 Photo-oxidation of Citric Acid
Mineralization Profile in Batch Reactor
Model vs Experimental Results

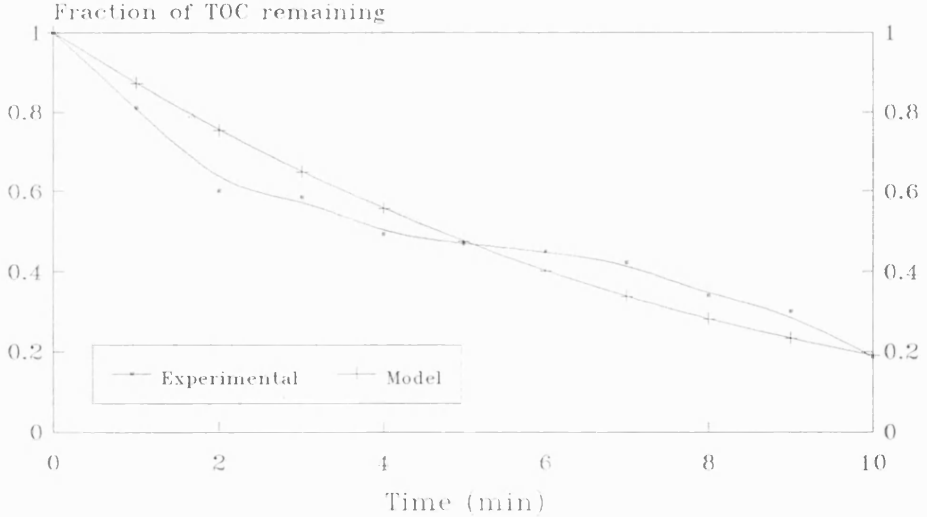

Medium Pressure Lamp(Nominal Power=250W)
Moles H2O2:Citric Acid=30
Initial TOC = 500ppm

Fig 9.3 Photo-oxidation of Citric Acid
Mineralization Profile in Batch Reactor
Model vs Experimental Result

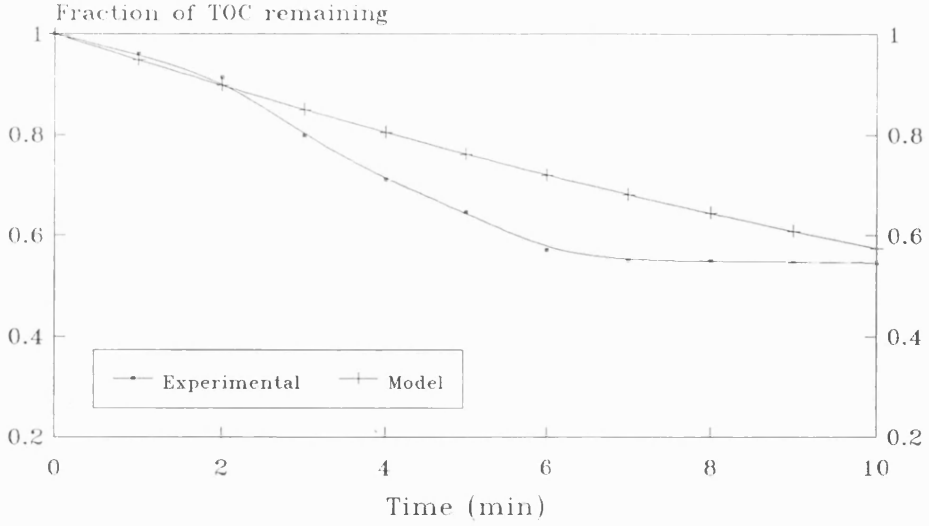

Medium Pressure Lamp(Nominal Power=600W)
Moles H202:Citric Acid=5
Initial TOC = 500ppm

Fig 9.4 Photo-oxidation of Citric Acid
Mineralization Profile in Batch Reactor
Model vs Experimental Result

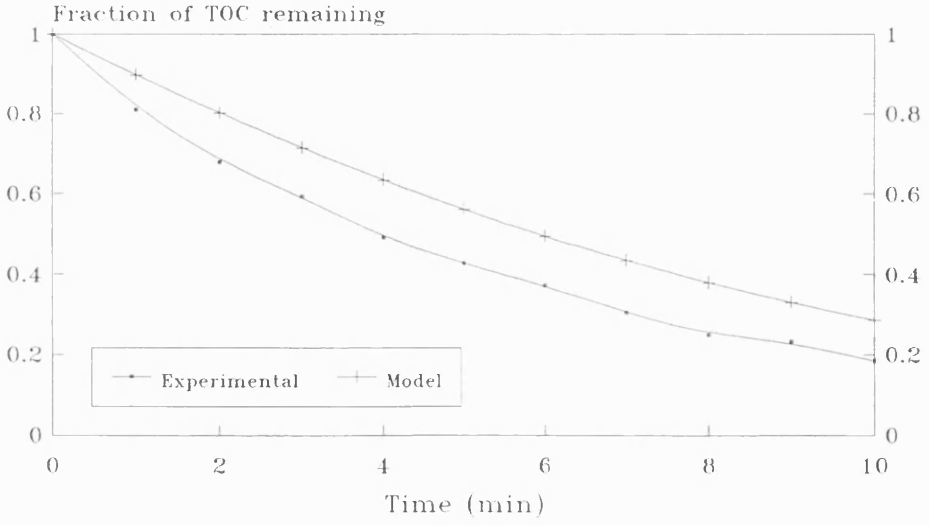

Medium Pressure Lamp(Nominal Power=600W)
Moles H202:Citric Acid=30
Initial TOC = 500ppm

Fig 9.5 Photo-oxidation of Citric Acid
Mineralization Profile in Batch Reactor
Model vs Experimental Result

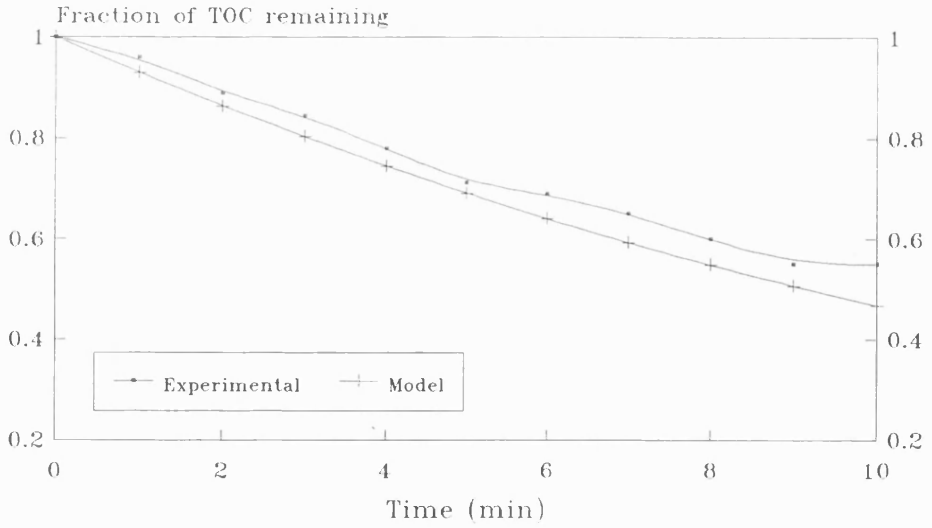

Medium Pressure Lamp(Nominal Power=250W)
Moles H2O2:Citric Acid=5
Initial TOC = 2500ppm

Fig 9.6 Photo-oxidation of Citric Acid
Mineralization Profile in Batch Reactor
Model vs Experimental Result

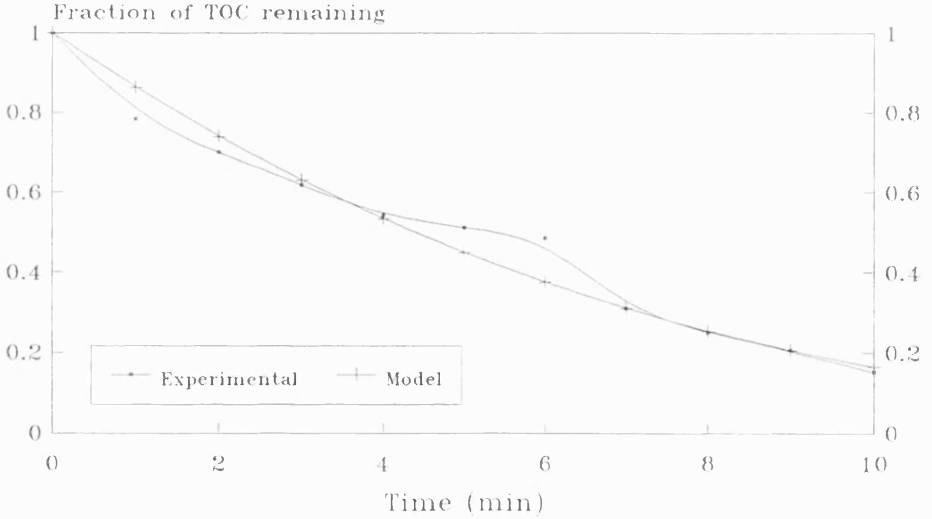

Medium Pressure Lamp(Nominal Power=250W)
Moles H2O2:Citric Acid=30
Initial TOC = 2500ppm

Fig 9.7 Photo-oxidation of Citric Acid
Mineralization Profile in Batch Reactor
Model vs Experimental Result

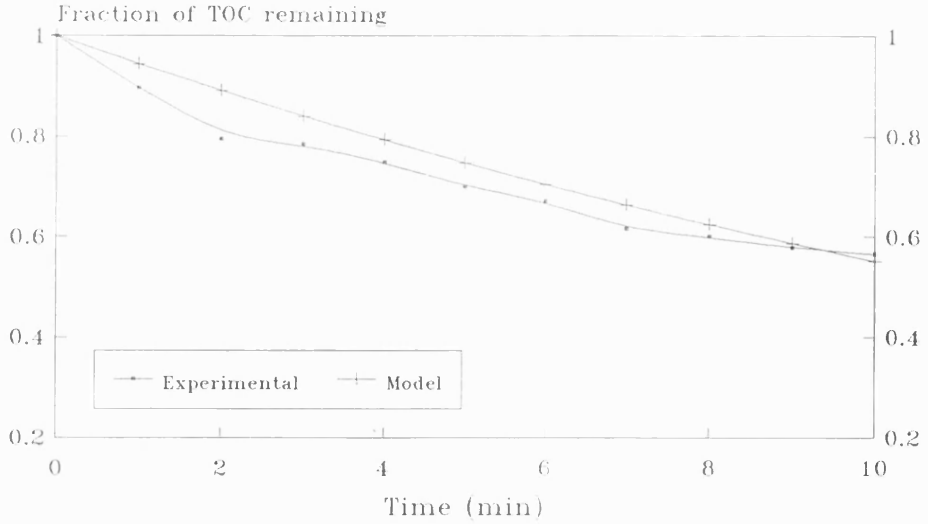

Medium Pressure Lamp(Nominal Power=600W)
Moles H2O2:Citric Acid=5
Initial TOC = 2500ppm

Fig 9.8 Photo-oxidation of Citric Acid
Mineralization Profile in Batch Reactor
Model vs Experimental Result

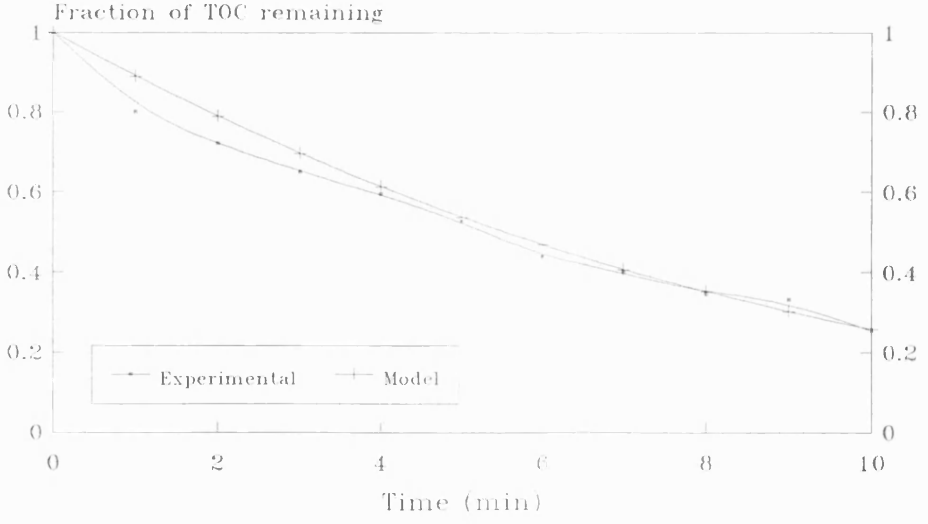

Medium Pressure Lamp(Nominal Power=600W)
Moles H2O2:Citric Acid=30
Initial TOC = 2500ppm

CHAPTER 10
PILOT PLANT :
MODEL AND EXPERIMENTAL

With the mineralization rate model established and tested in the last chapter, it is now time to apply the model to the prediction of the mineralization profile for the pilot plant. The following sections will show all the physical and financial constraints which restricted the number of experiments being done, and their reaction conditions. Before the actual calculation for the mineralization profiles can be performed, assumptions are made so that mass balances for the pilot plant can be carried out. The mass balances over the reactor and tank are then made for the individual reactants. Results obtained by computer simulation show large differences between the models and the experimental mineralization profile. Three approaches were then adopted to determine the reasons behind the poor results. New assumptions were made and refined and new mineralization rate equations were modelled. The results obtained are discussed, and finally conclusions and recommendations are made.

10.1 Physical Constraints

In Chapter 3 the physical dimensions of the pilot plant were described. It had been determined that the volume of the reactor was 88.41 litres and the reservoir tank had a volume of more than 130 litres. However it was not possible to carry out experiments using the whole volume of the pilot plant as this would have meant huge quantities of reactants being needed. Thus it was decided to use the minimum volume of fluid necessary to create a continuous flow into the reactor. After some trials, the total volume needed for that purpose was found to be 138 litres. With volume of the reactor known and the volume of the pipeworks was calculated to be about 13 litres,

thus the volume of fluid that should remained almost constant in the tank during experimental operation was 37 litres. The recycling volumetric rate of the fluid was maintained at a maximum rate of 2.53 litres s^{-1} (obtained from calibration graph provided by manufacturer) for all experiments.

10.2 Reaction Conditions

As mentioned previously, due to financial constrains a limited number of key experiments were carried out in the pilot plant. A well spaced selection of reaction conditions were selected, except the nominal power of the UV lamp and the concentration of ferric sulphate pentahydrate. The former was fixed by the manufacturer and the photon flux it produced was 1.75×10^{-4} ein s^{-1} (Sec. 8.4). The concentration of the ferric salt used was fixed 0.01 mol l^{-1} as determined in Chapter 8. A total of three experiments were carried out : (i) citric acid concentration of 1500 ppm with molar ratio of hydrogen peroxide to citric acid of 6:1; (ii) citric acid concentration of 2000 ppm with molar ratio of hydrogen peroxide to citric acid of 7:1; and (iii) citric acid concentration of 2500 ppm with molar ratio of hydrogen peroxide to citric acid of 12:1. The experimental procedures were described in Chapter 3.

10.3 Assumptions Made

A few assumptions had to be made before any calculations could be done to establish the mineralization profile. The first assumption was that the reactants were perfectly mixed in the reactor and in the tank at all times. In other words, concentrations of the reactants in the outlet were the same as that inside the vessels. Secondly, it had been calculated that fluid spent about 35 seconds in the reactor and 6 seconds in the paperworks and tank. Since it spend a relatively short time outside the reactor this can be ignored. Thirdly, reaction occurs in the reactor only and none

occurs in the pipeworks and tank. Although Chapter 6 has shown that although some oxidation processes can occur even without the assistance of UV light, the reaction rates are so slow that they can be ignored.

10.4 Mass Balances

In order to calculate the mineralization profile in the pilot plant mass balances incorporating the mineralization rate equation were needed. The mineralization rate equation which had been established in the last chapter was $r = -1.0094\text{x}10^{-4}[TOC]_o^{0.74}[H_2O_2]_o^{0.39}[I_{abs}]_o^{-0.11}$. The other known variables were the volume of fluid in the reactor and tank, the volumetric flow rate of the recycling fluid and the initial concentrations of the reactants as stated in sections above.

Mass balances were carried out over the reactor and tank for the TOC and hydrogen peroxide individually. In the following section, C_1 and H_1 represented the concentration of TOC and hydrogen peroxide (ppm) respectively leaving the tank and entering the reactor; while C_2 and H_2 represented the same reactants concentration leaving the reactor and entering the tank. F, r, V_R and V_T were the volumetric flow rate (litre s^{-1}), mineralization rate (ppm s^{-1}), volume of fluid in the reactor and tank respectively (litre).

10.4.1 Reactor

Consider TOC:

(Mass Flow Rate of TOC in) - (Mass Flow Rate of TOC out) -

(Rate of Conversion of TOC) = (Rate of Accumulation of TOC)

$$FC_1 - FC_2 - rV_R = -\frac{dC}{dt}V_R$$

let $a=F/V_R$

$$aC_1 - aC_2 - r = -\frac{dC}{dt}$$

At small time interval t,

$$aC_1 - aC_2 - r = -\frac{C_{t=0} - C_{t=t}}{t}$$

At t=0, C=C_1 and at t=t, C=C_2

$\therefore$

$$aC_1 - aC_2 - r = -\frac{C_1 - C_2}{t}$$

$$C_2 = \frac{t(aC_1 - r) + C_1}{1 + at} \qquad ...(10.1)$$

In the same way, mass balance for the hydrogen peroxide produced :

$$H_2 = \frac{t(aH_1 - r) + H_1}{1 + at} \qquad ...(10.2)$$

10.4.2 Tank

Consider TOC in small time increment t:

Mass of TOC in = $C_2 F\, t$

Mass of TOC remaining = $C_1(V_T - F\, t)$

$\therefore$ Concentration of TOC in tank = $\frac{C_2 Ft + C_1(V_T - Ft)}{V_T}$

$\therefore$ Concentration of TOC in the outlet = $\frac{C_2 Ft + C_1(V_T - Ft)}{V_T}$ ...(10.3)

Similarly for hydrogen peroxide,

Concentration of hydrogen peroxide in the outlet = $\frac{H_2 Ft + H_1(V_T - Ft)}{V_T}$ ...(10.4)

10.5 Model vs Experimental Results

To produce a simulation of the mineralization profile in the pilot plant a Fortran computer programme was compiled using the above mass balances (Appendix D). The time increment used was one second.

Both the model and experimental results for the three experiments were compared graphically in Figures 10.1 - 10.3. It can be seen clearly that the model fails to described within limits of errors the actual mineralization profile of citric acid in the pilot plant. Why this was so while it should showed good fit for the batch

experiments as seen in the last chapter was not clear. The next section attempts to determine the reasons for this discrepancy.

10.6 Alternative Models

Efforts were made to discover the reasons behind the large discrepancies between the model and experimental results. In the course of these attempts new assumptions were made and new mineralization rate models were proposed. Three approaches were used and are described below.

Approach A assumed that the rate equation was wrong because the statistical data used in its determination covered too wide a concentration range. New rate equations were determined which used a narrower band of concentration and these equations were applied to pilot plant where appropriate.

Approach B proposed a new assumption. The pilot plant was assumed to be more efficient than the batch reactor due to its more powerful lamp and size of the reactor; hence its mineralization rate was faster by a certain factor over the batch reactor. To simulate this, the mineralization rate was multiplied by a factor of 6, 8, 10 and exp(t), where t was the time in minutes.

The last approach, Approach C, assumed that the initial assumption made in Sec.10.3 was wrong. New assumption are proposed that change the mass balances in the pilot plant. The volume of fluid in the tank was assumed to be so small that it did not affect in any way the concentration of fluid entered the tank. In fact this assumption treats the pilot plant like a big batch reactor with its reaction fluid being constantly recycle.

10.6.1 Approach A

One possible reason for the poor fit might be because of too wide a concentration range used in the modelling of the mineralization rate. In this section, mineralization rate equations are determined as in Chapter 9, but used only over a specific range of hydrogen peroxide concentrations. These rate equations are applied to simulate the mineralization profile of pilot plant where their hydrogen peroxide concentrations were similar. The mineralization rate equations determined are tabulated in Table 10.1. Figs.10.4 - 10.6 showed the results of the mineralization profiles derived from these models, as compared with actual experimental results. They do not show any significant improvement over the mineralization profiles obtained in the previous section.

10.6.2 Approach B

From Fig.10.1 to Fig.10.3 it can be seen that the actual mineralization rates were much faster than those of the model. This might be due to the higher power of the UV lamp (however in the last chapter it had been shown that the initial mineralization rate decreased with increased lamp power) or larger size of the reactor. Whether this trend can be applied to the high power lamp is not certain since the only way to determine this is experimentally. However, for present circumstances, efforts were made to correct the differences in the mineralization rates between the model and the experimental results. It was assumed, for demonstrative purpose, that the assumptions made above were correct and the mineralization rate model can be used if only it was multiplied by a factor. The mineralization rate was multiplied by a factor of 6, 8, 10 and exponential of time, exp(t) and the mineralization profile for each experiments was determined as before in Sec.10.4 and Sec.10.5. The results were as shown in Fig.10.7 to Fig.10.9.

10.6.3 Approach C

In Sec.10.3 an assumption was made that fluid from the reactor enters the tank and is perfectly mixed with the fluid in the tank before being pumped into the reactor again. This assumption is commonly made and applied in reaction engineering. This section will modified this assumption. Since the volume of fluid maintained in the tank was small and the volumetric flow rate was high, it can be assumed that the fluid did not mix well in the tank but was pumped straight back into the reactor. In other words the existence of the tank was ignored. Thus only the mass balance over the reactor (Sec.10.4.1) was required. The computer programme in Sec.9.4 was modified and used here (Appendix E). The results of this model were presented as Model E in Fig.10.10 to Fig.10.12. It can be seen that the model describes the actual mineralization profile quite well for the first ten minutes, before divergence occurs. An extension to the assumption made above is proposed : after ten minutes the fluid in the tank has an effect on the lower concentration of the incoming fluid. In other words, for the first ten minutes Model E is applied and subsequently reverts back to the original model described in Sec.10.4. The mineralization profiles described by this new model are represented as Model F in Figs.10.10 - 10.12.

10.7 Results and Discussion

The results from Approach A provided little improvement to the mineralization profile over the initial model. Results from Fig.10.4 to Fig.10.6 showed that the mineralization profiles produced by models have very different trends to those seen experimentally. The mineralization profiles of the models were more or less straight lines while those of the actual profiles were more like exponential or polynomial; it was similar to the results obtained in Sec.10.5. This showed that the problem probably did not lie with the data.

Approach B also showed poor results. It was clear that the exponential factor can be ruled out as a possible factor while the rest produced mineralization profiles

which had similar trends to those seen experimentally. The similarity ends here. The same factor did not produce the same profile relative to the actual profile. The differences or errors between the model and actual profile were too great to consider this model as a possibility. Thus this model was found to be invalid.

Results from Approach C showed Model E worked rather well for the first ten minutes of the experiments. And the errors in this period were well below 10% (with the exception of a 12.4% error in Fig.10.12). Thus it had been shown that the mineralization rate equation determined in the last chapter could work very well in predicting the mineralization profile in the pilot plant, up to a point. Its success depends very much on the whether the assumptions made described accurately the situations inside the pilot plant. The initial assumptions made were merely following the norm in reaction engineering and the results had showed that it was not suitable in this case. From the graphs Fig.10.10 to Fig.10.12 it can be seen that for the first ten minutes the actual mineralization profile showed an almost constant steep gradient and then a pronounced changed in gradient which was less steep. The most probable explanation was that the mineralization rate in the pilot plant was very fast in the first ten minutes due to the high initial concentration of the reactants. However after ten minutes when the concentrations of the reactants had fall below a certain level, they affected the mineralization rate such that it began to proceed more slowly. Another probable reason was that more intermediate compounds were formed which were less easily mineralised.

10.8 Conclusion and Recommendations

There appears to be nothing wrong in the mineralization rate equation determined from the last chapter, and it can be used successfully in a pilot plant environment. However, caution is required to make sure the assumptions made are applicable to the actual situation in the pilot plant. In addition there is a limit imposed on the model : it can only predict the mineralization profile, within reasonable limits

of errors, in the pilot plant for the first ten minutes. To require the model to predict the mineralization profile for a longer period will required more studies and research, or the development of a totally new model. More pilot plant experiments are needed to verify the reliability of the above model for different reaction conditions. However all these are beyond the scope of this current study.

TABLE 10.1 Alternative Mineralization Rate Models Using Specific Range of Concentration of Hydrogen Peroxide

Model	Molar Ratio of $[H_2O_2]$:[Citric Acid]	Mineralization Rate Equation
A	5:1 & 10:1	$r = 8.1616\text{x}10^{-5}[TOC]_o^{0.15}[H_2O_2]_o^{0.97}[I_{abs}]_o^{-0.13}$
B	10:1	$r = 2.1806\text{x}10^{-4}[TOC]_o^{0.52}[H_2O_2]_o^{0.52}[I_{abs}]_o^{-0.11}$
C	10:1 & 30:1	$r = 2.0191\text{x}10^{-4}[TOC]_o^{0.89}[H_2O_2]_o^{0.20}[I_{abs}]_o^{-0.10}$
D	30:1	$r = 9.4946\text{x}10^{-5}[TOC]_o^{0.56}[H_2O_2]_o^{0.56}[I_{abs}]_o^{-0.09}$

Fig. 10.1 Mineralization Profiles
Model vs Experimental Result

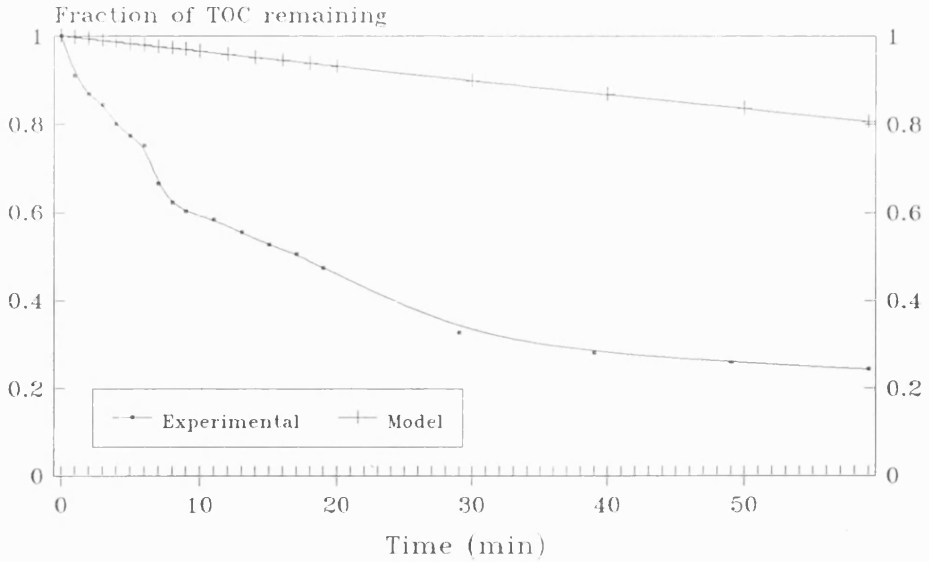

Medium Pressure Lamp (Nominal Power=3kW)
Moles H202 : Citric Acid = 6
Initial TOC = 500 ppm

Fig. 10.2 Mineralization Profile
Model vs Experimental Result

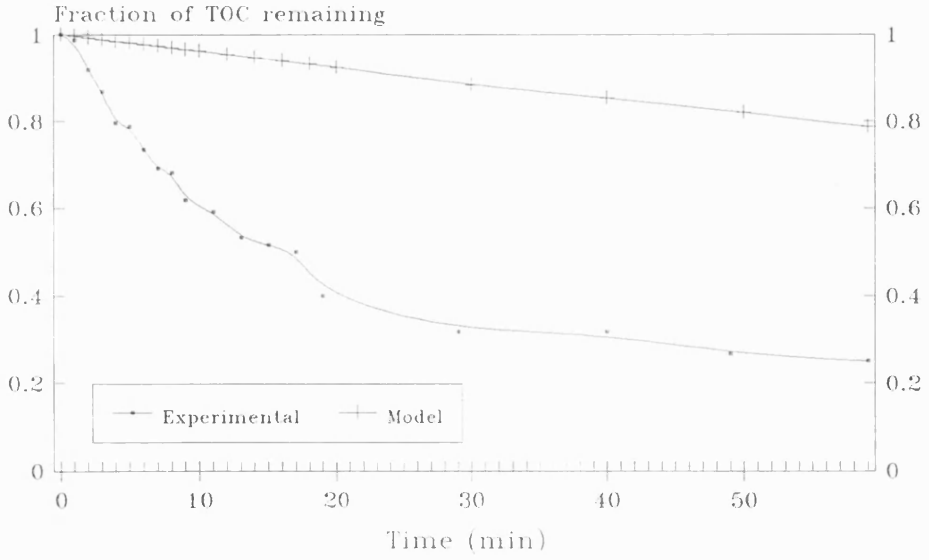

Medium Pressure Lamp (Nominal Power=3kW)
Moles H202 : Citric Acid = 7
Initial TOC = 667ppm

Fig. 10.3 Mineralization Profile
Model vs Experimental Result

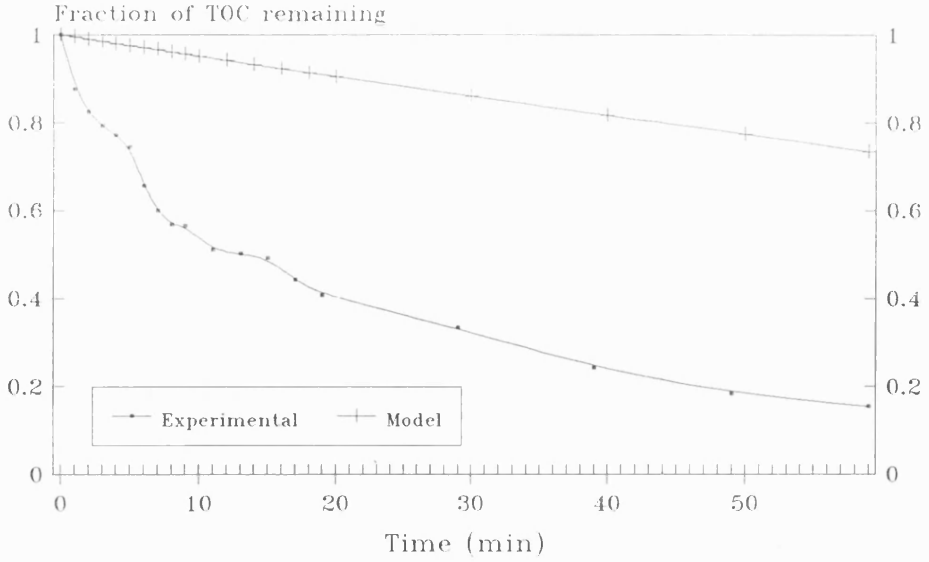

Medium Pressure Lamp (Nominal Power=3kW)
Moles H202 : Citric Acid = 12
Initial TOC = 834 ppm

Fig. 10.4 Mineralization Profiles
Models vs Experimental Result

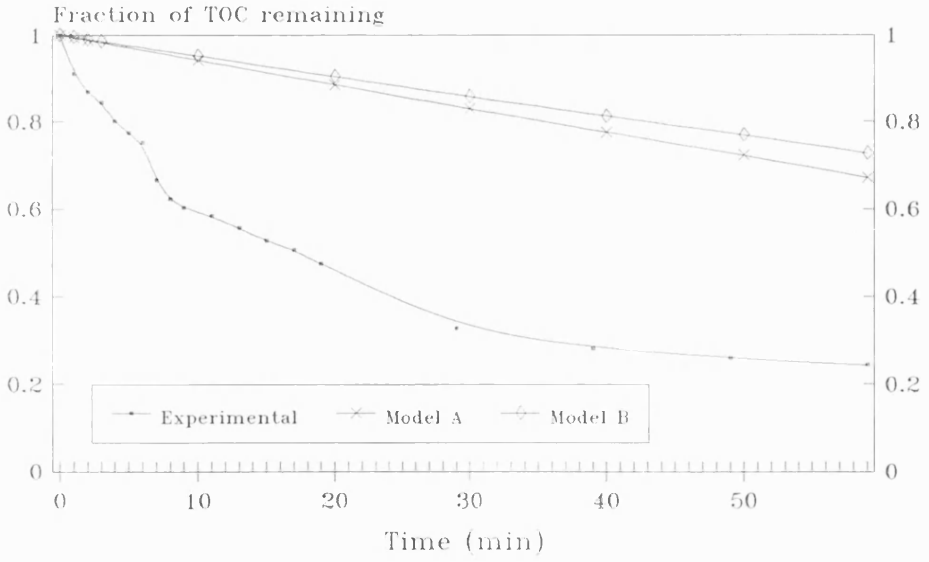

Medium Pressure Lamp (Nominal Power=3kW)
Moles H202 : Citric Acid = 6
Initial TOC = 500 ppm

Fig. 10.5 Mineralization Profile
Models vs Experimental Result

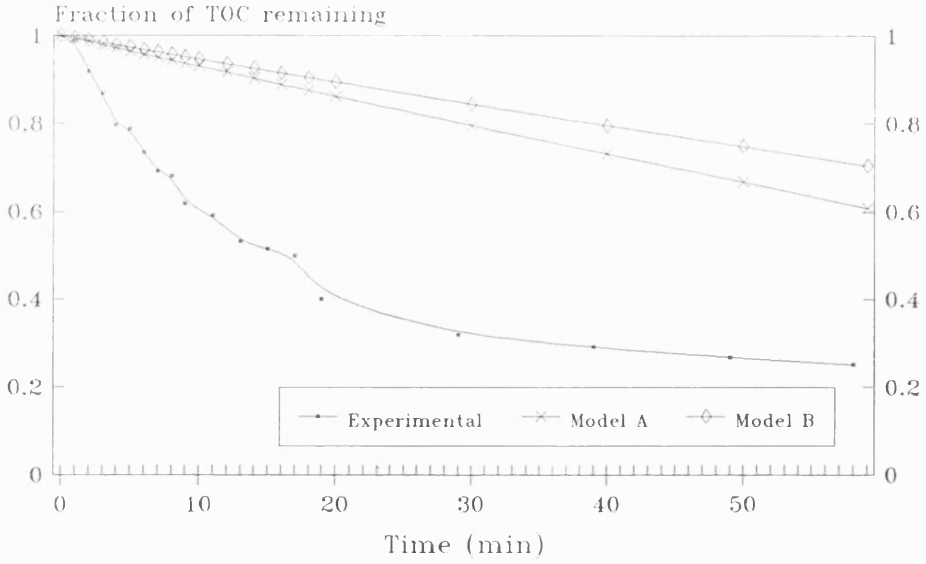

Medium Pressure Lamp (Nominal Power=3kW)
Moles H202 : Citric Acid = 7
Initial TOC = 667ppm

Fig. 10.6 Mineralization Profile
Models vs Experimental Result

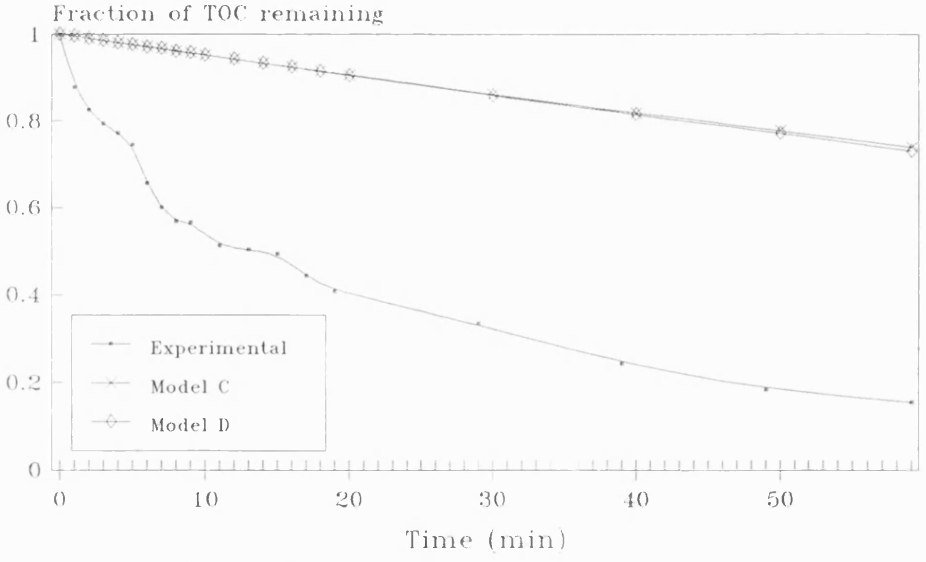

Medium Pressure Lamp (Nominal Power=3kW)
Moles H202 : Citric Acid = 12
Initial TOC = 834 ppm

Fig. 10.7 Mineralization Profiles
Models vs Experimental Results

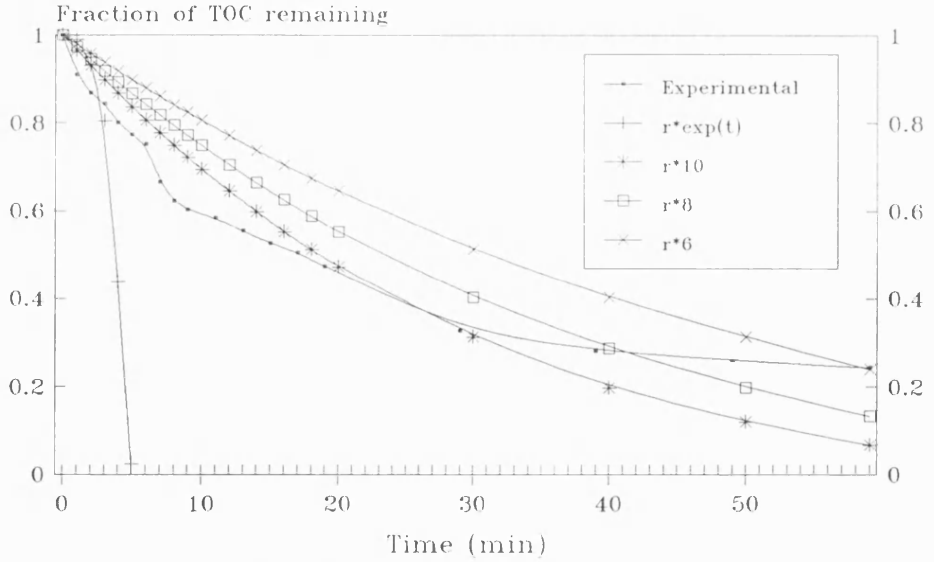

Medium Pressure Lamp (Nominal Power=3kW)
Moles H202 : Citric Acid = 6
Initial TOC = 500 ppm

Fig. 10.8 Mineralization Profile
Model vs Experimental Result

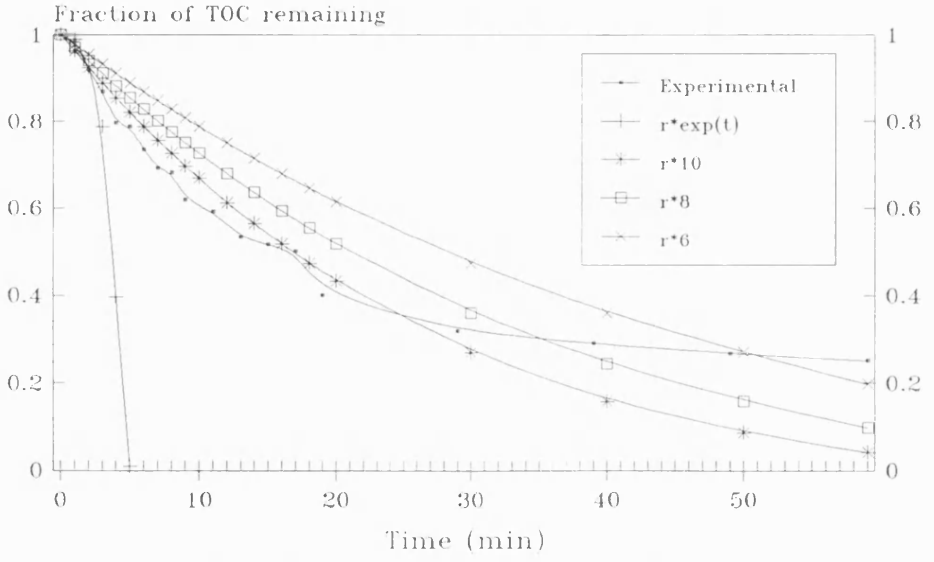

Medium Pressure Lamp (Nominal Power=3kW)
Moles H202 : Citric Acid = 7
Initial TOC = 667ppm

Fig. 10.9 Mineralization Profile
Model vs Experimental Result

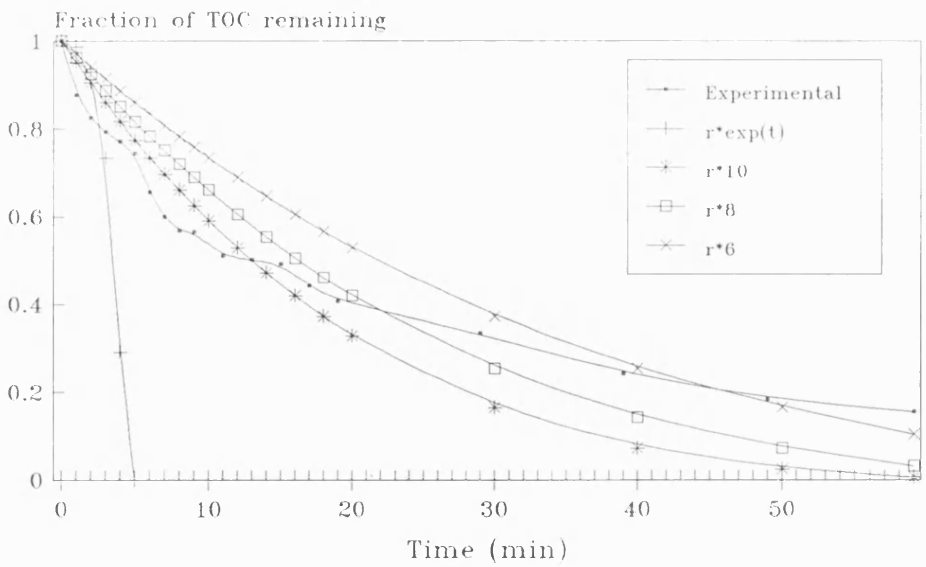

Medium Pressure Lamp (Nominal Power=3kW)
Moles H202 : Citric Acid = 12
Initial TOC = 834 ppm

Fig. 10.10 Mineralization Profile
Model vs Experimental Result

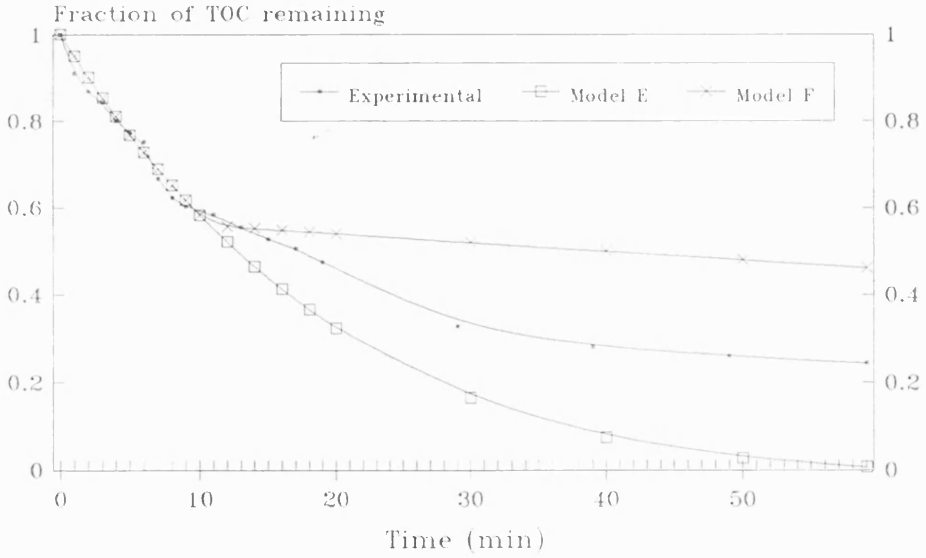

Medium Pressure Lamp (Nominal Power=3kW)
Moles H202 : Citric Acid = 6
Initial TOC = 500 ppm

Fig. 10.11 Mineralization Profile
Model vs Experimental Result

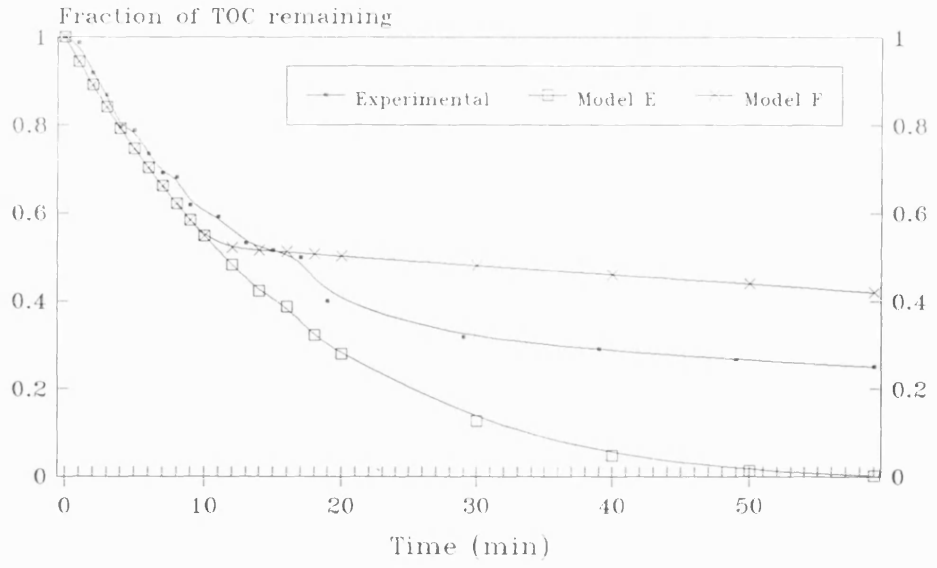

Medium Pressure Lamp (Nominal Power=3kW)
Moles H202 : Citric Acid = 7
Initial TOC = 667ppm

Fig. 10.12 Mineralization Profile
Model vs Experimental Result

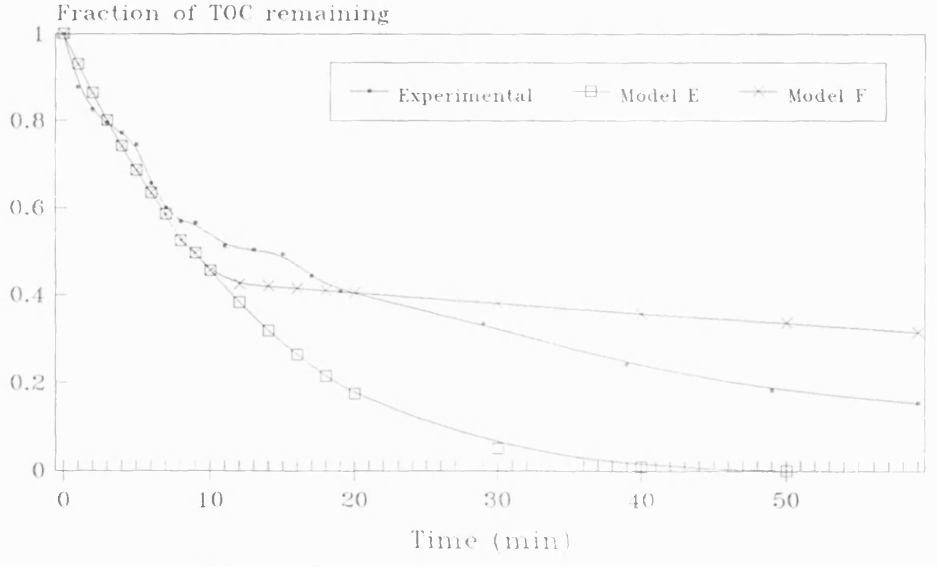

Medium Pressure Lamp (Nominal Power=3kW)
Moles H202 : Citric Acid = 12
Initial TOC = 834 ppm

CHAPTER 11
CRITICAL APPRAISAL
AND RECOMMENDATIONS

The very first thing that must be said about this research is that the whole approach to this environment pollution study had been very idealistic in that only one organic compound was studied without consideration being given to other organic, inorganic and humic compounds which are always present in the real environment. Natural systems and waste waters are very complex and contain many organic (living and non-living) and inorganic substances that influence the degradation and transformation of pollutants. Theoretical speculation and investigation of model systems appears to be irrelevant to the process of gaining an understanding of transformations which occur in nature or in a waste water treatment plant. However as in every other area of research, before detailed studies that approach real situations can be done, one needs to begin with the simple cases, and in this work several important discoveries had been made precisely because the situation was not too complicated to be analysed. A knowledge of the fundamental mechanisms of photochemical and/or photocatalytical decay, as determined from model solutions, will help to determine the most efficient and inexpensive process for the oxidation of pollutants. That said, recommendation (i) is to carry out more detailed studies which reflect the situation found in the environment or in industry more closely. For example, organic compounds such as EDTA are present with citric acid in the waste effluent from the nuclear power industry.

(ii) Studies from this research have found the most efficient advanced oxidation process to degrade and mineralise citric acid which is the $UV/H_2O_2/Fe^{3+}$ process. This study has shown that the presence of a little ferric salt improves the efficiency of the UV/H_2O_2 process many times over. The possibility and potential

that it can greatly reduce others organic compounds is tremendous. It has been demonstrated that the presence of each reactant is essential for the efficiency of the process; lacking of any one will greatly reduce the efficiency (Chapter 6). Also the amount of hydrogen peroxide needed to produced high mineralization rate was clearly shown in Chapter 5. The photo-oxidation rate and hence the efficiency of the process is very much dependent upon the amount of ferric salt and hydrogen peroxide used. Although higher, the amount of these reactants used can achieved greater degradation and mineralization rate a balance is needed not least because of financial reasons. An important factor to take into consideration is the sudden release of great amount of heat produced from exothermic reactions and likelihood of runaway reaction which could be difficult to control. Even though iron salts are abundant in the environment it does not justify one to add more into the environment which might upset the ecosystem. The literature had indicated that the presence of oxygen might improved the efficiency of the $UV/H_2O_2/Fe^{3+}$ process (Sec.6.4). Since oxygen is an oxidant and can play an important role in the process, its involvement may reduce the amount of hydrogen peroxide needed and hence the operational cost. Thus further experiments and studies involving the introduction of oxygen or air should be carried out.

(iii) The literature has identifies two intermediate compounds as the products of photo-oxidation of citric acid using $UV/H_2O_2/Fe^{3+}$ process. However, the findings from this research do not support these claims. Chapter 7 shows that the reactions involved could well be more complicated than those proposed in the literature. This research has also shown that there are more than two intermediate compounds formed. Therefore more efforts are needed to identify these unknown compounds, so that the reaction paths can be determined in order to have a clearer understanding of the process. Any toxic compounds produced can then be identified and a decision made as to the suitability of the process.

(iv) Though ultra-violet light plays an important role in the $UV/H_2O_2/Fe^{3+}$ process its intensity appears not to (Chapter 9). The mineralization rate was found to

be inversely proportional to the photon flux produced by the UV lamp. Further studies should be carried out to determine the lowest intensity that can produce the same efficient mineralization rate.

(v) This study has narrowed the gap between two fields of research : photoreaction engineering and advanced oxidation processes. Radiation field models, proposed by researchers to describe the radiation flux in the vicinity of a ultra-violet source, are used in this research to model the mineralization rate of the advanced oxidation process. It had been determined that the two radiation field models, LSSE and ESVE models, cannot be applied to processes which have a high absorption medium (Chapter 8).

(vi) Most importantly of all, the main aim of this research has been achieved. A mineralization rate model has been determined which can predict the mineralization profile both in the batch and pilot plant reactor. However the model can only be used for this purpose in the first ten minutes for the pilot plant, in which time about 40% of TOC had been mineralised (Chapter 10). There is no such problem for the batch experiments since the photo-oxidation reaction occur almost completely in the first ten minutes (Chapter 6). There are also restrictions on the usage of the mineralization rate model. It can safely be use only if (i) the ferric salt is ferric sulphate pentahydrate and its concentration is 0.01 mol/l; (ii) the concentration of citric acid is between 2500 and 1500 ppm; (iii) molar concentration of hydrogen peroxide to citric acid is between 5:1 and 30:1. The mineralization rate equation thus obtained is $r = -1.0094\text{x}10^{-4}[TOC]_o^{0.74}[H_2O_2]_o^{0.39}[I_{abs}]_o^{-0.11}$. To model a mineralization rate equation which is able to predict the mineralization profile for more than ten minutes in the pilot plant requires more experimental studies. This could mean instead of collecting the initial rate data from the batch experiments, sets of experiments should be carry out in the pilot plant. This will inevitably leads to a much higher operational cost.

CHAPTER 12
CONCLUSIONS AND FUTURE WORK

The previous chapter discussed the results obtained in this research, their implications and their short falls. This chapter will draw conclusions from all these findings and propose works which need to be done to achieve a successful application of this AOP in industry. The main objective of this research has been fulfilled with the successful determination of the most efficient AOPs in degradation and mineralization of citric acid, and the determination of its mineralization rate model. UV/H_2O_2/Ferric sulphate pentahydrate had shown to be the most efficient process in the mineralization of citric acid and there is little doubt that it can perform equally well with other organic compounds. Each individual reactants plays an important role in the process without which the mineralization rate will be greatly affected. In general, the photo-oxidation rate increases with increases in concentration of hydrogen peroxide and the ferric salt. However, a higher concentration of these reactants also means the more likelihood of runaway reaction, thus a balance is needed. The mineralization rate was determined to be $r = -1.0094\text{x}10^{-4}[TOC]_o^{0.74}[H_2O_2]_o^{0.39}[I_{abs}]_o^{-0.11}$. Incorporating mass balances it can predict within reasonable limits of error, the mineralization profile in the batch and the first ten minutes of the pilot plant operation.

The results have been very encouraging and they indicate strongly the feasibility of using this AOP on an industrial scale. However, further work needs to be done before this goal can be realised. Firstly, a more detailed study should be carried out on organic waste which reflects more closely conditions used in industry since the systems tend to be more complex. Secondly, the process can be operated more efficiently and economically if a balance is found in the usage of reactants. In addition, introduction of oxygen/air might further increase the process efficiency and

reduce the operational cost. Thus further studies should be carried out to improve the efficiency of the process and reduce its operational cost. Lastly but not least, all intermediate compounds should be identified to make sure no toxic compounds are created by the process.

REFERENCES

Alcock, N W, "Separation of Citric Acid Cycle and Related Compounds by Gas Chromatography", *Methods Enzymol*, 1969, **13**, 397 - 415.

Alfano, O M, Romero R L, and Cassano, A E, "Radiation Field Modelling in Photoreactors - 1. Homogeneous Media", *Chem Eng Sci*, 1986, **41(3)**, 421 - 444.

Anbar, M., and Neta, P, "A Compilation of Specific Bimolecular Rate Constant for the Reaction of Hydrated Electrons, Hydrogen Atoms and Hydroxyl Radicals with Inorganic and Organic Compounds in Aqueous Solution", *Intl J Appl Radiat Isotopes*, 1967, **18(7)**, 493 - 523.

Anderson, P J, Fitch, W L, and Halpern, B, "Rapid and Simplified Extraction Procedure for Gas Chromatographic-Mass Spectrometric Profiling of Urinary Organic Acids", *J Chromatogr*, 1978, **146(3)**, 481 - 484.

Andrews, C A, "Photooxidation Treatment of TNT Contaminated Waste Waters", Report No. WQEG/C 80-137, Naval Weapons Support Center, 1980.

Barb, W G, Baxendale, J H, George, P, and Hargrave, K R, "Reactions of Ferrous and Ferric Ions with Hydrogen Peroxide. Part I - The Ferrous Ion Reaction", *Trans Faraday Soc*, 1951, **47**, 462 - 500.

Barb, W G, Baxendale, J H, George, P, and Hargrave, K R, "Reactions of Ferrous and Ferric Ions with Hydrogen Peroxide. Part II - The Ferric Ion Reaction", *Trans Faraday Soc*, 1951, **47**, 591 - 616.

Barbeni, M, Minero, C, Pelizzetti, E, Begarello, E, and Serpone, N, "Chemical Degradation of Cholophenols with Fenton Reagent ($Fe^{2+}+H_2O_2$)", *Chemosphere*, 1987, **16(10-1)**, 2225 - 2237.

Baxendale, S H, and Wilson, J A, "The Photolysis of Hydrogen Peroxide at High Light Intensities", *Trans Farad Soc*, 1957, **53**, 344 - 347.

Behar, B, and Stein, G, "Photochemical Evolution of Oxygen From Certain Aqueous Solutions", *Science*, 1966, **154**, 1012 - 1013.

Benrath, A, "Über Photochemische Reaktionen in waBrigen Lösung", *Liebigs Ann*, 1911, **382**, 222 - 235.

Benrath, A, "Über Photochemische Reaktionen in waBriger Lösung", *J Prakt Chem*, 1912, **86**, 336 - 344.

Benrath, A, "Mitteilung aus dem Chemischem Institut der Universitat Bonn. Über Photochemishe Reaktionen in waBrigen Lösung. II", *J Prakt Chem*, 1917, **96**, 190 - 201.

Bielski, B H J, "Revolution of the Spectral and Kinetic Properties of $HO_2\cdot$ and of $\cdot O_2^-$ Free Radicals", *Photochem Photobiol*, 1978, **28(4/5)**, 645 -649.

Bishop, D F, Stern, G, Fleischman, M, and Marshall, L S, "Hydrogen Peroxide Catalytic Oxidation of Refactory Organics in Municipal Waste Waters", *I & EC Process Design and Developmen*t, 1968, **7(1)**, 110 - 117.

Braun, A M, Maurette, M T, and Oliveros, E, Photochemical Technology, Mikheev, L D ed, Wiley, Chichester, England, 1991.

Brunet, R, Bourbigot, M M, and Dore, M, "Oxidation of Organic Compounds Through the Combination Ozone-Hydrogen Peroxide", *Ozone Sci & Eng*, 1984, **6(3)**, 163 - 183.

Buhler, R E, Staehelin, J, and Hoigne, J, "Ozone Decomposition in Water Studied by Pulse Radiolysis 2.OH and HO_4 as Chain Intermediates", *J Phys Chem*, 1984, **88(24)**, 5999 - 6004.

Calvert, J G, and Pitts, J N Jr, Photochemistry, J. Wiley and Sons, N.Y., 1966.

Cassano, A E, Silveston, P L, and Smith, J M, "Photochemical Reaction Engineering", *Ind Eng Chem*, 1967, **59(1)**, 18 - 38.

Cassano, A E, Alfano, O M, and Romero, R L, "Photoreactor Engineering : Analysis and Design", in Concepts and Design of Chemical Reactors, Whitaker, S, and Cassano, A E ed, Gordon and Breach Science Publishers, N.Y., 1986, pp 339 - 512.

Cater, S R, Brown, P M, Buckley, J A, and Stevens, R D S, "Treating Contaminated Effluents and Ground Waters", U.S Patent No.5,043,080, 1991.

Cerda, J, Marchetti, J L, and Cassano, A E, "The Use of Simple Radiation Models for the Case of Direct Irradiation of Photochemical Reactors", *Lat Am J Chem Eng Appl Chem*, 1978, **8**, 15 - 25.

Chalmers, R A, and Watts, R W, "The Quantitative Extraction and Gas-Liquid Chromatographic Determination of Organic Acids in Urine", *Analyst*, 1972, **97(1161)**, 958 - 967.

Ciamician, G, and Silber, P, "Chemische Lichtwirkungen. XXVI. Autooxydationen. IV", *Berichte der Deutschen Gesellschaft*, 1913, **46**, 1558 - 1565.

Clarke, N, and Knowles, G, "High Purity Water Using H_2O_2 and UV Radiation", *Effluent and Water Treatment Journal*, 1982, **22(9)**, 335.

Dalgleish, C E, Horning, E C, Horning, M G, Knox, K L, and Yarger, K, "A Gas Liquid Chromatographic Procedure for Separating a Wide Range of Metabolites Occuring in Urine or Tissue Extracts", *Biochem J*, 1966, **101**, 792 - 810.

Discher, L A, Smith, P F, Lippman, I, and Turse, R, "A Revaluation of the Quantum Efficiency of the Uranyl Oxalate System", *J Phys Chem*, 1963, **67**, 2501.

Dixon, W T, and Norman, R O C, "An Intermediate in Homolytic Aromatic Substitution", *Proc Chem Soc*, 1963, 97 - 98.

Dixon, W T, and Norman, R O C, "Electron Spin Resonance Studies of Oxidation Part III. Some Alicyclic Compounds", *J Chem Soc*, 1964, **V**, 4850 - 4860.

Esplugas, S, Ibarz, A, and Vicente, M, "Influnce of Lamp Position on the Annular Photoreactor", *Chem Eng J*, 1983, **27(2)**, 107 - 111.

Esplugas, S, Vicente, M, Ibarz, A, Prat, C, and Costa, J, "Influnce of Lamp Position on Available Radiation Flux in an Annular Photoreactor", *Chem Eng J*, 1987, **34(3)**, 111 - 115.

Esplugas, S, Yue, P L, and Pervez, M I, "Degradation of 4-Chlorophenol by Photolytic Oxidation", *Wat Res*, 1994, **28(6)**, 1323 - 1328.

Farhataziz, P C, and Ross, A B, "A Selected Specific Rates of Reactions of Transients from Water in Aqueous Solution. III. Hydroxyl Radical and Perhydroxyl Radical and Their Radical Ions", NSRDS-NBS 59, U.S. Department of Commerce, Washington D.C., 1977.

Fenton, H J H, "Oxidation of Tartaric Acid in Presence of Iron", *J Chem Soc*, 1894, **65**, 899 - 910.

Fitch, W L, Anderson, P J, and Smith, D H, "Isolation, Identification and Quantitation of Urinary Organic Acids", *J Chromatogr*, 1979, **162(3)**, 249 - 259.

Frahn, J L, "The Photochemical Decomposition on the Citrate-Ferric Iron Complex : A Study of the Reaction Products by Paper Ionopheresis", *Australian J Chem*, 1958, **11**, 399 - 405.

Francis, P D, "Oxidation by UV and Ozone of Organic Contaminants Dissolved in Deionized and Raw Mains Water", *Ozone Sci & Eng*, 1987, **9(4)**, 369 - 390.

Fry, H S, and Gerwe, E G, "Action of Ultra-violet Light Upon Ferric Citrate Solutions", *Industr and Engng Chem*, 1928, **20(12)**, 1392 - 1394.

Glaze, W H, Peyton, G R, and Sohm, B, "Pilot Scale Evaluation of Photolytic Ozonation for Trihalomethane Precursor Removal", Final Report to USEPA/DWRD/MERL, Cincinnati, OH, Cooperative Agreement #CR-808825, J Keith Carswell, Project Officer, Aug. 1984.

Glaze, W H, Kang, J W, and Chapin, D H, "The Chemistry of Water Treatment Processes Involving Ozone, Hydrogen Peroxide and Ultraviolet Radiation", *Ozone Sci & Eng*, 1987, **9(4)**, 335 - 352.

Glaze, W H, and Lay, Y, "Oxidation of 1,2-dibromo-3-chloropropane (DBCP) Using Advanced Oxidation Processes", 9th Ozone World Conference of IOA, New York City, June 3 - 9, 1989.

Glikman, T S, Kalibabchuk, V A, and Sosnovskaya, V P, "Effect of the Addition of Ferric salts on Photolysis and Radiolysis Process of Hydroxy Acids", *J Gen Chem USSR*, 1965, **35**, 1533-1636.

Greter, J, and Jacobson, C E, "Urinary Organic Acids : Isolation and Quantification for Routine Metabolic Screening", *Clin Chem*, 1987, **33(4)**, 473 - 486.

Groves, J T, "Mechanism of Metal-Catalyzed Oxygen Insertion", in Metal Ion Activation of Dioxygen, Spiro, T G ed, Wiley, N.Y., 1980, pp 125 - 162.

Guittonneau, S, De Laat, J, Dore, M, Duguet, J P, and Bonnel, C, "Etude dela Degradation de Quelques Composes Organochlores Volatils par Photolyse du Peroxyde Dhydrogene en Milienx Aqueux", *Revul des Sciences de l'Ean*, 1987, **1(1&2)**, 35.

Guittonneau, S, De Laat, J, Duguet, J P, Bonnel, C, and Dore, M, "Oxidation of Parachloronitrobenzene in Dilute Aqueous Solution by O_3+UV and H_2O_2+UV, A Comparative Study", *Ozone Sci & Eng*, 1990, **12(1)**, 73 - 93.

Haag, W R, and Yao, C C D, "Rate Constants for Reaction of Hydroxyl Radicals With Several Drinking Water Contaminants", *Environ Sci Technol*, 1992, **26(5)**, 1005 - 1013.

Hager, D G, "UV-Catalyzed Hydrogen Peroxide Chemical Oxidation of Organic Contaminants in Water", *Innovat Hazard Wastes Treat Technol Ser*, 1990, **2**, 143 - 153.

Hamm, R E, Schull, C M, and Grant, D M, "Citrate Complexes With Iron (II) and Iron (III)", *J Am Chem Soc*, 1954, **76(7)**, 2111 - 2114.

Harmon, M A, and Doelle, H W, "Gas Chromatographic Separation and Determination of Microquantities of the Esters of the Tricarboxylic Acid Cycle Acids and Related Compounds", *J Chromatogr*, 1969, **42**, 157 - 169.

Harris, P R, and Dranoff, J S, "A Study of Perfectly Mixed Photochemical Reactors", *AIChE J*, 1965, **11(3)**, 497 - 502.

Hart, E J, Forni, L, and Bahnemann, D, "Mechanism of the Hydroxide Ion Initiated Decomposition of Ozone in Aqueous Solution", *J Phys Chem*, 1982, **86(2)**, 255 - 259.

Heidt, L J, Tregay, G W, and Middleton, F A, "Influence of pH Upon the Photolysis of the Uranyl Oxalate Actinometer System", *J Phy Chem*, 1970, **74(9)**, 1876 - 1882.

Hill, F B, and Felder, R M, "Effects of Mixing on Chain Reactions in Isothermal Photoreactors", *AIChE J*, 1965, **11**, 873 - 885.

Hoigne, J, and Bader, H, "Combination of Ozone/UV and Ozone/Hydrogen Peroxide; Formation of Secondary Oxidants", in Proc 8th Ozone World Congress Vol. 2, Zurich, Switzerland : Intl Ozone Assoc. Headquarters, 1987, pp K83 - K97.

Horning, M G, Boucher, E A, Muss, A M, and Horning, E C, "Gas Chromatographic Study of Derivatives of Acids of the Krebs Cycle and Related Compounds", *Anal Lett*, 1968, **1(11)**, 713 - 723.

Horning, E C, and Horning, M G, "Human Metabolic Profiles Obtained by GC and GC/MS", *J Chromatogr Sci*, 1971a, **9**, 129 - 140.

Horning, E C, and Horning, M G, "Metabolitic Profiles : Gas-phase Methods for Analysis of Metabolites.", *Clin Chem*, 1971b, **17**, 802 - 809.

Horrocks, R H, Hindle, E J, Lawson, P A, Orell, D H, and Poole, A J, "A New Method for the Gas Chromatographic Examination of Urinary Organic Acids", *Clin Chem Acta*, 1976, **69**, 93 - 100.

Irazoqui, H A, Cerda, J, and Cassano, A E, "Radiation Profiles in an Empty Annular Photoreactor With a Source of Finite Spatial Dimensions", *AIChem J*, 1973, **19(3)**, 460 - 467.

Irazoqui, H A, Cerda, J, and Cassano, A E, "The Radiation Field for the Point and Line Source Approximation and the Three-Dimensional Source Models: Applications to Photoreactions", *Chem Eng J*, 1976, **11**, 27 - 37.

Jaakonmaki, P Z, Knox, K L, Horning, E C, and Horning, M G, "The Characterisation by Gas-Liquid Chromatograhphy of ethyl-D-glucosiduronic Acids as a Metabolite of Ethanol in Rat and Man", *Eur J Pharmacol*, 1967, **1**, 63.

Jacob, S M, and Dranoff, J S, "Radial Scale-up of Perfectly Mixed Photochemical Reactors", *Chem Eng Prog Symp Ser*, 1966, **62(68)**, 47 - 55.

Jacob, S M, and Dranoff, J S, "Light Intensity Profiles in a Perfectly Mixed Photoreactor", *AIChE J*, 1970, **16(3)**, 359 - 363.

Kochany, J and Choudhry, G G, "Photochemistry of Halogenated Benzene Derivatives. 12. Effects of Sodium-Nitrile on the Environmental Phototransformation of Bromoxynil (3,5-dibromo-4-hydroxybenzonitrile) Herbicide in Water. The Photoincorporation of Nitrile Ions Into Bromoxynil", *Toxicol Environ Chem*, 1990, **27(4)**, 225 - 239.

Kochany, J, Choudhry, G G, and Webster, G R B, "Photochemistry of Halogenated Benzene Derivatives. 10. Effects of Sodium-Chloride on the Aquatic Photodegradation of Bromoxynil (3,5-dibromo-4-hydroxybenzonitrile) Herbicide", *Archiv Environ Contam Toxicol*, 1990, **19(3)**, 325 - 331.

Kolthoff, I M, Sandell, E B, Meehan, E J, and Bruckentein, S, Quantitative Chemical Analysis, 4th ed, MacMillan, N.Y., 1969.

Kozlov, Y N, Nadezhdin, A D, and Pourmal, A P, "Initiation Process in the System $Fe^{3+} + H_2O_2$", *Int J Chem Kinet*, 1974, **6**, 383 - 394.

Kremer, M L, and Stein, G, "The Catalytic Decomposition of Hydrogen Peroxide by Ferric Perchlorate", *Trans Faraday Soc*, 1959, **55**, 959 - 973.

Kremer, M L, "Nature of Intermediates in the Catalytic Decomposition of Hydrogen Peroxide by Ferric Ions", *Trans Faraday Soc*, 1962, **58**, 702 - 707.

Kremer, M L, "Oxidation Reduction Step in Catalytic Decomposition of Hydrogen Peroxide by Ferric Ions", *Trans Faraday Soc*, 1963, **59**, 2535 -2542.

Kremer, M L, "'Complex' versus 'Free Radical' Mechanism for the Catalytic Decomposition of H_2O_2 by Ferric Ions", *Int J Chem Kinet*, 1985, **17(12)**, 1299 - 1314.

Lanford, O E, and Quinan, J R, "A Spectrophotometric Study of the Reaction of Ferric Iron and Citric Acid", *J Am Chem Soc*, 1948, **70**, 2900 - 2903.

Larson, R A, Schlauch, M B, and Marley, K A, "Ferric Ion Promoted Photodecomposition of Triazines", *J Agric Food Chem*, 1991, **39(11)**, 2057 - 2062.

Legrini, O, Oliveros, E, and Braun, A M, "Photochemical Processes for Water Treatment", *Chem Rev*, 1993, **93(2)**, 671 - 698.

Leigton, W G, and Forbes, G S, "Precision Actinometry with Uranyl Oxalate", *J Am Chem Soc*, 1930, **52**, 3139 - 3152.

Li-Puma, G, "Photocatalytic Destruction of Multicomponent Organic Pollutants in Wastewater", MPhil Thesis, University of Bath, U.K., 1995.

Lunak, S, Sedlak, P, Brodilova, J, and Lederer, P, "Photocatalytic Effects of Fe(III) Compounds on the Hydroxylation of Benzoic Acid by Hydrogen Peroxide Initiated by 589 nm Radiation and Sensitized by Methylenes Blue", *Tetrahedron Lett*, 1989, **30(17)**, 2277 - 2280.

Malaiyandi, M, Sadar, M, Lee, P, and Grady, R O, "Removal of Organic in Water Using Hydrogen Peroxide in Presence of Ultraviolet Light", *Wat Res*, 1980, **14(8)**, 1131 - 1134.

Mansour, M, Parlar, H, and Korte, F, "Removal of Pollutants in the Aquatic Environment by Photooxidations", presented at 4th International Conference of Chemistry for Protection of the Environment, Toulouse, France, 1984, pp457 - 461.

Matsuura, T, and Smith, J M, "Light Distribution in Cylindrical Photoreactors", *AIChE J*, 1970, **16(2)**, 321 - 324.

Mukherjee, K K R, Fundamental of Photochemistry, John Wiley and Sons, N.Y., 1978.

Murov, S L, Handbook of Photochemistry, Dekker, N.Y., 1973.

Paillard, H, Brunet, R, and Dore, M, "Application of Oxidation by a Combined Ozone/Ultraviolet Radiation System to the Treatment of Natural Water", *Ozone Sci & Eng*, 1987, **9(4)**, 391 - 418.

Paul, D and Canter, L W, "Evaluation of Photochemical Oxidation Technology for Remediation of Ground Water Contaminated With Organic", *J Environ Sci Health*, 1990, **A25(8)**, 953 - 985.

Pervez, I M, private communication, Bath University, 1992.

Peyton, G R, Huang, F Y, Burleson, J L, and Glaze, W H, "Destruction of Pollutants in Water with Ozone in Combination with Ultraviolet Radiation : 2.Natural Trihalomethane Precursors", *Environ Sci Technol*, 1982, **16(8)**, 448 - 453.

Peyton, G R, and Glaze, W H, "Photolytic Ozonation : A Mechanistic Perspective", *Oznews*, 1985, **13**, #4.

Peyton, G R, and Glaze, W H, "The Mechanism of Photolytic Ozonation", in Proc. of the Symposium in Aquatic Photochemistry, 189th Annual Meeting of the American Chemical Society, April 1985, Vol. 189, pp5 - Geoc.

Peyton, G R, and Glaze, W H, "Mechanism of Photolytic Ozonation", in Photochemistry of Environmental Aquatic Systems, Zika, R G, Cooper, W J ed, American Chemical Society Symposium Series, No 327, Washington, D C, 1986, pp76 - 88.

Peyton, G R, Smith, M A, and Peyton, B M, "Photolytic Ozonation for Protection and Rehabilation of Ground-Water Resources, A Mechanistic Study", Water Resources Centre Research Report Number 206, University of Illinois, Project No. S - 104 - ILL, Jan 1987a.

Peyton, G R, and Glaze, W H, "Mechanism of Photolytic Ozonation", in Photochemistry of Environmental Aquatic Systems, Zika, R G, and Cooper, W J ed, ACS Symposium Series, No. 327 (Washington, D C : American Chemical Society), 1987b, pp76 - 88.

Peyton, G R, and Glaze, W H, "Destruction of Pollutants in Water with Ozone in Combination with Ultraviolet Radiation, 3.Photolysis of Aqueous Ozone", *Environ Sci Technol*, 1988, **22(7)**, 761 - 767.

Peyton, G R, "Oxidative Treatment Methods for Removal of Organic Compounds from Drinking Water Supplies", in Significance and Treatment of Volatile Organic

Compounds in Water Supplies, Ram, N M, Christman, R F, and Cantor, K P ed, Lewis Publishers, Chelsea, Micigan, 1990, Chp 14, pp 313 - 361.

Pignatello, J J, and Sun, Y, "Photoassited Mineralization of Herbicide Waste by Ferric Ion Catalyzed Hydrogen Peroxide", in Emerging Technologies in Hazardous Waste Management Vol III, Tedder, D W, and Pohland, F G ed, Vol. 518 of ACS Symposium Series, American Chemical Society, Washington, D C, 1993, Chp. 4, pp77 - 84.

Pinkston, D, Spiteller, G, Von Henning, H, and Matthaei, D, "High Resolution Gas Chromatography-Mass Spectrometry of the Methyl Esters of Organic Acids From Uremic Hemofiltrates", *J Chromatogr*, 1981, **223(1)**, 1 - 19.

Pignatello, J J, "Dark and Photoassited Fe^{3+} Catalyzed Degradation of Chlorophenoxy Herbicides by Hydrogen Peroxide", *Environ Sci Technol*, 1992, **26(5)**, 944 - 951.

Prengle, H W, "Ozone/UV Process Effective Wastewater Treatment", *Hydrocarbon Processing*, 1975, **54(10)**, 82 - 87.

Prengle, H W, "Experimental Rate Constants and Reactor Considerations for the Destruction of Micropollutants and Trihalomethane Precursors by Ozone With Ultraviolet Radiation", *Environ Sci Technol*, 1983, **17(12)**, 743 - 747.

Rabeck, J F, Experimental Methods in Photochemistry and Photophysics, Wiley, N.Y., 1982.

Rao, G G, and Aravamudan, G, "Analytical Application of the Photochemical Action of Light. I. Determination of Ferric Iron by Photochemical Reduction in the Presence of Citric and Mandelic Acids", *Analytica Chimica Acta*, 1955, **13**, 328 - 333.

Schumb,W E, Satterfield, C N, and Wentworth, R L, Hydrogen Peroxide, Reinhold Publishing Co., N.Y., 1955.

Sedlak, P, Lunak, S, and Lederer, P, "Comparision of Photocatalytic Activities of 3d Transition Metal Ions for Hydrogen Peroxide Photoinitiated Hydroxylation of 2-Hydroxybenzoic Acid", *Collection Czechoslovak Chem Commun*, 1987, **52(10)**, 2451 - 2456.

Simons, M S, and Zepp, R G, "Influnce of Humic Substances on Photolysis of Nitroaromatic Compounds in Aqueous System", *Wat Res*, 1986, **20(7)**, 899 - 904.

Sims, P, Truscott, R, and Halpern, B, "Improved Procedure for the Anion-Exchange Isolation of Urinary Organic Acids", *J Chromatogr*, 1981a, **222(3)**, 337 - 344.

Sims, A F E, "Phenol Oxidation With Hydragen Peroxide", *Effluent Water Treatment J*, 1981b, **21(3)**, 109 - 112.

Snell, F D, and Ettre, L S, "Hydrogen Peroxide", in Snell-Ettre Encyclopedia of Industrial Chemical Analysis, Vol 14, Interscience Publishers, N.Y., 1971, pp432 - 438.

Staehelin, J, and Hoigne, J, "Decomposition of Ozone in Water : Rate of Initiation by Hydroxide Ion and Hydrogen Peroxide", *Environ Sci & Technol*, 1982, **16(10)**, 676 - 681.

Staehelin, J, Buhler, R E, and Hoigne, J, "Ozone Decomposition in Water Studied by Pulse Radiolysis. 1. HO_2/O_2^- and HO_3/O_3^- as Intermediates", *J Phys Chem*, 1983, **88(12)**, 2560 - 2564.

Staehelin, J, and Hoigne, J, "Mechanism and Kinetics of Decomposition of Ozone in Water in the Presence of Organic Solutes", *Vom Wasser*, 1983, **61**, 337 - 348.

Staehelin, J, and Hoigne, J, "Decomposition of Ozone in Water in the Presence of Organic Solutes Acting as Promoters and Inhibitors of Radical Chain Reactions", *Environ Sci Technol*, 1985, **19(12)**, 1206 - 1213.

Stramigioli, C, Santarelli, F, and Foraboschi, F P, "Photosensitized Reactions in an Annular Continuous Photoreactor", *Appl Sci Res*, 1977, **33**, 23 - 42.

Stumm, W and Morgan, J J, Aquatic Chemistry, 2nd ed, Wiley-Interscience, N.Y., 1981.

Sun, Y, and Pignatello, J J, "Photochemical Reactions Involved in the Total Mineralization of 2,4-D by $Fe^{2+}/H_2O_2/UV$", *Environ Sci Technol*, 1993, **27(2)**, 304 - 310.

Sundstrom, D W, Klei, H E, Nalette, T A, Reidy, D J, and Weir, B A, "Destruction of Halogenated Aliphatics by Ultraviolet Catalyzed Oxidation With Hydrogen Peroxide", *Hazardous Waste and Hazardous Materials*, 1986, **3(1)**, 101 - 110.

Taube, H, "Photochemical Reactives of Ozone in Solution", *Trans Farad Soc*, 1956, **53**, 656 - 665.

Thompson, J A, and Markey, J P, "Quantitative Metabolic Profiling of Urinary Organic Acids by Gas Chromatography-Mass-Spectrometrym : Comparison of Isolation Methods", *Anal Chem*, 1975, **47(8)**, 1313 - 1321.

Turkelson, V T, and Richards, M, "Separation of the Citric Acid Cycle Acids by Liquid Chromatography", *Analytical Chemistry*, 1978, **50(11)**, 1420 - 1423.

Verhaeghe, B J, Lefevere, M F, and Leenheer, A P X, "Solid- Phase Extraction with Strong Anion - Exchange Columns for Selective Isolation and Concentration of Urinary Organic Acids", *Clin Chem*, 1988, **34(6)**, 1077 - 1083.

Walling, C, and Goosen, A, "Mechanism of the Ferric Ion Catalyzed Decomposition of Hydrogen Peroxide. Effect of Organic Substrates", *J Amer Chem Soc*, 1973, **95(9)**, 2987 - 2991.

Walling, C, and Weil, T, "The Ferric Ion Catalyzed Decomposition of Hydrogen Peroxide in Perchloric Acid Solution", *Int J Chem Kinet*, 1974, **6**, 507 - 516.

Walling, C, "Fenton's Reagent Revisited", *Acc Chem Rev*, 1975, **8**, 125 - 131.

Walling, C, and Cleary, M, "Oxygen Evolution as a Critical Test of Mechanism in the Ferric-Ion Catalyzed Decomposition of Hydrogen Peroxide", *Int J Chem Kinet*, 1977, **9**, 595 - 601.

Warner, R C, and Weber, I, "The Cupric and Ferric Citrate Complexes", *J Am Chem Soc*, 1953, **75**, 5086 - 5094.

Weir, B A, Sundstrom, D W, and Klei, H E, "Destruction of Benzene by Ultraviolet Light - Catalyzed Oxidation with Hydrogen Peroxide", *Hazardous Waste and Hazardous Materials*, 1987, **4(2)**, 165 - 176.

Williams, V P, Ching, D K, and Cederbaum, S D, "Adsorption of Organic Acids From Amniotic Fluid and Urine Onto Silica Gel Before Analysis by Gas

Chromatography and Combined Gas Chromatography/Mass Spectrometry", *Clin Chem,* 1979, **25**, 1814 - 1820.

Yue, P L, and Legrini, O, "Photochemical Destruction of Trace Organics in Water", Paper 52 D, AIChE National Meeting, San Francisco, 1989.

Yue, P L, private communication, Bath University, 1991.

Yue, P L, and Legrini, O, "Photochemical Degradation of Organics in Water", *Water Pollut Res J Can*, 1992, **27(1)**, 127 - 137.

Zepp, R G, "Factors Affecting the Photochemical Treatment of Hazardous Waste", *Environ Sci Technol*, 1988, **22(3)**, 256 - 257.

Zepp, R G, Faust, B C, and Hoigne, J, "Hydroxyl Radical Formation in Aqueous Reactions (pH 3 - 8) of Iron (III) with Hydrogen Peroxide. The Photo-Fenton Reaction", *Environ Sci Technol*, 1992, **26(2)**, 313 - 319.

NOMENCLATURE

a	average interfacial area per unit volume of liquid, also exponent in power law (Eqn.2.8)
A	area, cm^{-2}
A_V	interfacial area per unit volume, cm^{-1}
b,d,f,g	exponents in kinetic equations
m,n,p,q	exponents in kinetic equations
C	concentration of TOC, ppm
D_u	utilised ozone dose rate
e	ellipse eccentricity
e^a	local volumetric rate of energy absorption, ein s^{-1} cm^{-3}
E	energy flow rate, ein s^{-1}
F	flow rate, l s^{-1}
h	Planck's constant, joule s
H	Henry's constant, atm cm^3 $mole^{-1}$, or height, m
I	intensity, ein s^{-1} cm^{-2} sr^{-1}
I^o	intensity for a point source with spherical emission, ein s^{-1} sr^{-1}
I"	intensity for the line source with spherical emission, ein s^{-1} cm^{-1} sr^{-1}
I_e	photon rate emitted from the lamp at wavelength λ
I_{abs}	photon rate absorbed by the raection medium, ein s^{-1}
K_e	characteristic emission property of the lamp
k_p	rate constant of direct photolysis of M in Eqn.2.7
k_{ps}	rate constant for induced decomposition by the photosensitizer PS in Eqn.2.7
k_u	UV/ozone reaction rate constant
L	length of lamp, cm
n	unit normal vector
N_e	number of emitters per unit volume of source, cm^{-1}
$[OH]_{ss}$	steady state concentration of OH radicals
P	total pressure, atm
P_ν	probability density distribution function for emission per unit time per unit frequency, ν
|q|	radiation flux density, ein cm^{-2} s^{-1}
r	radial coordinates, cm, or mineralization rate, ppm s^{-1}
R	decomposition rate of oxalic acid, mol s^{-1}
R_s	overall rate of reaction
t	time, s
V	liquid or reactor volume, cm^3
ν	velocity, m s^{-1}
$W_{L,\lambda}$	photon rate emitted by the lamp at the wavelength λ, ein s^{-1}
x,y,z	rectangular Cartesian coordinates

Greek Symbols

α	stoichiometric coefficient for TOC reduction by ozone
υ	frequency
$\mu_{e\upsilon}$	effective attenuation coefficient or absorbance for frequency υ, cm^{-1}
ϕ,θ,ρ	cylindrical coordinates, rad
κ	characteristic property of the lamp emission
λ	wavelength, cm
ρ	spherical coordinate, cm
ϕ	spherical coordinate, cm
Φ_λ	quantum yield of ranyl oxalate at wavelength λ, mol ein^{-1}
Ω	reaction rate or solid angle

Subscripts

e	emission value
g	gas
i	inlet, initial state or interior
l	liquid phase
L	lamp property or relative to liquid phase
n	relative to the normal
o	outlet or outer
r	reception point
R	reactor
ss	relative to the steady state approximation
1	lower limit of integration
2	upper limit of integration
λ	wavelength dependence
υ	frequency dependence

Superscripts

o	initial or standard state value
*	modified property
a	absorbed value

APPENDIX A

```
C     Line Source Spherical Emission Model
C     ****************************

      real mu, h, ri, ro, w, l, sum1, sum2, sum3, Iz, Io, Iabs, Ir, Iave
      real r, z, z1, a, b, c, d, rho, f, y, q
      dimension sum1(1200), sum2(200), sum3(1200)
      dimension r(500), z(200), z1(1100)
      dimension Io(1200), Ir(200), Iz(1200), Iabs(500), Iave(500)
      dimension b(1200), c(1200), d(1200), rho(1200), f(1200), y(1200)
      dimension q(1200), mu(35), w(35)

      data mu(1),w(1)/78.36,1.27E-5/
      data mu(2),w(2)/76.62,4.12E-6/
      data mu(3),w(3)/72.88,3.99E-6/
      data mu(4),w(4)/70.70,1.63E-6/
      data mu(5),w(5)/68.31,1.66E-6/
      data mu(6),w(6)/65.79,2.81E-6/
      data mu(7),w(7)/60.30,2.9E-6/
      data mu(8),w(8)/54.60,7.72E-6/
      data mu(9),w(9)/49.93,7.88E-6/
      data mu(10),w(10)/42.11,2.07E-5/
      data mu(11),w(11)/28.11,4.02E-6/
      data mu(12),w(12)/13.80,3.67E-5/
      data mu(13),w(13)/3.95,3.16E-5/
      data mu(14),w(14)/1.44,4.89E-5/
      data mu(15),w(15)/0.04,6.9E-5/
      data mu(16),w(16)/0.03,2.9E-5/
      data mu(17),w(17)/69.14,1.27E-5/
      data mu(18),w(18)/67.26,4.12E-6/
      data mu(19),w(19)/64.21,3.99E-6/
      data mu(20),w(20)/62.72,1.63E-6/
      data mu(21),w(21)/60.92,1.66E-6/
      data mu(22),w(22)/59.15,2.81E-6/
      data mu(23),w(23)/56.25,2.9E-6/
      data mu(24),w(24)/50.85,7.72E-6/
      data mu(25),w(25)/46.75,7.88E-6/
      data mu(26),w(26)/39.60,2.07E-5/
      data mu(27),w(27)/26.26,4.02E-6/
      data mu(28),w(28)/12.35,3.67E-5/
      data mu(29),w(29)/2.80,3.16E-5/
      data mu(30),w(30)/1.13,4.89E-5/
      data mu(31),w(31)/0.03,6.9E-5/
      data mu(32),w(32)/0.03,2.9E-5/


      h=30
      ri=1.75
      ro=5
      l=14
      xo=8

      z1(1)=xo
      z(1)=0
```

```
      pi=3.141593
      dr=0.05
      dz=0.05
      dz1=0.1
       n=0

      x1=h/dz1
      x2=(ro-ri)/dr
      x3=l/dz

      open(5,file='test.dat')


C     Calculation for different W and mu
C     ^^^^^^^^^^^^^^^^^^^^^^^^^^^^^^^^^^
5     n=n+1
         a=w(n)/(4*pi*l)
         sum1(0)=0
         sum2(0)=0
         sum3(0)=0
         Iz(0)=0
         Iabs(0)=0
         i=0
         j=0
         k=0


C     Calculation at different axial position
C     ^^^^^^^^^^^^^^^^^^^^^^^^^^^^^^^^^^^^^^^
10    i=i+1
         z(i)=z(1)+(i-1)*dz


C     Calculation at different radius
C     ^^^^^^^^^^^^^^^^^^^^^^^^^^^
20    j=j+1
         r(j)=ri+(j-1)*dr
         b(j)=r(j)*r(j)
         c(j)=(r(j)-ri)/r(j)

         Print 100,z(i)
         Print 200,r(j)
         Print 300


C     Photon flux from different point along the lamp
C     ^^^^^^^^^^^^^^^^^^^^^^^^^^^^^^^^^^^^^^^^^^^^^^^^^^^^^^
30    k=k+1
         z1(k)=z1(1)+(k-1)*dz1
         d(k)=(z(k)-z1(k))*(z(k)-z1(k))
         rho(k)=sqrt(b(j)+d(k))
         f(k)=exp(-mu(n)*c(j)*rho(k))
         q(k)=(f(k)/(b(j)+d(k)))
         sum1(k)=sum1(k-1)+q(k)

         print 400, z1(k), q(k), sum1(k), sum3(k)
```

```
      if(k.le.x3)goto 30

          Io(k)=a*(sum1(k)/k)*l
          Iz(k)=2*pi*r(j)*Io(k)
          sum3(k)=sum3(k-1)+Iz(k)

          sum2(j)=sum2(j-1)+sum3(k)
          Ir(j)=(sum2(j)/j)*(ro-ri)

          write(5,*)'sum2(j),Ir(k)=',sum2(j),Ir(j)
          print 500,sum2(j),Ir(j)
          k=0

      if(j.le.x2)goto 20

          Iabs(i)=Iabs(i-1)+Ir(j)
          write(5,*)'Iabs(i)=',Iabs(i)
          j=0

      if(i.le.x1)goto 10

          Iave(i)=(Iabs(i)/i)*h
          print 600,mu(n),w(n),Iave(i)
          write (5,600)  mu(n),w(n),Iave(i)
          i=0

      if(n.lt.32) goto 5

      close (5)

100   Format(10X,'Axial position, z=',F10.5)
200   Format(10X,'Radial position, r=',F10.5)
300   Format(10X,'Radiation flux : q, sum q, ave q')
400   Format(1X,'Point source at z1=',1X,F5.3,3E15.5)
500   Format(1X,'Concentric,sum over annulus:',2E20.9)
600   Format(1X,3E20.9)


      stop
      end
```

APPENDIX B

```
c       Extense Source with Volumetric Emission (ESVE) Model
c       ************************************************

        Parameter (NOUT=6)
        External FA, P1, P2
        External D01DAF
        Dimension qr(1000), sumr(1000), sumz(1000), rave(1000), Lave(1000)
        Double precision mu, W, Vl, rl, r, L, z, Pi
        Double precision qr, sumr, sumz, rave, Lave, dr, dz, Vr, ro, ri
        Double precision FA, P1, P2, Y1, Y2
        Real ABSACC, ANS
        Integer NOUT, IFAIL, NPTS, i, j
        Common mu, W, Vl, rl, r, L, z, Pi

        mu=78.36
        W=1.27E-5
        rl=1.0
        L=14
        Pi=3.141593
        Vl=Pi*rl*rl*L
        ro=5
        ri=1.75
        Vr=Pi*L*(ro*ro-ri*ri)
        dr=0.05
        dz=0.5
        sumr(1)=0
        sumz(1)=0
        i=0
        j=0
        ABSACC=1.0E-6
        IFAIL=0

c       Calculation at different z
c       ^^^^^^^^^^^^^^^^^^^^
20      j=j+1
        z=0.1+dz*(j-1)

c       Calculation at different r
c       ^^^^^^^^^^^^^^^^^^^^
30      i=i+1
        r=ri+dr*(i-1)
        Y1=-acos(sqrt(r*r-rl*rl)/r)
        Y2=acos(sqrt(r*r-rl*rl)/r)


        call D01DAF(Y1,Y2,P1,P2,FA,ABSACC,ANS,NPTS,IFAIL)

        write (NOUT,99999) 'Integral =', ANS
        write (NOUT,99998) 'Number of function evaluations =', NPTS
        if (IFAIL.GT.0) write (NOUT,99997) 'IFAIL =', IFAIL
```

```
      qr(i)=ANS*2*Pi*r
      sumr(i)=sumr(i)+qr(i)
      rave(i)=(sumr(i)/i)*(ro-ri)
      ABSACC=1.0E-6
      IFAIL=0

      if (r.lt.ro) goto 30

      sumz(j)=sumz(j)+rave(i)
      i=0

      if (z.le.L-0.1) goto 20
      Lave(j)=(sumz(j)/j)*(L-0.05-0.01)
      print*,Lave(j)

      stop

99999 Format (1X,A,E10.4)
99998 Format (1X,A,I5)
99997 Format (1X,A,I2)

      end

      DOUBLE PRECISION FUNCTION P1(y)
c     ** Scalar Arguments **
      double precision y
      double precision rl,L,z,r,mu,W,Vl,Pi
      common mu,W,Vl,rl,r,L,z,Pi
c     ** Intrinsic Functions **
      intrinsic sqrt,cos,atan
c     ** Executable Statements **
      P1=atan((r*cos(y)-sqrt(r*r*cos(y)*cos(y)-r*r+rl*rl))/(L-z))

      return
      end

      DOUBLE PRECISION FUNCTION P2(y)
c     ** Scalar Arguments **
      double precision y
      double precision rl,L,z,r,mu,W,Vl,Pi
      common mu,W,Vl,rl,r,L,z,Pi
c     ** Intrinsic Functions **
      intrinsic sqrt,cos,atan
c     ** Executable Statements **
      P2=Pi+atan((r*cos(y)-sqrt(r*r*cos(y)*cos(y)-r*r+rl*rl))/(-z))

      return
      end

      DOUBLE PRECISION FUNCTION FA(x,y)
c     ** Scalar Arguments **
      double precision x,y
      double precision rl,L,z,r,mu,W,Vl,Pi
      common mu,W,Vl,rl,r,L,z,Pi
c     ** Intrinsic Functions **
      intrinsic sqrt,cos,sin
c     ** Executable Statements **
      FA=mu*W/(2*Pi*Vl)*sin(x)*cos(y)*sqrt(r*r*cos(y)*cos(y)-r*r+rl*rl)
```

```
$exp(-mu*((r*cos(y)-sqrt(r*r*cos(y)*cos(y)-r*r+rl*rl))/sin(x)))

return
end
```

APPENDIX C

```
c       Mineralization Profile Simulation for Batch Reactor
c       ********************************************

        Real k, C1, H1, C2, H2, I, n, r
        Integer time, j, dt

        k=1.0094E-4
        C1=834
        H1=2022.461
        I=8.66E-5

        time=60
        dt=1
        n=time/dt
        j=0

10      j=j+1
        t=j*dt

c       Mineralization Rate Equation
c       ^^^^^^^^^^^^^^^^^^^^^^^^^^^^
        r=k*C1**(0.74)*H1**(0.39)*I**(-0.11)

c       MASS BALANCE OVER REACTOR
c       *************************
c       For TOC
c       ^^^^^^^^
        C2=C1-r*dt

c       For Hydrogen Peroxide
c       ^^^^^^^^^^^^^^^^^^^^^^
        H2=H1-r*dt

        print *, t, r, C2, H2
        C1=C2
        H1=H2
        if(j.lt.n) goto 10

        stop
        end
```

APPENDIX D

```
c       Mineralization Profile Simulation for Pilot Plant
c       ****************************************

        Real k, C1, H1, C2, H2, I, Vr, Vt, n, r, a, b, F
        Integer time, j, dt
        k=1.0094E-4
        C1=834
        H1=4853.907
        I=1.75E-4
        Vr=88.41
        Vt=37
        F=2.53
        a=F/Vr
        b=F/Vt
        time=60
        dt=1
        n=time/dt

        j=0
10      j=j+1
        t=j*dt

c       Mineralization Rate Equation
c       ^^^^^^^^^^^^^^^^^^^^^^^^^^^
        r=k*C1**(0.74)*H1**(0.39)*I**(-0.11)

c       MASS BALANCE OVER REACTOR
c       *************************
c       For TOC
c       ^^^^^^^^
        C2=(dt*(a*C1-r)+C1)/(1+a*dt)

c       For Hydrogen Peroxide
c       ^^^^^^^^^^^^^^^^^^^^^
        H2=(dt*(a*H1-r)+H1)/(1+a*dt)

c       MASS BALANCE OVER TANK
c       **********************
c       For TOC
c       ^^^^^^^^
        C=(C2*F*dt+C1*(Vt-F*dt))/Vt

c       For Hydrogen Peroxide
c       ^^^^^^^^^^^^^^^^^^^^^
        H=(H2*F*dt+H1*(Vt-F*dt))/Vt

        print *, t, r, C, H
        C1=C
        H1=H
        if(j.lt.n) goto 10
        stop
        end
```

APPENDIX E

```
c       Mineralization Profile Simulation for Pilot Plant
c       ****************************************

        Real k, C1, H1, C2, H2, I, Vr, n, r, a, F, Vr
        Integer time, j, dt

        k=1.0094E-4
        C1=834
        H1=4853.907
        I=1.75E-4
        Vr=88.41
        F=2.53
        a=F/Vr
        time=60
        dt=1
        n=time/dt

        j=0

10      j=j+1
        t=j*dt


c       Mineralization Rate Equation
c       ^^^^^^^^^^^^^^^^^^^^^^^^^^^
        r=k*C1**(0.74)*H1**(0.39)*I**(-0.11)


c       MASS BALANCE OVER REACTOR
c       *************************
c       For TOC
c       ^^^^^^^^
        C2=(dt*(a*C1-r)+C1)/(1+a*dt)

c       For Hydrogen Peroxide
c       ^^^^^^^^^^^^^^^^^^^^
        H2=(dt*(a*H1-r)+H1)/(1+a*dt)


        print *, t, r, C2, H2
        C1=C2
        H1=H2
        if(j.lt.n) goto 10


        stop
        end
```